Biochemical and Biophysical Investigations of Non-Zinc Dependent Glyoxalase I Enzymes

by

Nicole Sukdeo

A thesis
presented to the University of Waterloo
in fulfillment of the
thesis requirement for the degree of
Doctor of Philosophy
in
Chemistry

Waterloo, Ontario, Canada, 2008

AUTHOR'S DECLARATION

I hereby declare that I am the sole author of this thesis. This is a true copy of the thesis, including any

required final revisions, as accepted by my examiners.

I understand that my thesis may be made electronically available to the public.

Abstract

The principal methylglyoxal (MG)-detoxifying system in most living organisms is the two-metalloenzyme Glyoxalase system. Glyoxalase I (GlxI) initially converts the non-enzymatically formed MG-GSH hemithioacetal to the thioester S,D-lactoylglutathione. The hydrolase, Glyoxalase II (GlxII) regenerates GSH and liberates the product D-lactate. Ni^{2+}/Co^{2+}- and Zn^{2+}-activated GlxI enzymes exist in nature. The Ni^{2+}/Co^{2+}-activated GlxI are not active as Zn^{2+}-holoenzymes in spite of the structural similarities to the Zn^{2+}-dependent enzymes. The Zn^{2+}-GlxI enzymes have been investigated heavily relative to the Ni^{2+}/Co^{2+}-activated enzymes, which have been isolated more recently. As part of this study the three GlxI homologs isolated from *Pseudomonas aeruginosa* were characterized. The homologous genes encode GlxI enzymes of both metal activation type. The Zn^{2+}-activated *P. aeruginosa* GlxI is difficult to de-metallate compared to the Ni^{2+}/Co^{2+}-activated enzymes, reflecting a difference in metal-binding/insertion between the two types of GlxI. The *E. coli* GlxII was isolated and characterized to determine whether Ni^{2+}/Co^{2+}-activation is a characteristic of the Glx system as a whole in this organism. Inductively coupled plasma mass spectrometry on purified *E. coli* GlxII confirms that the active protein is a binuclear Zn^{2+}-metalloenzyme. The results to date indicate a detectable isotope effect for the Cd^{2+}-holoenzyme but not the Ni^{2+}-reconstituted enzyme. Chemical crosslinking experiments indicate that the SlyD Ni^{2+} metallochaperone does not form a complex with *E.coli* GlxI. This indicates that the *E. coli* active site is not metallated *in vivo* by this accessory protein. The principal biophysical experiment in this project was determining of Ni^{2+}-binding stoichiometry for *E. coli* GlxI by ^{1}H-^{15}N heteronuclear single quantum coherence (HSQC) NMR. The GlxI dimer reorganization ceases when the metal:dimer stoichiometry reaches 0.5 during apoenzyme titration. This finding supports previous studies that indicate half-of-the-sites metal binding in this enzyme.

Acknowledgements

"One does not become fully human painlessly." – Rollo May

I would like to thank my supervisor Dr. John Honek for giving me the opportunity to investigate metalloenzymes under his guidance. I appreciate that I have been able to pursue intensive study of a subject that interested me greatly during undergraduate study. As a graduate researcher I have been able to interact with persons investigating a diversity of experimental systems. These individuals (students, technicians, faculty) exemplify many qualities that define a thorough, responsible investigator. For as long as I remain involved in biochemical research, these are attributes that I aspire towards incorporating in my work. I am grateful that Dr. Honek has provided a gateway to rewarding experiences in the laboratory and in other related contexts, while fostering a competence for enzymological research. His patience and mentorship have helped to make my doctoral project a positive experience.

Dr. Elisabeth Daub and Dr. Susan Clugston were most supportive and helpful providing the instruction I needed to go about my studies with confidence. They were instrumental in allowing me to become comfortable with the laboratory environment that has been my place of study for several years.

My advisory committee has provided a patient ear, and constructive criticism as well as being a gracious panel that followed my progress through the Glyoxalase project. I extend my thanks to Dr.'s Gary Dmitrienko, Guy Guillemette and Janet Wood for their advice, support and insight.

I am indebted to Dr. Trevor Charles for allowing me to undertake in a research project for the first time. His approachability and enthusiasm for bacterial genetics made my first encounters with "bench work" easier. It has been a pleasure over the years to converse with him on from time to time, where we might discuss my current project, future plans and anything conceptual that we were fixated on at the time. His advice and insight have been of great value to me throughout my studies at University of Waterloo.

Dr. Deborah Zamble at the University of Toronto must be acknowledged for her collaboration to investigate the potential for metallochaperone involvement in *Escherichia coli* GlxI metallation *in vivo*. Dr. Zamble and her technician Kathleen Zhang generously provided the required *E. coli* strains for this part of the project and evalutated *E. coli* GlxI for possible complexation with the SlyD metallochaperone.

Dr. Richard Smith, Valerie Robertson and Mike Ditty have all been instrumental in providing technical assistance for mass spectrometric and NMR analyses in the context of my project. Their help was much appreciated and their advice was helpful on all occasions.

The members of the Honek laboratory have provided companionship, support and intellectual discourse throughout the completion of this degree. The peers I worked alongside included Dr. Susan Clugston, Jennifer Coggan, Pei Hang, Christine Hand, Danish Khan, Meijun Lu, Ignace Moya, Kadia Mullings, Jason O' Young, Uthaiwan Suttisansanee, Dr. Mark Vaughan, Paula Walasek, Ronald

Table of Contents

List of Figures

xi

xii

List of Tables

List of Abbreviations

Amino acids are referred to in text by the standard one-letter or three-letter codes.

α-deuterioPG	α-deuteriophenylglyoxal
AGE	Advanced glycation end product
AR	Aldose reductase
Da	Dalton
DHAP	Dihydroxyacetone phosphate
DIE	Deuterium isotope effect
DmPBGS	*Drosophila melanogaster* porphobilinogen synthase
DMSO	Dimethylsulfoxide
DNA	Deoxyribonucleic acid
DPA	2,6-pyridinedicarboxylic acid
DTNB	5, 5'-dithiobis-(2-nitrobenzoic acid)
EDC	1-(3-dimethylaminopropyl)-3-ethylcarbodiimide hydrochloride
EDTA	Ethylenediamine tetraacetic acid
EPR	Electron paramagnetic resonance
ESMS	Electrospray ionization mass spectrometry
EXAFS	X-ray absorption fine structure
FluoroMG	Fluoromethylglyoxal
FPLC®	Fast peptide and protein liquid chromatography

Gdn-HCl   Guanidinium hydrochloride

Glx   Glyoxalase

GlxI   Glyoxalase I

GlxII   Glyoxalase II

GSH   Glutathione

HEPES   *N*-2-Hydroxyethylpiperazine-*N'*-2-ethanesulfonic acid

HIPC-GSH   *S*-(*N*-hydroxy-*N*-*p*-iodophenylcarbamoyl)glutathione

HPLC   High performance liquid chromatography

HSQC NMR   Heteronuclear single quantum coherence nuclear magnetic resonance

ICP-AES   Indcutively coupled plasma atomic emission spectroscopy

ICP-MS   Inductively coupled plasma mass spectrometry

IPTG   Isopropyl-β-D-thiogalactopyranoside

ITC   Isothermal titration calorimetry

kDa   Kilodalton

KIE   Kinetic isotope effect

MES   2-(*N*-morpholino)ethanesulfonic acid

MG   Methylglyoxal

MM   Molecular mass

MW   Molecular weight

MOPS   3-(N-morpholino)propanesulfonic acid

mRNA	messenger ribonucleic acid
NADPH	Nicotinamide adenine dinucleotide phosphate (reduced)
NCBI	National Centre for Biotechnology Information
NMR	Nuclear magnetic resonance
PAR	4-(2-pyridylazo)resorcinol
PCR	Polymerase chain reaction
PBGS	porphobilinogen synthase
PDB	Protein Databank
PG	Phenylglyoxal
pI	Isoelectric point
PMSF	Phenylmethylsulfonyl fluoride
QTOF	Quadrupole time-of-flight
RNA	Ribonucleic acid
SDS-PAGE	Sodium dodecylsulfate polyacrylamide gel electrophoresis
SLG	*S*-D-lactoylglutathione
Salmonella	*Salmonella enterica* serovar Typhimurium
TIGR	The Institute for Genomic Research
TIM	Triosephosphate isomerase
TSH	Trypanothione
w/ and w/o	with and without

Chapter 1

Review of the Glyoxalase System and Project Synopsis

1.1   The Glyoxalase System and Methylglyoxal Toxicity

The glyoxalase (Glx) system is a well-studied carbon metabolism pathway conserved in many living organisms. This enzyme system is generally considered a major detoxification pathway of cytotoxic methylglyoxal (MG) and related α-ketoaldehyde substrates (10). There are two metalloenzymes that comprise the Glx system and the tripeptide glutathione (GSH) participates in the reactions as a co-substrate (Figure 1.1) (11). Glyoxalase I (GlxI: *S*-D-lactoylglutathione methylglyoxal lyase (isomerizing) E.C. 4.4.1.5) converts the hemithioacetal of MG and GSH to the corresponding thioester *S*-D-lactoylglutathione (Figure 1.1). The MG-GSH hemithioacetal is formed non-enzymatically prior to enzymatic conversion. The second enzyme in the pathway Glyoxalase II (GlxII: *S*-2-hydroxyacylglutathione hydrolase E.C. 3.1.2.6) hydrolyzes the thioester to generate the α-hydroxyacid D-lactate and the co-substrate GSH (Figure 1.1).
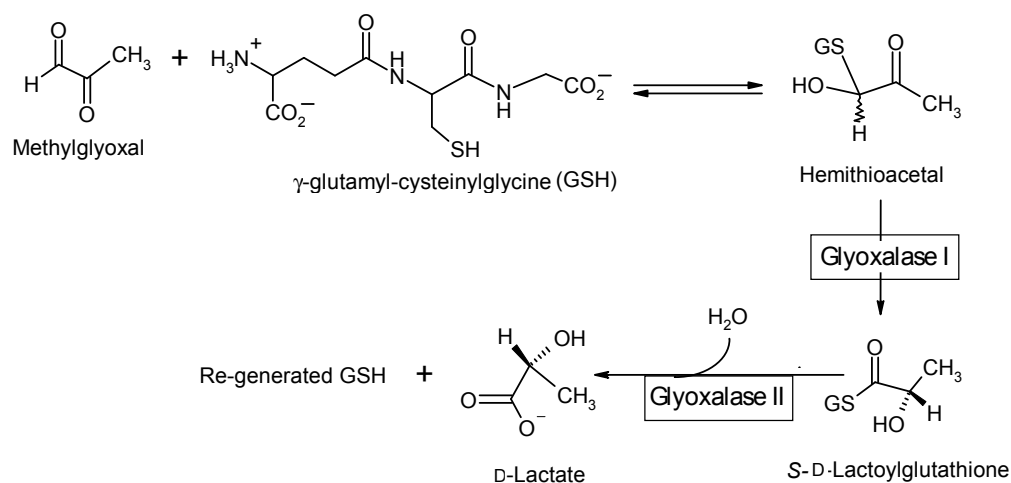
Figure 1.1: The reactions of the Glyoxalase system

α-Ketoaldehyde byproducts are potent electrophiles that are deleterious to biological systems, because of their propensity to form covalent adducts with protein and nucleic acid molecules (12, 13). Adduct formation is due to the tendency of the aldehydic group of α-ketoaldehydes to undergo attack by a nucleophile (See structure of MG in Figure 1.1).

Protein glycation is a consequence of MG reactivity that constitutes a form of long-term tissue damage in diabetic pathologies (14). Cysteine, lysine and arginine residues in proteins are particularly prone to MG modification (15, 16). Irreversible covalent adducts formed by the interaction of MG with protein are called "advanced glycation end products" or AGE's (17). The conversion of a protein to an AGE frequently eliminates or reduces function of the molecule. Arginine is the most commonly observed site of modification and a recent study of MG-modification on human hemoglobin demonstrates that this residue is most frequently converted into a hydroimidiazolone derivative (18).

The guanidine modification of tobacco mosaic virus ribonucleic acid (RNA) is one of the earliest documented examples of MG-dependent nucleic acid adduct formation (19). Krymkiewicz, Zwaig and Dieguez characterized the deleterious effects of RNA and DNA adduction by MG during the 1970's. These two research groups resolved that MG toxicity inhibits protein synthesis as a consequence of nucleic acid modification at the genetic level (DNA) and transcriptional (mRNA) level (20). Since then, small molecule analysis techniques such as mass spectrometry have enhanced detection of MG modification on genomic and transcript material. For instance, Frischmann *et al.* have detected the formation of N^2-1-carboxyethyl)-2'-deoxyguanosine following the incubation of salmon sperm DNA with MG at physiological concentrations (10 µM) at 37 degrees Celsius (21). The identification of guanosine adducts in this study was possible because the investigators used liquid chromatography mass spectrometry to analyze the DNA.

1.2 Non-Glx Pathways for MG Detoxification

The glyoxalase enzymes in mammalian systems are the predominant methylglyoxal detoxifying components in liver tissue. A different enzyme called aldose reductase (AR) also detoxifies MG in eukaryotes. This enzyme has been identified in mammals and *Saccharomyces cerevisiae* (14, 22). AR is expressed at relatively higher levels in cardiovascular and renal tissues of multi-organ system eukaryotes. This enzyme is an NADPH-dependent aldo-keto reductase that converts MG to acetol. AR can be considered an extrahepatic detoxification system for diverse aldehyde-containing substrates. The products of reduction are the corresponding alcohols of the substrates. AR can reduce glucose, catecholamines and steroid metabolites to sorbitol, phenylglycol derivatives, and androstandiol derivatives respectively (23, 24, 25, 26).

Recently Yabe-Nishimura and co-workers were able to demonstrate upregulation of AR activity in response to physiologically relevant MG concentrations (27). Their experimental system involves incubating isolated rat aortic smooth muscle cells with MG. They observed an increase in the amount of AR-encoding mRNA transcript generated by the cells exposed to MG. The increase in the amount of AR-encoding transcript was proportional to MG exposure time as well as dosage. Additionally AR activity levels and protein quantity (as assessed by Western blot analysis) increased with longer MG exposure times.

Another interesting finding is that intracellular reactive oxygen species (ROS) production increases following MG exposure, but precedes transcriptional induction of AR by several hours (27). This observation suggests that MG may mediate AR induction with ROS as the signaling molecule(s) for the process. Finally Yabe-Nishimura and co-workers noted that the p38 kinase pathway might be involved in AR regulation in response to MG stress. Thus, AR constitutes a secondary, thiol independent route for MG detoxification that may be more important for responding to MG stress outside of the liver.

1.3 Metabolic Routes of MG Production

The origin of MG in biological systems can be attributed to several metabolic sources. Enzymatic routes of production include, direct enzymatic formation (from MG synthase), amino acid degradation, cytochrome P450 IIE1 isozymes and amine oxidases. The triosephosphate isomerase (TIM) reaction in the glycolytic pathway can produce MG as an unwanted side reaction and this will be discussed in the following section.

1.3.1 MG Formation by Triose Phosphate Isomerase

The glycolytic enzyme TIM normally catalyzes the interconversion of dihydroxyacetone phosphate (DHAP) and glyceraldehyde-3-phosphate. The reaction typically proceeds via the formation of an enediolate intermediate. However the TIM-catalyzed reaction can result in an unwanted side reaction where inorganic phosphate is eliminated from the intermediate resulting in the generation of MG (Figure 1.2) (28). This elimination mechanism may occur at a sufficient frequency that cells could accumulate MG at a rate of 0.4 mM/cell/day (28). This reaction constitutes a significant contribution to MG formation in organisms with a glycolytic pathway.
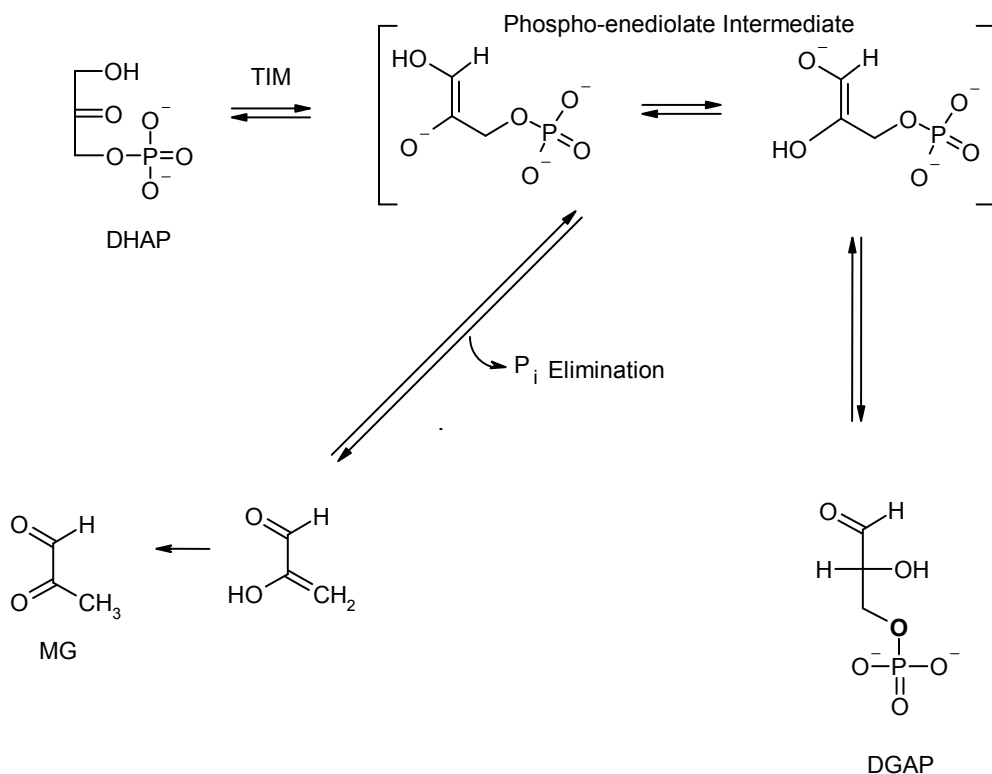
Figure 1.2: TIM-catalyzed isomerization and elimination reactions

1.3.2 MG and the Glycolytic Bypass

One of the most interesting aspects of MG metabolism is that production of this toxic electrophile

may be metabolically relevant to some organisms. The enzyme MG synthase catalyzes the formation

of MG from dihydroxyacetone phosphate with liberation of inorganic phosphate (29). MG synthase

was first isolated from *E. coli*, but has also been purified from *Saccharomyces cerevisiase*,

Pseudomonas saccharophila, goat liver and *Clostridium acetobutylicum* (30, 31, 32, 33). Inorganic

phosphate (P_i) is an allosteric inhibitor of MG synthase. The enzyme is also negatively regulated by

3-phosphoglycerate, phosphoenolpyruvate and pyrophosphate, but not to the same extent as with P_i

(30). In organisms possessing MG synthase, the enzyme is thought to function within a metabolic

5

pathway that bypasses phosphorylating glycolysis (Figure 1.3) (34, 35). The bypass functions under conditions of intracellular P_i limitation, such that there is an accumulation of DHAP. Consequently MG synthase activity increases, so that there is an increased amount of intracellular MG. The MG can be converted to pyruvate via the glyoxalase system enzymes and D-lactate dehydrogenase, thereby conserving the existing pool of P_i within the cell (Figure 1.3). The bypass enzymes therefore constitute a non-phosphorylating means for producing the end glycolytic product, pyruvate.

1.3.3 MG Formation during Amino Acid Degradation

The glyoxalase system is also proposed to play a role in amino acid degradation. Glycine and threonine degradation yields the product aminoacetone (1). The accumulation of methylglyoxal has been observed during the feeding of *S. cerevisiae* of L-threonine as a nitrogen source and also in goat plasma (36, 37). Investigation of methylglyoxal production from aminoacetone suggests that conversion occurs using the enzyme monoamine oxidase (Figure 1.3) (Elliot 1959, (38). The existence of amine oxidases that produce methylglyoxal has been confirmed in *Saccharomyces cerevisiae* and *Staphylococcus aureus* (36, 39).

1.3.4 Cytochrome P450-Catalyzed MG Production

Isozymes of the cytochrome P450 IIEI subfamily are also capable of producing MG from acetone as part of the gluconeogenic pathway (See Figure 1.3)(40). Acetone-converting monooxygenases were characterized as part of this pathway from analysis of hepatic microsomes from rats that consumed acetone in drinking water. The analysis revealed the presence of an acetone monooxygenase that converts acetone to acetol (See Figure 1.4). A second acetol monooxygenase converted the acetol to methylglyoxal (40).
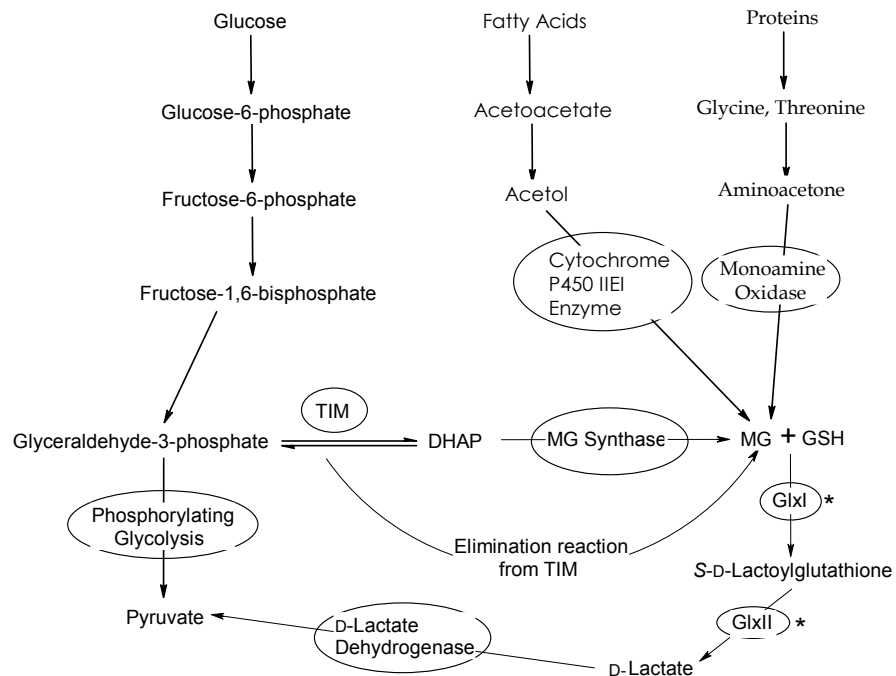
Figure 1.3: Summary of MG sources in living systems. This diagram was adapted from (1)**.**

1.4 Microbial GlxI enzymes with Alternative Roles in Cellular Physiology

A number of putative glyoxalase-like proteins have been identified recently as gene products that are

upregulated in expression during colonization activities by prokaryotic pathogens. The host

specificity of these bacterial species is quite diverse as they include plant and human pathogens.

These recent investigations are stimulating additions to this research area because they connect the

Glx system to cellular functions other than MG detoxification. These novel contexts for the Glx

system include type III secretion, host-cell colonization, and acid tolerance as described in the following sections.

1.4.1 *Ralstonia solanacearum*

The vascular pathogen *Ralstonia solanacearum* has a protein with predicted GlxI function that is upregulated by the HrpB transcriptional activator (41). This AraC-type activator controls expression of the type III secretion system common to many Gram-negative bacteria (41). The type III secretion system consists of a needle- (animal pathogens) or pilus-like (phytopathogens) assembly that facilitates protein translocation into the host organism during the colonization process (41). The promoter region of this putative GlxI -encoding gene contains a plant-inducible-promoter box motif, which is associated with regulation by HrpB (41). Secretion analysis revealed that the putative GlxI can accumulate to significant levels in the *R. solanacearum* cells grown in *hrp*-inducing medium, but remains in the cytoplasm of the bacteria (42). Deletion of this gene increased the MG susceptibility of *R. solanacearum*, indicating that it likely codes for a GlxI enzyme (42).

1.4.2 *Salmonella typhimurium*

The pathogen *Salmonella enterica* serovar Typhimurium (*Salmonella*) has also been examined using proteomic analysis to identify genes upregulated during macrophage colonization. Shi *et al.* recently identified 39 proteins that were strongly upregulated during *in vitro* macrophage infection by *Salmonella*, including a putative GlxI sequence (43). The deletion of the GlxI-encoding gene called STM3117 rendered *Salmonella* less viable during macrophage infection (43). The impaired viability was apparent as a reduced rate of replication in the macrophages. This finding implicates a GlxI-like protein as a potential virulence determinant for *Salmonella*. Several other genes upregulated during infection included a monoamine oxidase, which can produce MG from aminoacetone and an acetyl-CoA hydrolase, which produces acetate. Shi *et al.* postulated that the coordinate upregulation of all three genes might be pertinent to cell wall modification during *Salmonella* replication and host cell

colonization. The reason for this inference is that D-lactate, the final product of Glx system MG

detoxification can be used to make peptidoglycan, the principal constituent of bacterial cell walls.

Also, the acetate from the acetyl-CoA hydrolase can be used to modify peptidoglycan, conferring

resistance to enzymatic degradation. Further study is necessary and may reveal a novel role for MG

synthesis and turnover in the adaptive physiology of Gram-negative pathogens.

1.4.3 *Bacillus anthracis*

Bacillus anthracis is a Gram-positive animal pathogen lacking enzymes for glutathione synthesis, but

contains several GlxI-family genes that are transcriptionally upregulated when cells are subjected to

paraquat-induced superoxide stress (44). Transcription of these putative GlxI-encoding genes is

upregulated in wild type cells and in an isogenic oxidative stress-prone mutant (containing a deletion

of the superoxide dismutase-encoding gene) when subjected to paraquat stress (44). Futhermore,

paraquat priming of the cells increased their MG resistance as assessed by disk diffusion assay (44).

Although this data suggests a redox-response by a putative *B. anthracis* Glx system, there may be

other detoxification/resistance mechanisms that are pleiotropically regulated in the presence of

oxidative stress (44).

1.4.4 *Streptococcus mutans*

The Gram-positive bacterium *Streptococcus mutans* is associated with the formation of dental caries

in humans. *S. mutans* facilitates the formation of dental caries by producing acidic metabolites in

substantial quantities (45). The accumulation of acidic byproducts is believed to be due to

modulation of the flux through the glycolytic pathway by *S. mutans* (45). The glycolytic rate in *S.*

mutans is directly influenced by the "feast-or-famine" conditions in the oral cavity which is

dependent upon the host diet (45). The net result of these physiological changes is a substantial

increase in the *S. mutans* biofilm layer, which contributes to the destructive invasion of dental enamel

(45). The increased flux through the glycolytic pathway can result in the accumulation of toxic

metabolites, including MG from the TIM side reaction. Therefore MG detoxification systems should be present in *S. mutans* to prevent premature cell death in the biofilm.

Recently a putative GlxI sequence has been identified in *S. mutans* strain UA159 that appears to be regulated as part of the aciduric response by this organism (45). No putative GlxII-encoding gene has been identified in the *S. mutans* genome, yet the degradation of *S*-lactoylglutathione is detectable in lysates of *S. mutans* cultures (45). Interestingly, *S. mutans* also does not synthesize the glutathione co-substrate commonly associated with glyoxalase system activity. However *S. mutans* can import glutathione from its surrounding based on culture experiments, so it may rely on host-provided thiols for intracellular redox and detoxification activities. Korithoski *et al.* also deleted the GlxI-encoding gene, which decreased MG resistance in *S. mutans* strain UA159 and increased the glycolytic rate under acidic growth conditions. Acid tolerance for the GlxI knockout strain was diminished in a biofermentor growth competition experiment against the isogenic wild type strain (45). Korithoski *et al.* were able to demonstrate that GlxI activity in *S. mutans* strain UA159 increases under conditions of acid adaptation.

Transcriptional profiling experiments confirm that the GlxI-encoding gene expression increases, as indexed by level of mRNA transcripts under acidic growth conditions (pH 5.0 versus pH 7.0) and also under acid-adapted conditions (grown to mid-logarithmic phase at pH 7.5, then exposed to pH 5.0 for 2 hours) (45). GlxI-mRNA levels also increases with the exposure of cultures to exogenous MG (45).

1.5 Glx as a Metalloenzyme System

Davis and Williams first described the metal ion requirement of GlxI in 1966 (46). They were characterizing calf liver GlxI when the metal activation of this enzyme was discovered. GlxI enzymes were initially described as Mg^{2+}-dependent because some preparations of the enzyme (calf liver, sheep liver, human liver, rat erythrocyte and porcine erythrocyte) could be successfully

reconstituted with this ion (46, 47, 48, 49). However in 1978 Aronsson, Marmstal and Mannervik determined that purified preparations of human erythrocyte, porcine erythrocyte, rat liver and yeast GlxI enzymes contained bound Zn^{2+} as determined by atomic absorption spectroscopy (50). Since the publication of this study all GlxI enzymes were considered Zn^{2+}-dependent in nature.

The first example of a non-Zn^{2+} activated GlxI enzyme was *Escherichia coli* GlxI (51). When this enzyme was first isolated for characterization, the similarity of the amino acid sequence and conservation of active site residues (36% identity to human GlxI) seemed indicative of a Zn^{2+}-activated GlxI enzyme (51). However, initial screens of metal activation revealed that *E. coli* GlxI becomes maximally activated by Ni^{2+}-ions and not Zn^{2+}-ions (51).

Since *E. coli* GlxI was the first non-activated Zn^{2+}-dependent form of this enzyme, a comparative biochemical survey of several other bacterial GlxI enzymes was carried out in the laboratory of Honek *et al.* The GlxI-encoding genes of *Yersinia pestis*, *Pseudomonas aeruginosa* and *Neisseria meningitidis* have been cloned and overexpressed in *E. coli* (3). The recombinant GlxI enzymes have been characterized to ascertain whether the non-Zn^{2+}-dependent metal activation profile is present in other prokaryotes with similar enzymes. The results indicate that all three GlxI enzymes characterized are similar in catalytic efficiency (3). These enzymes also exhibit optimal activation with Ni^{2+} and Co^{2+} ions, similar to *E. coli* GlxI (3). Therefore the GlxI enzymes can be broadly classified into two groups based on metal activation: Zn^{2+}-dependent and non-Zn^{2+}-dependent (Ni^{2+}/Co^{2+}-activated).

1.5.1 Structure of GlxI Enzymes

E. coli GlxI is the first crystallographically characterized non-Zn^{2+}-dependent GlxI enzyme (52). The crystal structure for the archetypal Zn^{2+}-dependent human GlxI was available three years prior to the bacterial enzyme data (53). Having both structures available allowed for comparisons to be made that could be potentially correlated to the difference in metal activation between these two enzymes.

Overall, human and *E. coli* GlxI enzymes exhibit a highly conserved topology within a homodimeric framework (Figure 1.4) (52). The monomer of the human enzyme is larger than that of *E. coli* GlxI because of the N-terminal arm region that wraps around the adjacent subunit (Figure 1.4). GlxI enzymes belong to a structural superfamily called the βαββ superfamily (9, 54). The superfamily consists of evolutionarily divergent proteins all containing tandem βαββ motifs (Figure 1.5) (9). In the case of the dimeric GlxI enzymes each consituent monomer is composed of two βαββ motifs connected by a linker. A semi-circular cleft is created by the approach of the β-sheet portion of two βαββ motifs in superfamily members (9, 54). This cleft is important, as it constitutes the active site in enzymatic superfamily members. In the case of the GlxI enzymes the active site/metal-binding cleft is formed from βαββ motifs at the dimeric interface, such that each motif is on a different polypeptide subunit. This arrangement is classified as a domain-swapped dimer (Figure 1.6). Other βαββ proteins such as methylmalonyl coA epimerase contain the active site cleft within one monomer, so that the dimer consists of back-to-back subunits (Figure 1.6) (55).

A   B
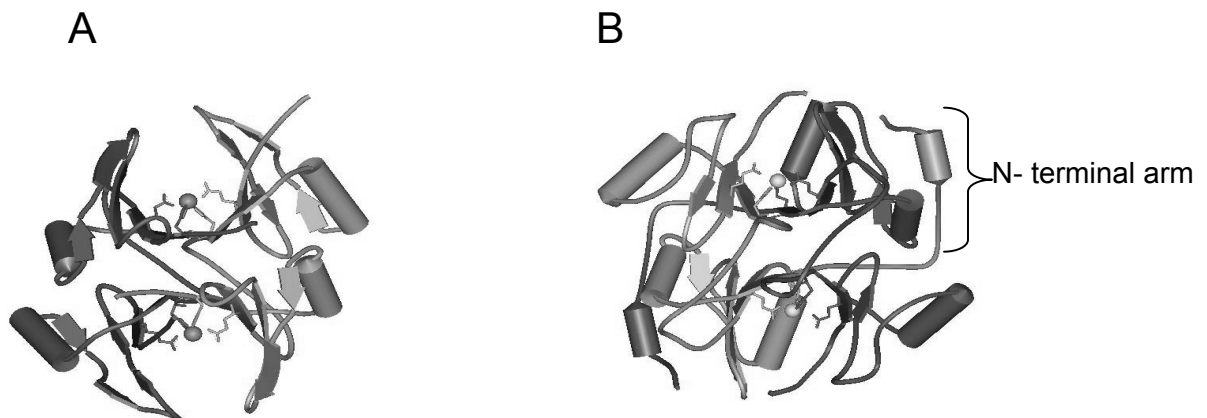
Figure 1.4: Crystal structures of A) *E. coli* **GlxI (PDB ID: 1F9Z) and B) human GlxI (PDB ID: 1QIN**). The subunits in each dimer can be distinguished from the shading in the diagram (dark grey module and light grey) module in each protein. The spheres at the dimeric interface represent bound metal ions. The N-terminal arm with a helical segment in the human enzyme is labeled in the above figure
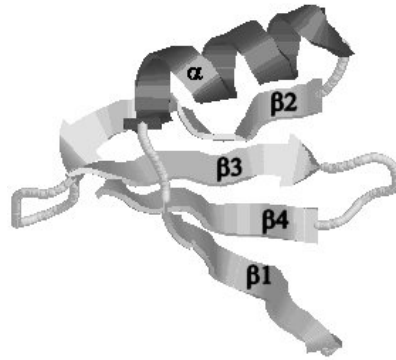
Figure 1.5: Structure of the βαβββ motif (from PDB ID: 1F9Z)
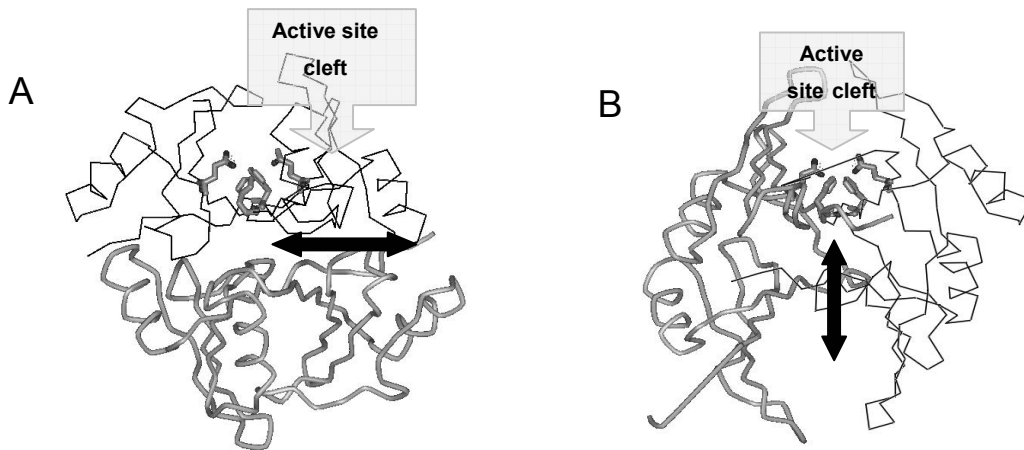
Figure 1.6: Structures of A) *P. shermanii* **MMCE (non-domain swapped, PDB ID: 1JC5) and B)** *E. coli* **GlxI (domain swapped, PDB ID: 1F9Z).** Individual subunits in each dimer can be distinguished by the grey tube trace of one subunit and the black wireframe trace of the other subunit. Active site residues are shown in stick form and the black double-headed arrow indicates the dimer interface of each protein. The cleft where the active site residues are located is labeled correspondingly.

The contiguous assembly of βαβββ motifs in these proteins is thought to originate from gene duplication and subsequent fusion events (9). This scheme can account for the occurrence of GlxI

13

enzymes as homodimers, which is common to human, bacterial, leishmanial and trypanosomal forms of the enzyme. Fused dimer GlxI enzymes also exist, which are monomeric forms of the enzyme with all four constitutive motifs in a single polypeptide. GlxI enzymes of this type tend to be found in plants, yeast (*Saccharomyces cerevisiae*) and *Plasmodium falciparum* (55, 56, 57, 58).

1.5.2 Human and *E. coli* GlxI Enzymes have Similar Active Sites

GlxI sequence comparisons and structural characterization shows that the four amino acid metal ligands are very well conserved (51, 52, 53). Two amino acid metal ligands are contributed from each monomer in human and *E. coli* GlxI (Figure 1.4 and Figure 1.7). These residues are generally two histidines and two glutamates (52). However the human enzyme has a Gln residue at position 34, which corresponds to His5 in *E. coli* GlxI (Figure 1.7) (53). The variation of this single metal ligand is not predictive of Zn^{2+}-dependent metal activation in GlxI enzymes. Several other GlxI enzymes known to be Zn^{2+}-activated, possess a histidine residue at the position that Gln34 would be located in the human enzyme. Such examples include the GlxI enzymes of *Saccharomyces cerevisiae* and *Pseudomonas putida* (57, 59).

Initial studies of *E. coli* GlxI led to the creation of a His5 → Gln5 variant, so that the active site residues were "humanized" in composition (60). The aim of this investigation was to assess whether amino acid variation at this position was a determinant of metal selectivity. The purified variant is substantially impaired for metal binding and activation, yet retains maximal activation in the presence of Ni^{2+} (60). A shift towards low levels of Zn^{2+} activation is detectable with this *E. coli* GlxI variant. This indicates that the ligand substitution could influence metal activation but it is not the dominant determinant of metal selectivity.

One notable finding in active site comparisons of the human and *E. coli* GlxI enzymes at the structural level is the coordination environment around the metal ion. The active human and *E. coli* GlxI enzymes (Zn^{2+}-bound and Ni^{2+}-bound respectively) both possess octahedral coordination

14

geometry around their active site metal ions (52, 61, 62). Four conserved amino acid residues at the

dimeric interface and two monodentate water ligands chelate metal ions at the active site. The

inactive Zn^{2+}-bound GlxI from *E. coli* exhibits trigonal bipyramidal geometry at the active site

(Figure 1.8) (52). The five-coordinate geometry around the Zn^{2+} ion is due to the loss of one of the

water ligands (Figure 1.8) (52). This finding indicates that octahedral coordination is a prerequisite

for the formation of active holoenzyme (52). GlxI enzymes do not exhibit catalytic activity in their

apo-forms (51). Inactive GlxI enzymes can result from the loss of metal during purification steps for

enzyme preparation, or by chelator treatment (EDTA, 1,10-phenanthroline) of holoenzyme samples.

The structure of *E. coli* GlxI does not undergo any major re-organization that can be detected by X-

ray crystallography, or circular dichroism spectroscopy when it converts from the apo- to the

holoform (51).
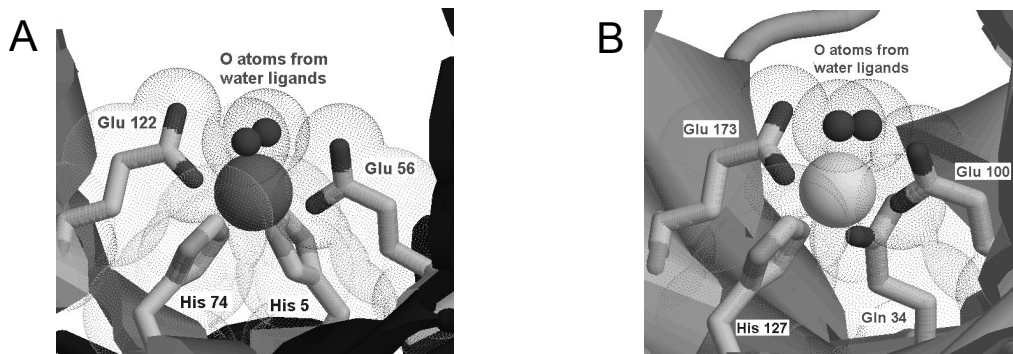
Figure 1.7: Active sites of A) *E. coli* **GlxI (PDB ID: 1F9Z) and B) Human GlxI (PDB ID: 1QIN).** The large spheres ligated with hexacoordinate geometry depict bound Ni^{2+} and Zn^{2+} ions in each enzyme respectively. The coordination environment shown is found in active GlxI holoforms.
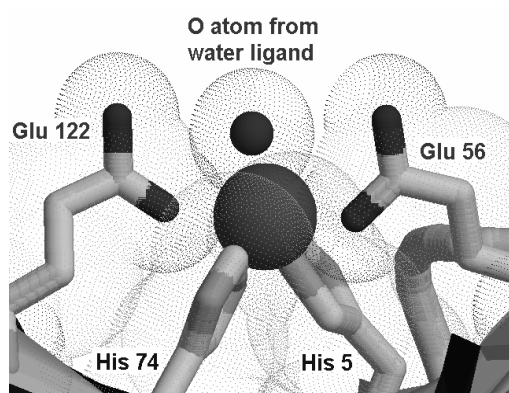
Figure 1.8: Active site of the Zn^{2+}-bound *E. coli* **GlxI (PDB ID: 1FA5).** Pentacoordinate geometry is apparent for the Zn^{2+} ion (large dark sphere) due to the loss of a water ligand

Besides coordination of the activating metal, the amino acid ligands have been implicated as catalytic bases in the function of GlxI enzymes. The glutamatic acid residues of the active site have been probed in human and *P. falciparum* GlxI by site-directed mutagenesis for their involvement in MG-GSH hemithioacetal isomerization (8, 63). Inspection of the active site for human and *E. coli* GlxI indicates that no residues other than the metal-coordinating glutamic acid residues are present as candidate catalytic bases for proton transfer (Figure 1.9) (52, 53).
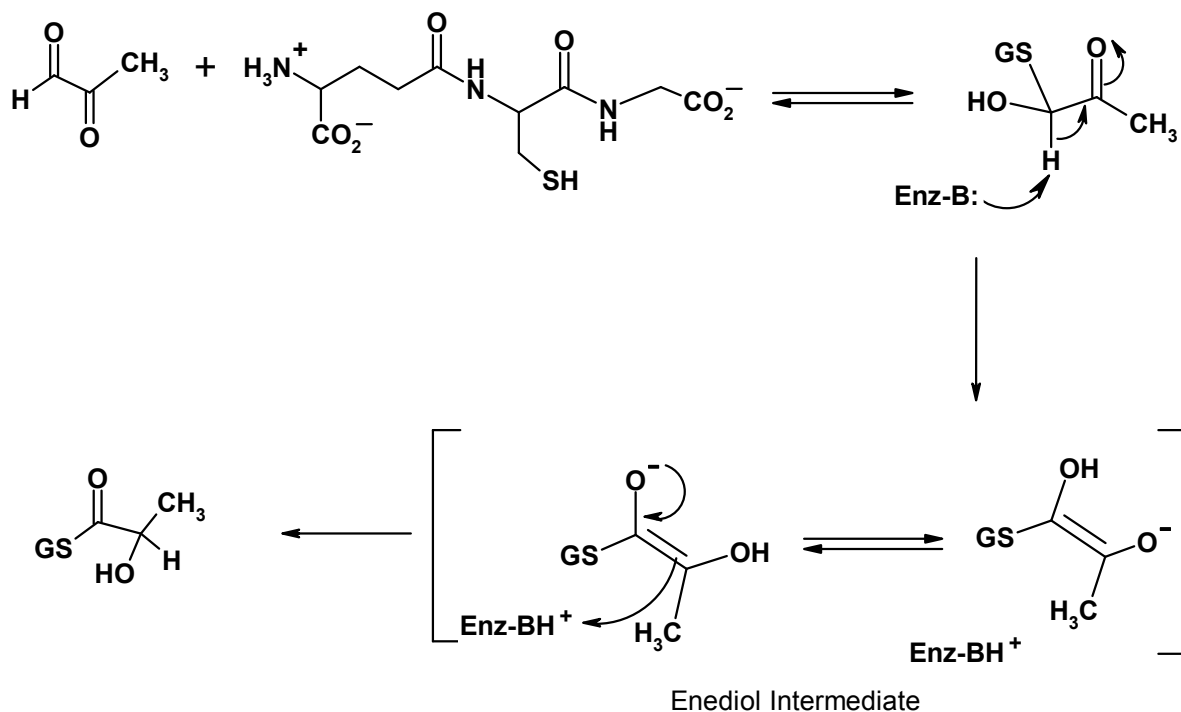
Figure 1.9: Proposed mechanism for GlxI-catalyzed isomerization

In human GlxI, Glu172 seems like a more plausible candidate for participation in catalysis because of the 3.3Å distance from the catalytic Zn^{2+} and its optimal position to re-protonate the bound

17

S-(*N*-hydroxy-*N*-*p*-iodophenylcarbamoyl)glutathione (HIPC-GSH) (transition state analogue) observed in the crystal structure (Figure 1.10) (64). Ridderstrom *et al.* have conducted a mutagenesis study on human GlxI comparing the activities of various active site Glu →Gln variants. The Glu99Gln mutant exhibits only 0.1% of the activity observed for the wild type GlxI (63). In contrast, the Glu172Gln variant exhibits less than 10^{-5} the activity of the wild type enzyme (63). The investigators concluded that Glu172 was relevant to the GlxI mechanism in part because of its proximity and positioning to substrate analogues in the active site. Glu172 also appeared catalytically relevant because of the large difference in activity loss when it was substituted for Gln versus modification of Glu99.

1.5.3 Evidence for Glutamate as a Catalytic Base

The co-crystallization of human GlxI and the transition state analogue HIPC-GSH (a mimic of the enediol intermediate) HIPC-GSH provides some evidence in favor of a Glu residue as a general base (Figure 1.10) (64). In this structure, direct coordination of the inhibitor coordinated directly to the active site metal, and the ligand Glu172 is 3.3 Å away from the Zn^{2+} ion. The 3.3 Å distance is too great for direct metal coordination with the Glu172 residue. Cameron *et al.* proposed an inner sphere catalytic mechanism based on these findings. In this mechanism, the incoming substrate would displace the ligating water molecules in addition to the catalytic glutamate residue (64). This change in coordination environment changes the Glu172 pKa so it can function as a proton abstractor (64). X-ray absorption fine structure (EXAFS) analysis of the *E. coli* GlxI in complex with a hydroxamate peptide inhibitor exhibits a similar change in coordination environment (65). The EXAFS data indicates that the inhibitor interacts directly with the active site metal, displacing the water molecule and Glu122 ligands (65). Although this mode of coordination is similar to the active site of the HIPC-bound human GlxI, an important caveat is that hydroxamate-based structures are inherently

prone to metal chelation. Therefore the *E. coli* GlxI-inhibitor complex must be interpreted with caution as the displacement of ligands observed may simply reflect the chelating capacity of the inhibitor.
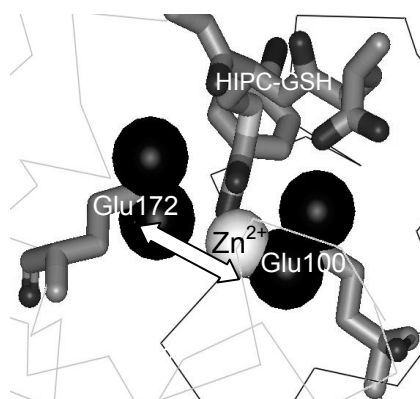
Figure 1.10: Active site of HIPC-GSH- bound human GlxI (PDB ID: 1QIN). The inhibitor, Zn^{2+} ion, and glutamic acid ligands are labeled in the above figure. The carboxylate oxygen atoms of the glutamic acid residues are depicted as dense black spheres. The increased distance between Glu172 and Zn^{2+} due to inhibitor binding is highlighted with the double-headed arrow.

1.5.4 Two Classes of Metal Activation for GlxI Enzymes

The metal activation class of a GlxI sequence can be inferred by amino acid sequence comparisons (Figure 1.11) (3, 66). The homodimeric Ni^{2+}/Co^{2+}-activated GlxI enzymes tend to have shorter amino acid sequences for the monomeric subunit with molecular masses under 20 kDa. The metal ligands tend to be the conserved two histidine and two glutamate residues, where the first histidine ligand in the sequence is not preceded by a long (>20 amino acids) N-terminus (Figure 1.11) (3, 66). In contrast, the homodimeric Zn^{2+}-activated GlxI enzymes tend to have the N-terminal arm preceding the first histidine or glutamine ligand. In the case of the human GlxI enzyme, the 29 amino acid long N-terminal engages in contacts with the opposing monomer in the native protein (Figure 1.4 and Figure 1.11). The N-terminal arm does not seem to be essential for dimerization, since the shorter

19

Ni^{2+}/Co^{2+}-activated GlxI enzymes are homodimers in apo- and holo- form (3, 51, 52). Sequence alignment of Zn^{2+}-dependent GlxI enzymes against Ni^{2+}/Co^{2+}-activated GlxI enzymes also reveals several short regions of amino acid sequence in the former proteins that are absent in shorter forms of this enzyme (Figure 1.11) (3, 66). These regions assume loop conformations in the human GlxI enzyme based on the published crystal structure (53). Thus it would appear that a longer module of βαββ motifs with greater intersubunit contacts evolved to facilitate the GlxI enzyme activation with Zn^{2+} ions. How the presence of an extended amino acid sequence promotes Zn^{2+}-binding and selectivity in contrast to GlxI enzymes like that of *E. coli* remains undefined in the inorganic biochemical literature.
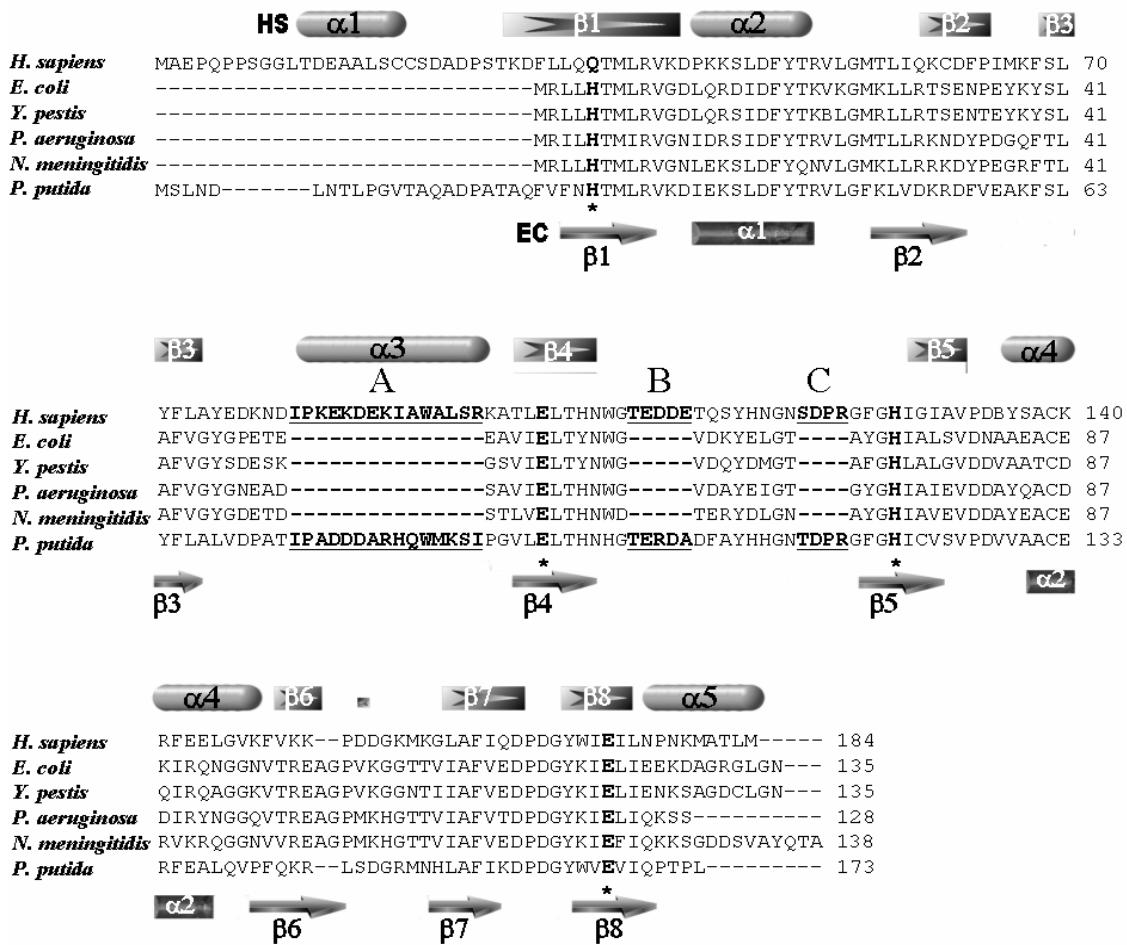
Figure 1.11: Sequence alignment comparing long and short dimeric GlxI enzymes. The longer Zn^{2+}-activated GlxI sequences are from *H. sapiens* and *P. putida* (National Centre for Biotechnology Information (NCBI) accession numbers are NP_006699 and NP_745896 respectively). The shorter Ni^{2+}/Co^{2+}-activated GlxI sequences are from *E. coli*, *Y. pestis*, *P. aeruginosa* (GloA1 homologue) and *N. meningitidis* (NCBI accession numbers are U57363, CAL21009, NP_252214 and NP_284840 respectively). The α-helix and β-strand structures in the GlxI enzymes are based on the human (HS) and *E. coli* (EC) sequences. The letters A, B and C represent sequences present in longer GlxI enzymes that are absent in the shorter non-Zn^{2+}-activated class of enzymes. The active site ligands are bolded and highlighted with asterisks in the above figure.

21

The Ni^{2+}/Co^{2+} activation profile for GlxI is not limited to enzymes of bacterial origin. Recently, GlxI enzymes have been isolated from the protozoan parasites *Leishmania major, L. donovani* and *Trypanosoma cruzi* that are very similar to the *E. coli* enzyme (67, 68, 69). The monomers of *L. major* and *T. cruzi* are 18.5 kDa and 16.6 kDa respectively (67, 69). As observed with other GlxI enzymes these proteins are active as homodimers. Sequence alignment indicates that these parasitic GlxI enzymes are comparable in length to the bacterial non-Zn^{2+}-activated GlxI enzymes (Figure 1.12). The metal activation profile for *L. major* GlxI closely mirrors that of *E. coli* GlxI, where the level of Ni^{2+}-activation of apoenzyme exceeds Co^{2+}-activation by approximately 74% (67). Another similar feature between *L. major* and *E. coli* GlxI is that they are not Zn^{2+}-activated (67). In contrast, *T. cruzi* GlxI exhibits a less stringent metal activation profile, such that Co^{2+} reconstitution is almost as effective for restoring maximal activity as Ni^{2+}. Furthermore, *T. cruzi* GlxI also exhibits low-level enzyme activation in the presence of Zn^{2+} (69).

```
E. coli       ----------------------------MRLLHTMLRVGDLQRSIDFYTKVLGMKLLR  30
T. cruzi      -------------------------MSTRRLMHTMIRVGDLDRSIKFYTEALGMRLLR  33
H. sapiens    MAEPQPPSGGLTDEAAL-SCCSDADPSTKDFLLQQTMLRVKDPKKSLDFYTRVLGMTLIQ  59
P. putida     MS--------LHDLQTLPGVTAQPDAATAQFVFNHTMLRVKDIEKSLDFYTRVLGFRLVD  51
L. major      -------------------------MPSRRMLHTMIRVGDLDRSIKFYTERLGMKVLR   33


E. coli       TSENPEYKYSLAFVGYGPETE--------------EAVIELTYNWGVDK-----YELGT  70
T. cruzi      KWDCPEDKFTLVFLGYGTESE--------------TAVLELTYNYGQSE-----YKHGD  73
H. sapiens    KCDFPIMKFSLYFLAYEDKNDIPKEKDEKIAWALSRKATLELTHNWGTEDDETQSYHNGN  119
P. putida     KRDFPEAAFSLYFLALVDPAQIPADDTARHQWMKSIPGVLELTHNHGTENDADFAYHNGN  111
L. major      KWDVPEDKYTLVFLGYGPEMS--------------STVLELTYNYGVTS-----YKHDE  76


E. coli       A----YGHIALSVDNAAEACEKIRQNGGNVTREAGPVKGGTTVIAFVEDPDGYKIELIEE  126
T. cruzi      A----YGHIAIGVEDVNEEIARLKKMNVPIDYES-----EDGFMAFIVDPDGYYIELLNT  124
H. sapiens    SDPRGFGHIGIAVPDVYSACKRFEELGVKFVKKP--DDGKMKGLAFIQDPDGYWIEILNP  176
P. putida     TDPRGFGHICISVPDVRAACARFEELEVPFQKRL--QDGRMNHLAFVKDPDGYWVEVIQP  168
L. major      A----YGHIAIGVEDVKELVADMRKHDVPIDYED-----ESGFMAFVVDPDGYYIELLNE  127


E. coli       KDAGRGLGN----------- 135
T. cruzi      ERM---LEKSREQMNEQGTA 141
H. sapiens    NKMATLM------------- 184
P. putida     TELEG-------------- 173
L. major      KTM---MEKAEADMKEQGTA 144
```

Figure 1.12: Sequence alignment comparing the GlxI enzymes from *E. coli*, *T. cruzi*, *H. sapiens*, *P. putida* and *L. major* (NCBI accession numbers are U57363, XM_813363, NP_006699, NP_745896 and AY604654 respectively) . The GlxI sequences from *E. coli*, *T. cruzi* and *L. major* are Ni^{2+}/Co^{2+}-activated and are similar in length. The *H. sapiens* and *P. putida* GlxI sequences are included in this alignment to highlight that the parasitic enzymes resemble the *E. coli* GlxI in length. The active site residues are shown with grey highlighting in the sequences

1.5.5 Non-GSH-Dependent GlxI Enzymes

The relatedness of Ni^{2+}/Co^{2+}-activated bacterial GlxI enzymes to Leishmanial and Trypanosomal GlxI enzymes is remarkable because the thiol co-substrate used for detoxification differs significantly. Unlike *E. coli*, leishmanial and trypanosomal parasites depend on trypanothione (TSH) as a major intracellular thiol for redox and detoxification processes (Figure 1.13) (70). The k_{cat}/K_m value for *L. major* GlxI utilization of MG-TSH hemithioacetal is 200 times greater than that observed with the MG-GSH hemithioacetal (67). Correspondingly, *L. major* GlxI k_{cat}/K_m values for phenylglyoxal(PG)-TSH are 147 times greater than for turnover of PG-GSH (67). *L. major* GlxI can also efficiently

isomerize hemithioacetals of N_1-glutathionylspermidine and MG (67). However the most significant

aspect of *L. major* GlxI substrate specificity is the selectivity for TSH over GSH.
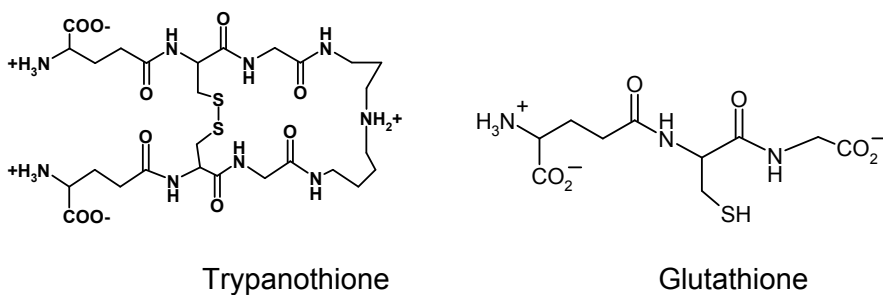
Figure 1.13: Structures of trypanothione and glutathione co-substrates

Kinetic characterization of *T. cruzi* GlxI indicates that it isomerizes MG hemithioacetals of

TSH and glutathionylspermidine 2400 and 14000 times more efficiently respectively, when compared

to MG-GSH hemithioacetal (69). In this case *T. cruzi* GlxI appears more selective for

glutathionylspermidine as a co-substrate, yet promastigotes of this organism tend to have higher

intracellular concentrations of TSH relative to the spermidine thiol (69)l. *T. cruzi* likely uses both co-

substrates for MG detoxification *in vivo*.

The crystal structure of *L. major* GlxI indicates that the active homodimer contains conserved

βαββ topology with an identically positioned active site as observed in *E. coli* and human GlxI

enzymes (Figure 1.14) (71). The dimer is more similar to the *E. coli* enzyme structurally with a root

mean squared deviation value for C-alpha of 0.9 Å versus 1.2 Å when compared to the human

enzyme (71).
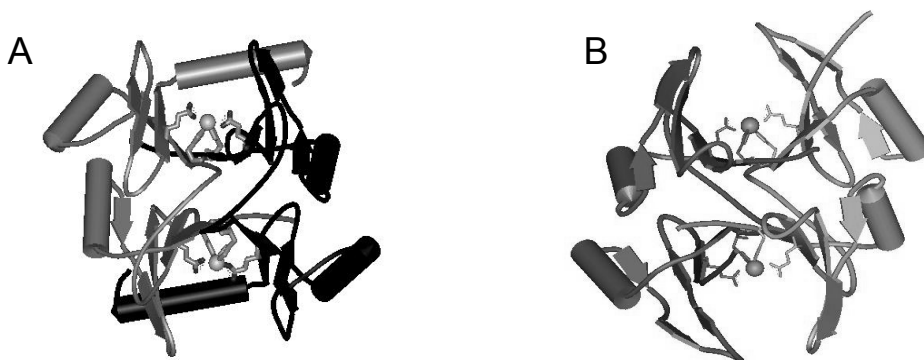
Figure 1.14: Crystal structures of A) *L. major* **GlxI (PDB ID: 2C21) and B)** *E. coli* **GlxI (PDB ID: 1F9Z).** Although the structure shown for *L. major* GlxI has electron density for two bound metal ions, only one active site was reported to contain electron density for bound Ni^{2+} in the crystallographic data set.

1.5.6 Half-of-the-Sites Metal Activation in Non-Zn^{2+}-Activated GlxI Enzymes

The metal coordination environment in *L. major* GlxI is highly similar to *E. coli* and human GlxI, so that the bound Ni^{2+} ion in the structure is ligated to two histidine residues, two glutamate residues and two water molecules (71). However, the *L. major* GlxI structure has only one metal ion bound per dimer, whereas the *E. coli* GlxI structure shows both active sites occupied for the holoforms containing Ni^{2+}, Co^{2+}, Cd^{2+} and Zn^{2+}(71). The presence of only one metal per dimer in the *L. major* holoenzyme structure is in agreement with estimates of the metal: enzyme stoichiometry from atomic absorption spectroscopy (71). The structure of *L. major* GlxI exhibiting half-of-the-sites metal binding converges with biochemical data indicating that active *E. coli* GlxI requires one metal ion per dimer (51, 71).

1.6 GlxII: Review of Biochemical and Structural Properties

Racker recognized GlxII as an enzyme involved in MG metabolism during the 1950's (11). The first extensively purified and characterized GlxII enzyme was derived from human liver (72). At the time,

the metal ion requirement of the hydrolase was suspected since metal-catalyzed thioester hydrolysis

had been observed in aqueous model systems not involving enzymes (73). Uotila noted that storage

of human liver GlxII in EDTA-containing buffer slowly deactivated the preparation (72). Attempts at

reconstitution of the EDTA-treated GlxII by adding metal ions (Mg^{2+}, Mn^{2+}, Co^{2+}, Ni^{2+}, Zn^{2+}, Ca^{2+},

Cu^{2+}) were ineffective, and could not provide unambiguous evidence for GlxII functioning as a

metalloenzyme (72).

Ridderstrom *et al.* characterized recombinant human GlxII but made no mention of a metal

ion requirement or the evaluation of metal-dependency as part of their report (74).   Ridderstrom and

Mannervik also isolated and characterized a GlxII enzyme from *Arabidopsis thaliana*, and concluded

from their studies that there was no metal ion requirement for the enzyme (75). The metal ion

requirement was discounted because they failed to observe any augmentation of activity in the

purified recombinant enzyme (expressed in *E. coli*) with the addition of Zn^{2+} or Mg^{2+} to the growth

medium (75). However in the same year, Crowder *et al.* published a characterization of a

recombinantly expressed cytosolic GlxII from *A. thaliana* (76). They reported a metal ion

requirement for the enzyme in this publication. Crowder *et al.* were able to determine from

inductively coupled plasma atomic emission spectroscopy that their purified recombinant GlxII

possessed two equivalents of Zn^{2+} per monomer (76). Additionally they performed a sequence

alignment comparing glyoxalase II enzymes from human and *A. thaliana*, to metallo-β-lactamase

sequences from several bacterial sources. They noted that the metal ligands in these proteins were all

well conserved (76).

A highly conserved T-H-X-H-X-D-H motif associated with metal binding is common to both

the GlxII enzymes and the metallo-β-lactamases (Figure 1.15) (77). Two additional histidine residues

can be found in GlxII that contribute to metal binding (Figure 1.15) (77). These residues are

conserved amongst all GlxII enzymes but external to the aforementioned binding motif. Based on

these findings it was postulated that all GlxII enzymes would likely have bound metal ions as part of

their structure.

```
H. sapiens       ------------------------------------------------------------
A. thaliana cyt  ------------------------------------------------------------
A. thaliana mit  MPVISKASSTTTNSSIPSCSRIGGQLCVWPGLRQLCLRKSLLYGVMWLLSMPLKTLRGAR
Sm MBL L1        ------------------------------------------------AEVPLPQLRA--
Pa MBL VIM-2     MFKLLSKLLVYLTASIMA---IASPLA-------FSVDSSGEYPTV--SEIPVGEVRL—-


H. sapiens       ----------------MKVEVLP----ALTDNYMYLVIDDETKEAAIVD--PVQPQKVV
A. thaliana cyt  ----------------MKIFHVP----CLQDNYSYLIIDESTGDAAVVD--PVDPEKVI
A. thaliana mit  KTLKITHFCSISNMPSSLKIELVP----CSKDNYAYLLHDEDTGTVGVVD--PSEAAPVI
Sm MBL L1        YTVDASWLQPMAPLQ--IADHTWQ----IGTEDLTALLVQTPDGAVLLDGGMPQMASHLL
Pa MBL VIM-2     YQIADGVWSHIATQS--FDGAVYPSNGLIVRDGDELLLIDTAWGA-------KNTAALLA


H. sapiens       DAARKHGV---KLTTVLTTHHHWDHAGGNEKLVKLESGLKV------------------
A. thaliana cyt  ASAEKHQA---KIKFVLTTHHHWDHAGGNEKIKQLVPDIKV------------------
A. thaliana mit  EALSRKNW---NLTYILNTHHHDDHIGGNAELKE-RYGAKV------------------
Sm MBL L1        DNMKARGVTPRDLRLILLSHAHADHAGPVAELKR-RTGAKVAANAESAVLLARGGSDDLH
Pa MBL VIM-2     EIEKQIGL---PVTRAVSTHFHDDRVGGVDVLR--AAGVAT------------------


H. sapiens       YGGD-D--RIGALTHKITHLSTLQVG-SLNVKCLATPCHTS--GHICYFVSKPGGSEPPA
A. thaliana cyt  YGGSLD--KVKGCTDAVDNGDKLTLGQDINILALHTPCHTK--GHISYYVNGKEG-ENPA
A. thaliana mit  IGSAVDKHRIPGIDILLKDSDKWMFA-GHEVRILDTPGHTQ--GHISFYFPGSAT-----
Sm MBL L1        FGDGIT-YPPANADRIVMDGEVITVG-GIVFTAHFMAGHTP--GSTAWTWTDTRNGKPVR
Pa MBL VIM-2     YASP--------STRRLAEVEGNEIP-THSLEGLSSSGDAVRFGPVELFYPGAAH-----


H. sapiens       VFTGDTLFVAGCGKFYEGTADEMCKALLEVLGRLPPDTRVYCGHEYTINNLKFARHVEPG
A. thaliana cyt  VFTGDTLFVAGCGKFFEGTAEQMYQSLCVTLAALPKPTQVYCGHEYTVKNLEFALTVEPN
A. thaliana mit  IFTGDLIYSLSCGTLSEGTPEQMLSSLQKIVS-LPDDTNIYCGRENTAGNLKFALSVEPK
Sm MBL L1        IAYADSLSAPGYQ--LQGNPR-----------YPHLIEDYRRSFATVRALPCDVLLTPH
Pa MBL VIM-2     STDNLVVYVPSASVLYGGCA-------------IYELSRTSAGNVADADLAEWPTSIE—


H. sapiens       NAAIREKLAWAKEKYSIGEPTVPSTLAEEFTYNPFMRVREKTVQQHAGETDPV---TTMR
A. thaliana cyt  NGKIQQKLAWARQQRQADLPTIPSTLEEELETNPFMRVDKPEIQEKLGCKSPI---DTMR
A. thaliana mit  NETLQSYATRVAHLRSQGLPSIPTTVKVEKACNPFLRISSKDIRKSLSIPDSATEAEALR
Sm MBL L1        PGA--SNWDYAAGARAG---------AKALTCKAYADAAEQKFDGQLAKETAGAR-----
Pa MBL VIM-2     ----RIQQHYPEAQFVIPGHGLPGGLD-------LLKHTTNVVKAHTNRSVVE-------


H. sapiens       AVRREKDQFKMPRD
A. thaliana cyt  EVRNKKDQWRG---
A. thaliana mit  RIQRARDRF-----
Sm MBL L1        --------------
Pa MBL VIM-2     --------------
```

Figure 1.15: Amino acid sequence comparison of *H. sapiens* GlxII, *A. thaliana* cytosolic GlxII, *A. thaliana* mitochondrial GlxII, *S. maltophilia* metallo-β-lactamase L1, and *P. aeruginosa* metallo-β-lactamase VIM-2 (NCBI accession numbers are Q16775, NP_187696, NP_565999, BAF47409 and ABR10840 respectively). The conserved T-H-X-H-X-D-H motif region is highlighted in grey. Additional active site His residues in the GlxII enzymes are highlighted in black.

28

The crystal structure for human GlxII was reported in 1999 by Cameron *et al.* and was resolved to 1.9 Å (78). The monomeric protein is approximately 29 kDa in size and composed of two structurally distinct domains (Figure 1.16). The N-terminal domain consists of a four-layered β sandwich, the first half of which possesses ββαβαββ topology and the second half assumes ββββαβ topology (Figure 1.16) (78). The two halves of the sandwich are rotated relative to each other and the overall layering in the domain is such that two mixed β-sheets are flanked by α-helices (78). The C-terminal α-helical domain is connected to the N-terminal β-sandwich domain via a β-hairpin region and it consists of five α-helices (Figure 1.16) (78). There is significant similarity between the topology of the N-terminal GlxII domain and that of the zinc-metallo-β-lactamases. In fact GlxII and metallo-β-lactamase are members of the zinc-metallohydrolase family of proteins (78).
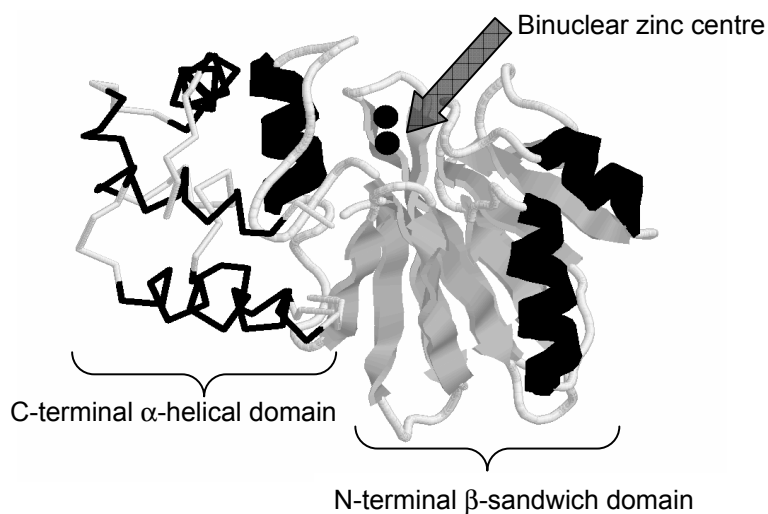
Figure 1.16: Crystal structure of human GlxII (PDB ID: 1QH5)

1.6.1 GlxII has a Binuclear Active Site

The electron density within the human GlxII crystal structure clearly indicates the presence of a binuclear metal centre at the active site of the protein (78). The enzyme was considered to be a Zn-

metalloenzyme even though metal analysis of the prepared protein indicated only 1.5 equivalents of the metal per monomer (78). Metal exchange during purification was assumed to be the reason for the less than binuclear stoichiometry observed by metal analysis. The positions of the metal binding sites in human GlxII are very similar to those found in metallo-β-lactamase enzymes. The coordination environment for the two Zn^{2+} ions in the human GlxII resemble the environment found in the binuclear centre or the metallo-β-lactamase L1 from *Stenotrophomonas maltophilia* (78). The catalytic metal ions are located along the edge of the β-sandwich when comparing the structures of both metalloenzymes (Figure 1.16) (78). The distance separating both metal ions is approximately 3.3-3.5 Å (78). Seven amino acid residues and a single water molecule ligate to the zinc ions according to the crystal structure (Figure 1.17) (78). There are bridging ligands between the metal ions consisting of the water molecule and Asp 134, via oxygen atoms (Figure 1.17). The ligands coordinating zinc atom 1 include His54, His56 and His110 (Figure 1.17) (78). The amino acids ligating to zinc atom 2 are Asp58, His59 and His173 (Figure 1.17) (78). The crystal structure of human GlxII with GSH bound to the active site contains an additional water molecule positioned such that the aqua and sulfur ligands (from GSH) gives each zinc ion octahedral or square pyramidal geometry in the protein (78).
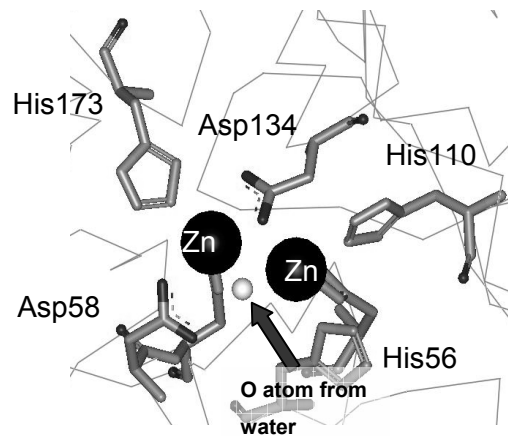
Figure 1.17: Active site of human GlxII (PDB ID: 1QH5). The arrow points to the oxygen atom from a bridging water ligand.

Although GlxII is a member of a zinc metalloprotein family, there is evidence that the enzyme can bind other activating metals in the active site. The *A. thaliana* GlxII enzymes have been the focus of most structural and metal activation studies. They have also been of interest in plant physiology owing to the presence of organelle specific isoforms. There are three mitochondrial forms of *A. thaliana* GlxII designated GLX2-1, 2-4 and 2-5 (2). The cytoplasmic isoform is designated GLX2-2. The isoform designated GLX2-3 deviates from the typical GlxII protein sequence especially for residues in substrate binding positions, and may not actually be a GlxII enzyme by function (2). Zang *et al.* conducted a series of experiments on GLX2-2 probing the effect of ligand substitutions on metal content of the enzyme (79). The metal ligand variants of the enzyme were created by site-directed mutagenesis and the purified enzyme was subjected to metal analysis by inductively coupled plasma atomic emission spectroscopy (79). Their findings revealed that GLXI2-2 tends to be expressed as a holoenzyme with a zinc:iron ratio of 1:2. From the mutagenesis study they concluded

that the first metal site in this GlxII enzyme has a preference for binding iron where the second

activating metal site was selective for zinc over iron (79).

1.6.2 Heterogeneous Metallation in GlxII

Schilling *et al.* performed a more biophysical investigation of metal binding in GLX2-2 by examining

the binuclear active site using EXAFS and electron paramagnetic resonance (EPR) techniques (80).

Their results were most interesting because the metal analysis they performed indicates

heterogeneous holoforms of recombinant GLX2-2 are produced in complex growth media (80). The

metal content of the purified enzyme from these conditions contained 0.8 ± 0.2 iron, 0.4 ± 0.2 zinc,

and 0.30 ± 0.05 manganese per protein (80). They also found that supplementation of the growth

medium with iron-, zinc- or managese- containing salts yields GLX2-2 with proportional amounts of

the exogenously supplied metal ion (80). The kinetic parameters of these holoforms are comparable

demonstrating that the GlxII enzyme structure is not stringently selective for activating metal ions.

The EXAFS analysis shows that metal-ligand distance varies depending on the metal ions bound at

the binuclear centre, demonstrating a flexibility of the coordination environment supplied by the

enzyme and associated water molecules (80). The EPR results reported by Schilling *et al.* indicate a

variety of binuclear configurations that can be found in GLX2-2 which include Fe(III)Fe(II),

Fe(III)Zn(II), and Mn(II)Mn(II) centres. The result of this investigation does not indicate biased

metal selectivity for each site in the binuclear centre as declared in the report by Zang *et al.* Again

these findings emphasize the flexible nature of metal binding in the GlxII scaffold, in contrast to the

hierarchical metal activation exhibited by GlxI enzymes, particularly the non-Zn^{2+} activated types.

Crowder's research group extended their study of metal loading in GLX2-2 to the analysis of recombinant enzyme produced by bacteria cultivated in minimal medium (81). Their objective was to clarify the influence of exogenous metal addition on the types of holoenzymes recovered from purification. The previous use of rich medium tended towards the production of recombinant GLX2-2 with mixtures of Zn, Fe and Mn in the active site (81). The metal stoichiometry of GLX2-2 produced in minimal medium was approximately one metal ion per monomer, with the bulk of the metal being Zn or Fe if salts of these respective metals were added to the growth medium (81). An interesting finding is that the substoichiometrically loaded GlxII from minimal growth conditions contains a mixture of dinuclear enzyme, and apoenzyme (81). This data demonstrates that the GlxII enzyme has a propensity for binding metals at both sites of the catalytic centre. In contrast the related metallo-β-lactamases have been isolated as both mono- and dimetallated forms from various soil bacteria (82).

Marasinghe *et al.* published the first detailed characterization of a mitochondrial GlxII enzyme from *A. thaliana* in 2005. This GlxII enzyme, designated GLX2-5 is isolated following expression of the recombinant protein in *E. coli* as a binuclear FeZn enzyme. Unlike GLX2-2, stoichiometrically significant quantities of Mn are not found associated with the enzyme (2). The EPR analysis of GLX2-5 indicates that the majority of the binuclear holoenzyme was Fe(III)Zn(II) occupied although there are some anti-ferromagnetically coupled Fe(II)Fe(II) metal centres detectable by this method (2).

The 1.74 Å resolution crystal structure of GLX2-5 confirmed the suspected difference in metal coordination environments at the active site, given the presence of an Fe(III)Zn(II) centre as opposed to the Zn(II) Zn(II) centre observed in human GlxII. Between these two enzymes 37% sequence identity is shared and there is conservation of all of the amino acids ligands (2). Instead of the five- and six- coordinate metal centres found in the human enzyme, GLX2-5 has tetrahedrally and

33

trigonal bipyramidal metal centres (2). Metal site 1 has four ligands supplied by His54, His56, His12 and a bridging water ligand (Figure 1.18)(2). Metal site 2 uses Asp58, His59, Asp131, His169 and a bridging water ligand to provide a pentacoordinate inner sphere at this location (Figure 1.19) (2).
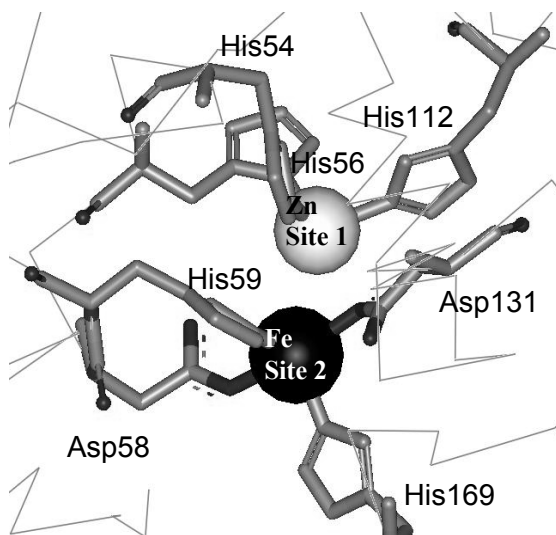
Figure 1.18: Active site of GLX2-5 (PDB ID: 1XM8). The bridging water ligands are not shown in this figure.

1.6.3 Outer Sphere Metal Ligation in GlxII

In contrast to structural studies of GlxI, the second-sphere or extended bonding network associated with the metal sites in GlxII have been characterized as part of the structure determination studies. The extended hydrogen-bonding network around the binuclear metal centre in GlxII is also a well-documented architectural feature observed in metallo-β-lactamase enzymes. The ligands associated with the second metal site in particular are observed in connection with outer sphere ligands (2). The second sphere hydrogen bonding interactions for human (GLX2-2) and GLX2-5 are summarized below (Table 1.1). Two interactions in the human enzyme are absent in GLX2-5, and it

may be this difference in extended coordination environment that confers the observed divergence in

metal selectivity between these two hydrolases (2).

Table 1.1: Ligands in Human GlxII and GLX 2-5 (2)

Human GlxII First Sphere Ligands	GLX2-5 First Sphere Ligands	Human GlxII Second Sphere Ligands	GLX2-5 Second Sphere Ligands
His54 (Site 1)	His54 (Site 1)	Lys143 → His54	Thr53 → His54 Lys140 → His54
His56 (Site 1)	His56 (Site 1)	Glu146 → H_2O → His56	No equiv ligand
His110 (Site 1)	His112 (Site 1)	No equiv ligand	Lys140 carbonyl
No equiv ligand (Site 1)	Bridging water (Site 1)		
Asp134 (Site 1)	No equiv ligand (Site 2)	Asp134 carbonyl	No equiv ligand
Asp58 (Site 2)	Asp58 (Site 2)		
His59 (Site 2)	His59 (Site 2)	No equiv ligand	Thr53 → Asp29 → His59
Asp134 (Site 2)	Asp131 (Site 2)		
His173 (Site 2)	His169 (Site 2)	No equiv ligand	Lys10 →Asp11→His169 Also Asp11 → H_2O
No equiv ligand (Site 2)	Bridging water ligand Site 2)		

36

1.6.4 Substrate Specificity of GlxII and Active Site Residues

GlxII enzymes can accept a wide variety of substituted thioester substrates including *S*-D-mandeloylglutathione, *S*-D-acetylglutathione, *S*-D-acetoacetylglutathione, *S*-D-formylglutathione, *S*-D-glycolylglutathione, and *S*-D-lactoylglutathione (72). Despite the broad substrate selectivity, the preferred target of hydrolysis is *S*-D-lactoylglutathione (72). Early efforts at identifying active site residues prior to the availability of GlxII crystal structures were largely conducted by using side chain modification reagents and inhibitors. The presence of an active site amine moiety was inferred from the observed inactivation of human liver GlxII by 2,4,6-trinitrobenzenesulphonate (72, 83). The inactivation is a pH dependent effect with a pK of 8.95 (83). The modification could be abated in the presence of the competitive inhibitor *N*-acetyl-*S*-(*p*-bromobenzyl)glutathione, leading to the conclusion that an active site amine was being modified by the sulphonate (83).

An arginine residue may be involved in GlxII-catalyzed hydrolysis due the observation of phenylglyoxal-induced inactivation at pH 8 (83). The histidine specific chemical modification agent diethylpyrocarbonate also inactivates GlxII (rat erythrocyte) at pH 6, providing indirect evidence for involvement of this residue in the catalytic cycle of the enzyme (83).

1.7 Rationale for Continued Characterization of GlxI Enzymes

Structure-function studies of GlxI enzymes have focused upon resolving the basis for metal activation

differences in spite of a highly conserved protein structure (52, 53, 57, 71). This aspect of GlxI

metalloenzyme chemistry has a substantial foundation in the seminal discovery of non-Zn^{2+} activation

in *E. coli* GlxI (51).

The discovery of non-Zn^{2+}-activated, Ni^{2+}/Co^{2+}-activated bacterial (*E. coli*, *P. aeruginosa*, *N.

meningitidis*, *Y. pestis*) and parasitic (*L. major*, *T. cruzi*) GlxI enzymes represents a recent addition to

the catalog of known Ni^{2+}-metalloenzymes. The biochemistry of nickel in proteins is a relatively

recent area of metalloenzyme research compared to the wealth of information collected on zinc

metalloproteins (84, 85). There are many unanswered questions about the structural nature of

divergent metal activation in a conserved protein scaffold exemplified by GlxI.

Attempts at metal ligand replacement and loop insertion mutagenesis were pursued with *E.

coli* GlxI previously. The intent of these studies was to create a "humanized" chimeric GlxI enzyme

exhibiting robust activation in by Zn^{2+}. These experiments are documented in the doctoral and

master's dissertations of Dr. Susan Clugston and Nicole Sukdeo respectively. Briefly, the ligand

replacement (His5 to Gln5) results in only a weak but detectable shift towards Zn^{2+}-activation.

Singular insertions of loop regions unique to human GlxI do not shift the selectivity of *E. coli* GlxI

towards Zn^{2+}-activation (60).   The addition of multiple loops in an attempt to create a more

thoroughly "human-like" GlxI scaffold from the *E. coli* enzyme generates constructs that produce

modest quantities of the variants as insoluble inclusion bodies.

Therefore, it can be concluded that the additional secondary structure associated in

homodimeric Zn^{2+}-activated GlxI enzymes is very specific to this metal activation subclass. Therefore

the Ni^{2+}/Co^{2+}-activated enzymes are not optimal scaffolds for subtle modification towards Zn^{2+}-

activation. However a rational and detailed structural basis for divergent metal activation in GlxI remains undefined and hopefully can be resolved with further research.

The difference in metal selectivity for GlxI enzymes may affect other properties of the enzyme, such as the metal stoichiometry in active enzyme, the process for metal insertion into the active site and enzyme-substrate interactions. This investigation addresses some of these topics and are described in the next section.

1.8 Synopsis of Project

Several aspects of biochemical research have been addressed in the scope of the doctoral dissertation presented herein. Since the *E. coli* GlxI enzyme has been characterized and well documented as a non-Zn^{2+}-dependent GlxI, it was of considerable interest to ascertain whether *E. coli* GlxII was also divergent in metal selectivity. Thus the isolation and characterization of *E. coli* GlxII has been carried out and the results are summarized in this document.

1.8.1 Characterization of GlxI Homologs from *Pseudomonas aeruginosa*

During the course of this project it became apparent that the genome of *Pseudomonas aeruginosa* strain PAO1 contained three GlxI-encoding homologs. The enzyme encoded by *gloA1* has been characterized previously and identified as a Ni^{2+}/Co^{2+}-activated GlxI enzyme. Interestingly the other two homologs in the *P. aeruginosa* genome appeared to encode one additional Ni^{2+}/Co^{2+}-activated GlxI enzyme as well as a Zn^{2+}-dependent enzyme. At the time, we were not aware of any other bacteria possessing multiple genes encoding GlxI, and subsequently characterized these sequences confirming that they encode functional forms of the lyase. Additionally the metal ion requirement inferred from sequence comparison was found to be correct from biochemical characterization.

39

1.8.2 Characterization of *E. coli* GlxII

The *gloB* gene from *E. coli* strain MG1655 was cloned and overexpressed in order to characterize the second component of the *E. coli* Glx system. We were particularly interested in determining whether the metal specificity of the hydrolase would be similar to those of *E. coli* GlxI, so that the entire Glx system in this organism is Ni^{2+}/Co^{2+}-activated. The results of this characterization indicate that *E. coli* GlxII is a Zn^{2+}-metalloenzyme with two Zn atoms occupying its binuclear active site.

1.8.3 Deuterium Isotope Effects on *E. coli* GlxI-Catalyzed Isomerization

In an attempt to address whether the mechanistic attributes of GlxI-catalyzed isomerization are retained in the non-Zn^{2+}-activated enzyme, the deuterium isotope effects exhibited by GlxI from *E. coli* have been examined using the substrates phenylglyoxal and α-deuteriophenylglyoxal. The deuterium isotope effects have been determined using Ni^{2+}- and Cd^{2+}-substituted GlxI. The present results indicate that the presence of an isotope effect depends to some extent upon the metal present at the active site.

A wealth of kinetic and mechanistic investigation has been conducted on Zn^{2+}-activated GlxI enzymes. The proton transfer mechanism proposed for GlxI was based upon solvent isotope incorporation experiments using the Zn^{2+}-dependent GlxI enzyme of *S. cerevisiae* (86, 87). Stereoselectivity of the GlxI enzymes has also been investigated by quantitating the relative rates of turnover of conformationally locked substrates using *S. cerevisiae* GlxI also (88). The results of this investigation revealed that GlxI exhibits no preference for either diastereomer of the MG-GSH hemithioacetal. Finally the kinetic isotope effects of yeast GlxI were determined using perdeuteriomethylglyoxal and α-deuteriomethylglyoxal as proposed by Vander Jagt and Han during the 1970's (86). These experiments indicate that the proton transfer step is partially rate determining for GlxI-catalyzed isomerization (86, 87). Considering that the GlxI enzymes can be sub-classified

on the basis of metal activation, the kinetic and mechanistic aspects of the Zn^{2+}-dependent GlxI-catalyzed reaction should be re-examined in the Ni^{2+}/Co^{2+}-activated system.

1.8.4 SlyD Metallochaperone and *E. coli* GlxI Ni^{2+}-Loading *in vivo*

The NiFe hydrogenase in *E. coli* is a well-studied example of a Ni^{2+}-dependent enzyme with a cognate set of metallochaperones that assist with co-factor insertion *in vivo* (89, 90). In an attempt to determine whether *E. coli* GlxI is subject to metallochaperone-mediated Ni^{2+}-insertion, a comparison of GlxI activity in *slyD*[+] versus Δ*slyD E. coli* strains was performed. The *slyD* gene product is a peptidylprolyl-cis-trans isomerase that participates in Ni^{2+} insertion into the NiFe hydrogenase protein (6, 91). Therefore it was of interest to determine whether the presence or absence of this metallochaperone would be of consequence to the magnitude of detectable GlxI activity in *E. coli* cell lysates.

The Zn^{2+}-dependent GlxI enzymes tend to be purified from various sources with Zn^{2+}-identified in the active site, but not all of them can be re-activated even partially with metal following EDTA de-metallation. For example *S. cerevisiae* GlxI cannot be reconstituted to exhibit any activity by addition of exogenous Zn^{2+} following metal removal with EDTA. These observations imply that the more extended structures of the Zn^{2+}-activated enzymes may reflect differences in the process for metallocentre assembly of these GlxI enzymes relative to the Ni^{2+}/Co^{2+}-activated forms.

1.8.5 Nuclear Magnetic Resonance (NMR) Studies of Metal Binding in *E. coli* GlxI

The half-of-the-sites metal activation and metal occupancy in *E. coli* GlxI is an interesting feature of this enzyme, given the homodimeric assembly as well as the availability of two identical active sites for metal recruitment . The one-metal per dimer sufficiency for catalytic activation has also been documented for the *L. major* GlxI and has been observed as an attribute of the holoenzyme crystal

structure for this parasitic enzyme. No structural changes are obvious in the *E. coli* apoenzyme versus the various holoforms as assessed by X-ray crystallography. To investigate the dynamics of metal binding in *E. coli*, and verify biophysically the enzyme's propensity for half-of-the-sites metallation, $^1H^{15}N$-heteronuclear single quantum correlation nuclear magnetic resonance (HSQC-NMR) was performed on ^{15}N-labelled enzyme during incremental titration with Ni^{2+}. Additional investigation of ligand binding effects on the backbone orientation of the *E. coli* GlxI was conducted by titration with an inhibitor. A metal titration on the less active ligand variant H74Q GlxI was performed for a comparison of metal-dependent structural reorganization with a weakly-binding active site.

Chapter 2   Glyoxalase I Homologs in *Pseudomonas aeruginosa*

2.1 Gene Transfer and *P. aeruginosa*

The *P. aeruginosa* genome has been analyzed extensively in an effort to understand how its composition of genes evolved. The complete genome sequence for *P. aeruginosa* strain PAO1 was reported in 2000 (92). In this publication Stover *et al*. reported that 10 regions of the genome, that were 3 kB or greater in size exhibited low G+C content (relative to the rest of the genome) and unusual codon usage (92). Regions of a genome that have a very different codon usage compared to the rest of the bacterial chromosome are typically suspected of originating from another species (93, 94, 95). The base composition and codon usage may be indicative of genomic regions acquired through horizontal gene transfer (92, 93). Horizontal or lateral gene transfer refers to gene transfer between different species; this includes mechanisms such as conjugation, transformation and transduction (96). This contrasts with the "vertical" gene transfer, which refers to inheritance of DNA from a parental/progenitor organism (96).

Genomic sequence data and protein sequence data have been used in most cases to postulate whether horizontal transfer has shaped the genome of an organism. Some indicators of horizontal transfer include the observation of highly similar homologs between two distantly related organisms (93). This evidence is most convincing when the homolog has the highest similarity to that of an organism in a distant taxon (93). This attribute is largely dependent on the cutoff values for similarity that are chosen when making these comparisons. Horizontal gene transfer may be suspected when a cluster orthologous genes in a given organism is highly similar to an organism from a distant taxon(93). Conservation of gene order for a set of orthologs between distant taxa may also be indicative of gene transfer that might have occurred via transfer by bacteriophage or animal viruses (93).

Analyzing the base composition of bacterial genomes has also been employed for inferring that a genomic region might have been laterally acquired. These regions include genomic islands, which are large chromosomal regions call ed genomic islands originating from horizontal transfers that are flanked by repeat sequences and situated nearby tRNA-encoding genes (97). Lateral gene transfer has been identified as a mechanism by which *P. aeruginosa* strains have acquired certain virulence determinants. Disseminating genetic material by these mechanisms may also contribute to the presence of multiple homologs of a given gene in an organism.

2.2 Gene Duplication

The presence of multiple homologs of a gene within a bacterium may indicate that gene transfer or gene duplication events have taken place. Duplication of genes may result from whole genome duplication, segmental duplication, retrotransposition of mature RNA's or tandem duplication of genes (98) Adaptive evolution may drive gene duplication events depending on the physiological requirements of the bacterium. For example comparative genomic studies on Mycobacteria species have revealed gene duplications in metabolic pathways that are non-uniform between the species examined. (99) For example two genes involved in lysine metabolism are present in multiple copies in the genome of *Mycobacterium avium* ssp.paratuberculosis (99). Marri *et al.* have suggested that the increased biosynthesis of lysine may be required to make the cell wall of this bacterium resistant to the acidity of the ruminant gut (99). A physiological basis for multiple GlxI organisms in *P. aeruginosa* has not yet been identified.

2.3 *pyrC*: An Example of Multiple Homologs in the *P. aeruginosa* Genome

There is precedent for redundant copies in *P. aeruginosa* since it contains three homologs for the *pyrC* gene that encodes dihydroorotase (100). Only two of the gene loci encode functional dihydroorotases in contrast to the GlxI homologs which are all functional (100). Dihydroorotases are

Zn^{2+}-dependent enzymes that catalyze the reversible cyclization of carbamoyl L-aspartate to L-dihydroorotate (100). In our investigation, we used the *P. aeruginosa* chromosomal map to determine whether the *gloA* homologs in *P. aeruginosa* clustered with any of the *pyrC* homologs, given the same number of duplicate genes/pseudogenes. Only *gloA1* was within 2.5 kilobases of the functional *pyrC* homolog designated PA3527 according to the *Pseudomonas* Genome Database (Figure 2.1). Thus it is not likely that the occurrence of multiple *pyrC* loci in the *P. aeruginosa* genome arose from the same mechanism or location as the multiple *gloA* homologs.
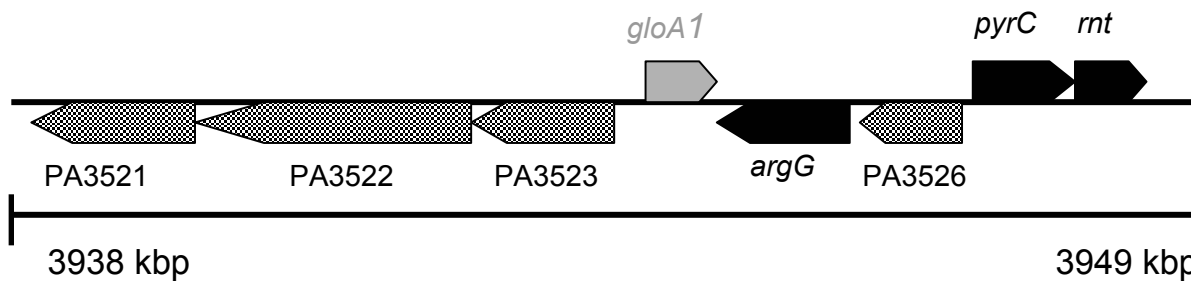
Figure 2.1: Chromosomal region surrounding *gloA1* gene in strain PAO1.

2.4 *P. aeruginosa* has Three GlxI-Encoding Genes

Although the mechanism by which genes become situated or duplicated in a genome may not always

be known, it is an interesting exercise to document the existence of homologs in bacterial genomes.

This genomic context is particularly intriguing, as bacterial genome organization tends to be

economical in the sense that all genes residing on the chromosome are expressed and contribute to the

overall cellular physiology of the organism. The published *Pseudomonas aeruginosa* PAO1 genome

indicates the existence of *three* putative GlxI-encoding open reading frames as delineated by

hypothetical functions in the PAO1 strain genome database (www.pseudomonas.com) (92, 101). The

gene designated *gloA1* (designated by the locus tag PA3524 in the *Pseudomonas* Genome Database),

in this database was initially identified and characterized in our previous comparative studies of

bacterial GlxI enzymes based on its similarity to the *E. coli* GlxI (Figure 2.2) (3, 66). The *E. coli*

GlxI polypeptide sequence was employed as a query in selecting candidate homologs for biochemical

analysis. GloA1 (gene product of *gloA1*) has been fully characterized as a non-Zn^{2+}-dependent,

homodimeric GlxI enzyme with a similar metal activation profile to the *E. coli* GlxI (Figure 2.2).

46

Additional sequences (*gloA2* and *gloA3,* designated by locus tags PA0710 and PA5111 respectively) with predicted lactoylglutathione lyase functions however appeared to be present in the *P. aeruginosa* genome (Figure 2.2).

```
                              20                    40                    60
                              |                     |                     |
    E. coli  - - - - - - - - - -  - - - - - - - - - -  - - - - - - - - -M  RLLHTMLRVG  DLQRSIDFYT  KVLGMKLLRT  31
     GloA1   - - - - - - - - - -  - - - - - - - - - -  - - - - - - - - -M  RILHTMIRVG  NIDRSIDFYT  RVLGMTLLRK  31
     GloA2   - - - - - - - - - -  - - - - - - - - - -  - - - - - - - - -M  RILHSMLRVA  DLEAALEFYT  RALDMRLLRR  31
     GloA3   MSFNT- - - - -  - - -EVQPGIC  MEPDAITQEY  VFNHTMLRVK  DPKRSLDFYS  RVLGMRLLRR  52
  P. putida  MSLHD- - - - -  - -LQTLPGVT  AQPDAATAQF  VFNHTMLRVK  DIEKSLDFYT  RVLGFRLVDK  53
  H. sapiens MAEPQPPSGG  LTDEAALSCC  SDADPSTKDF  LLQQTMLRVK  DPKKSLDFYT  RVLGMTLIQK  60

                              80                   100                   120
                              |                     |                     |
    E. coli  SENPEYKYSL  AFVGYGPETE  - - - - - - - - - -  - - - - -EAVIE  LTYNWG- - - -  -VDKYELGT-  70
     GloA1   NDYPDGQFTL  AFVGYGNEAD  - - - - - - - - - -  - - - - -SAVIE  LTHNWG- - - -  -VDAYEIGT-  70
     GloA2   RDYPEGRFTL  AFVGYQDERA  - - - - - - - - - -  - - - - -AAALE  LTHNWD- - - -  -RDGYTQGD-  70
     GloA3   LDFEEGRFSL  YFLAMTRGEE  VPDAVDERQR  YTFGRQSVLE  LTHNWGSESD  DSQ-YHNGNQ  111
  P. putida  RDFPEAAFSL  YFLALVDPAQ  IPADDTARHQ  WMKSIPGVLE  LTHNHGTEND  ADFAYHNGNT  113
  H. sapiens CDFPIMKFSL  YFLAYEDKND  IPKEKDEKIA  WALSRKATLE  LTHNWGTEDD  ATQSYHNGNS  120

                             140                   160                   180
                              |                     |                     |
    E. coli  - - -AYGHIAL  SVDNAAEACE  KIRQNGGNVT  REAGPVKGGT  TVIAFVEDPD  GYKIELIEEK  127
     GloA1   - - -GYGHIAI  EVDDAYQACD  DIRYNGGQVT  REAGPMKHGT  TVIAFVTDPD  GYKIELIQKS  127
     GloA2   - - -GYGHLAI  EVEDAAVTCA  RARALGYRVT  REAGLMQHGR  SVIAFLEDPD  GYKVELIQKG  127
     GloA3   DPRGFGHICF  SVPDLVAACE  RFETLGVNFV  K- - -PLDRGM  KNVAFISDPD  GYWVEIVQAS  168
  P. putida  DPRGFGHICI  SVPDVRAACA  RFEELEVPFQ  KR- -LQDGRM  NHLAFVKDPD  GYWVEVIQPT  171
  H. sapiens DPRGFGHIGI  AVPDVYSACK  RFEELGVKFV  KK- -PDDGKM  KGLAFIQDPD  GYWIEILNPN  178


    E. coli  DAGRGLGN- -  - 135
     GloA1   S- - - - - - - - -  - 128
     GloA2   TQFD- - - - - -  - 131
     GloA3   LNGEMGRG- -  - 176
  P. putida  ELEG- - - - - -  - 175
  H. sapiens KMATLM- - - -  - 184
```

Figure 2.2:   Sequence alignment of *P. aeruginosa* GlxI enzymes (GloA1, GloA2 and GloA3; NCBI accession numbers are: AAG06912, AAG04099 and AAG08496 respectively) with other representative enzymes from both metal activation classes. The other sequences displayed are from *E. coli*, *P. putida* and *H. sapiens* GlxI enzymes (Accession numbers are AAC27133, NP_745896 and NP_006699 respectively). Conserved residues directly involved in metal coordination are marked with an asterisk. The letters A, B and C denote internal regions of extended sequence present in the Zn^{2+}-dependent enzymes that are systematically absent in the non-Zn^{2+}-dependent GlxI sequences. The alignment was created in CLC Free Workbench (CLC bio A/S) version 3.0.1 using the accurate alignment algorithm.

P. aeruginosa and *S. typhimurium* are notable amongst bacteria for having three GlxI homologs encoded in its genome. The *P. aeruginosa* GlxI-encoding genes (*gloA1*: 3944184 - 3944570 nucleotides, *gloA2*: 782570 – 782965 nucleotides, *gloA3*: 5754144 – 5753614 nucleotides, according to annotation in *Pseudomonas* Genome Database, version 2) are located on chromosomal regions distant from each other, hence the *gloA* genes do not constitute an operon (Figure 2.3) (92, 100). The genomic organization of *P. aeruginosa* in general does not exhibit the discrete functional clustering observed in the operons of the Enterobacteriaciae (102). The completed genome sequence of strain PAO1 was reported in 2000 and there is little evidence for recent gene duplication events on the chromosome (92). This is indicated by the high G + C content of 66.6.% of the PAO1 chromosome, with only ten regions possessing a low G + C content and divergent codon usage suggestive of recent horizontal gene transfer (92). None of the GlxI-encoding genes in PAO1 reside in these regions of skewed G + C content.
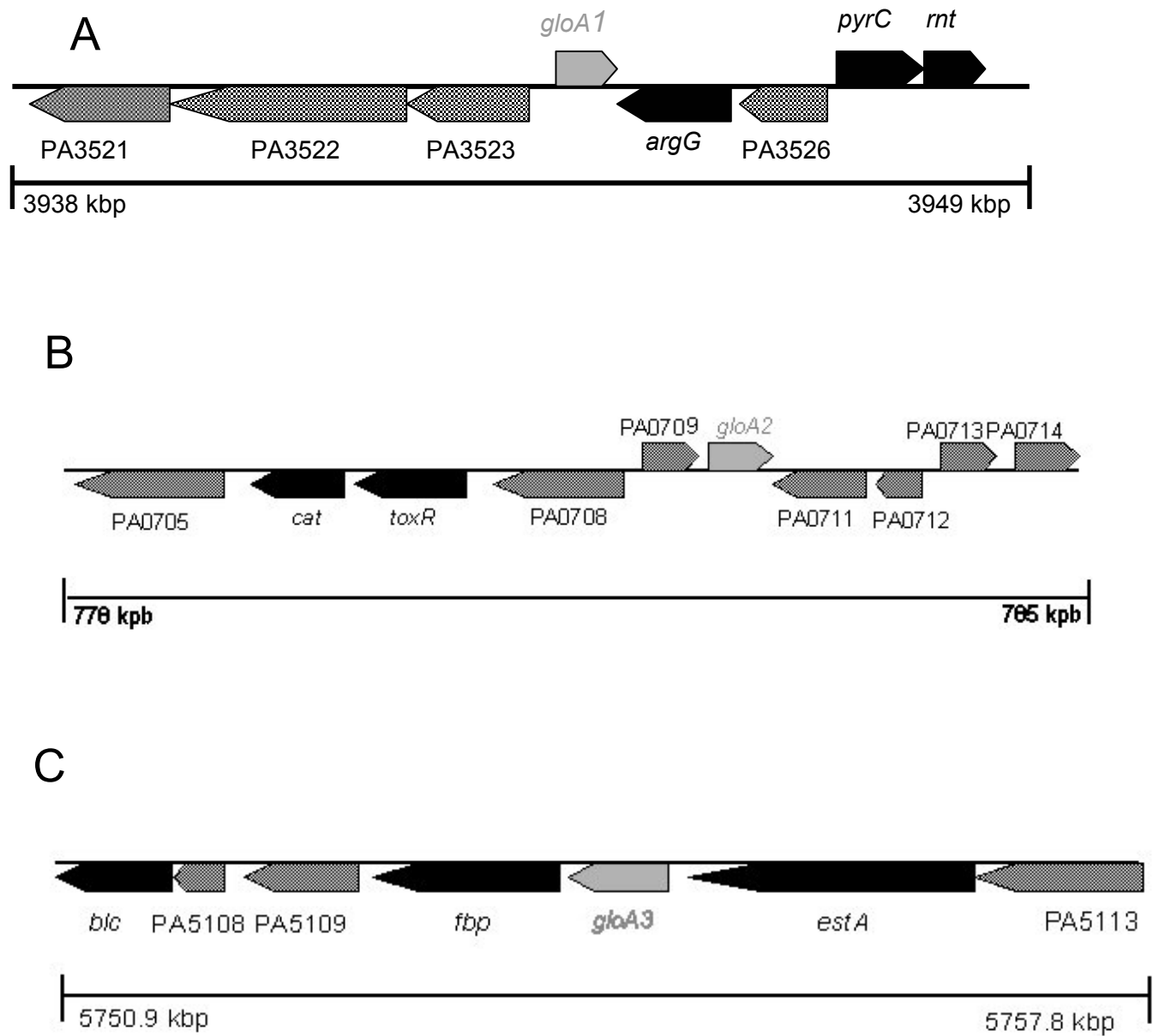
Figure 2.3: Chromosomal regions surrounding A) *gloA1*, **B)** *gloA2* **and C)** *gloA3* **genes in PAO1.** The ORF's code for hypothetical proteins: PA0705 - probable glycosyl transferase; PA0708 - transcriptional regulator; PA0709- hypothetical protein; PA0711 - hypothetical protein; PA0712 - hypothetical protein; PA0713 - hypothetical protein; PA0714 - hypothetical protein; PA5108 - hypothetical protein; PA5109 - hypothetical protein; PA5113 - hypothetical protein. *.cat* is a chloramphenicol acetyltransferase -encoding gene, *toxR* codes for transcriptional regulator ToxR, *blc* is the gene for the Blc outer membrane lipoprotein, *fbp* codes for fructose-1,6-bisphosphatase-encoding gene and *estA* codes for the EstA esterase.

49

In contrast *P. aeruginosa* only has one copy of a GlxII-encoding gene, as is the case for other pseudomonads (sp. *Fluorescens, putida, phaseocola, entomophila*), *E. coli*, and all other bacteria listed in the TIGR comprehensive microbial resource database (http://cmr.tigr.org/tigr-scripts/CMR/CmrHomePage.cgi). This gene resides in a genomic region that appears to be well conserved amongst the Pseudomonad genome sequences catalogued in the *Pseudomonas* Genome database.

Only one true pseudomonad listed in pseudomonas.com, *P. fluorescens* possesses a methylglyoxal synthase-encoding gene (103). Clearly the physiological context and evolution of methylglyoxal metabolism in pseudomonads is complex and not easily deciphered from preliminary genomic comparisons.

Considering the relatedness of the true pseudomonads (related to *P. aeruginosa* in the DNA-rRNA homology group I, within the Gammaproteobacteria class) *P. aeruginosa* stands out as the only species relative to *P. putida* KT2440, *P. fluorescens* Pf-5 and *P. syringae* DC3000 (whose genomes have all been completely sequenced) with three GlxI homologs in its genome (103, 104, 105, 106). The GlxI enzymes in the *Pseudomonas* species possess GlxI homologs with significant similarity to GloA3, representing the Zn^{2+}-dependent class. Genome region comparisons indicate no conservation of the chromosomal regions containing GlxI between the four species (101). This is not unusual considering that genome alignments indicate many chromosomal rearrangements have occurred within the distinct species in spite of the conservation of homologs (107). *P. aeruginosa* appears to diverge from the *fluorescens*, *putida* and *syringae* genomes at a phylogenetic level which may account for the higher percent identity between the latter two putative GlxI amino acid sequences as opposed the identity shared by *P. aeruginosa* GloA3 (107).

These putative *P. aeruginosa* GlxI sequences were cloned and characterized to verify whether they exhibited lactoylglutathione lyase activity (108). Interestingly, metal reconstitution studies of GloA2 and GloA3 have determined that the former is a non-Zn^{2+}-activated GlxI enzyme while the latter is isolated as an active Zn^{2+}-holoenzyme (108). It is clear from the present work that *P. aeruginosa* PAO1 has genes that encode several fully functional GlxI homologs with differing metal selectivities.

2.5 Materials

2.5.1 Reagents

The reagensts listed below were used in other experiments described in this thesis and are referred to accordingly. Nickel (II) chloride hexahydrate (99.9999% pure), 2,6-pyridinedicarboxylic acid (dipicolinic acid, DPA, 99% purity) were from Aldrich (Oakville, ON, Canada), cobalt chloride hexahydrate (assay, 100%, specification, 98–102%), cadmium chloride (assay, 99.4%), manganous chloride tetrahydrate (assay, 98.8%) and zinc chloride (assay, 99.3%) were obtained from J. T. Baker (Toronto, ON, Canada), and magnesium chloride hexahydrate (assay, 99.2%) and calcium chloride dihydrate (assay, 75.5%) was obtained from BDH (Toronto, ON, Canada). $ZnSO_4$ heptahydrate (assay 99%) was obtained from Fisher (Nepean, ON, Canada) and was obtained from Aldrich (Milwaukee, WI, USA). Aqueous methylglyoxal (MG) (40% v/v), S-D-lactoylglutathione (SLG), reduced glutathione, guanidinium hydrochloride and phenylglyoxal (PG) monohydrate was purchased from Sigma (Oakville, ON, Canada). Water used in experiments was purified using a Milli-Q RG Ultrapure water system (18 MΩ-cm; Waters Associates, Milford, MA, USA). Tris acid, Tris base, solid $(NH_4)_2SO_4$, Isopropyl β-D-thiogalactoside (IPTG), HEPES, MOPS and phenylmethylsulfonyl fluoride (PMSF) were purchased from Bioshop Canada (Burlington, ON). KCl was obtained from EMD Biosciences (Gibbstown, NJ, USA). Chelex 100 cation exchange resin was obtained from Bio-Rad (Mississauga, ON, Canada) for the removal of divalent cations from buffer solutions and water. Biolyte 4-6 commerical ampholyte (40% stock) was employed for purification of GloA2 and GloA3 at dilutions in the focusing cell to a final concentration of 1-1.5% v/v. Water used in all experiments and purification protocols was purified using a Milli-Q RG Ultrapure water system (18 MΩ-cm; Waters Associates, Milford, MA, U.S.A.).

2.5.2 Chromatography Resins

The chromatographic media listed below have been used in other experiments described in this thesis and are referred to accordingly. The chromatographic resins Q-Sepharose Fast Flow, Mono-Q anion exchange, Phenyl HP Hi Sub, and Superdex 75 were obtained from Amersham Biosciences (Uppsala, Sweden). The pre-packed Unosphere-Q anion exchange column was obtained from Bio-Rad (Mississauga, ON, Canada).

2.5.3 Centrifugation

Centrifugation of volumes exceeding 20 mL was carried out using a Beckman Avanti J-25I centrifuge (JA 25.5 rotor used for 20-50 mL volumes, JA 14.4 rotor used for volumes exceeding 50 mL up to 250 mL, and JA 10 rotor used for volumes exceeding 250 mL up to 500 mL) (Mississauga, ON). Centricon® concentrators were spun in a VWR Clinical 100 (Labnet International, Woodbridge NJ, USA) clinical centrifuge centrifuge at 3500 rpm. Centrifugation of volumes suitable for microcentrifuge tubes was performed using the Biofuge A microcentrifuge (Heraeus Sepatech GmbH, Germany). The microcentrifuge was used at speeds of 13 000 rpm for pelleting of cells for SDS-PAGE, and at speeds of 1000 rpm for pelleting precipitated GlxI from isoelectric focusing fractions.

2.5.4 Chromatographic Systems

Fast peptide and protein liquid chromatography (FPLC®) on cell lysate was performed using a Pharmacia (now Amersham Biosciences, Uppsala, Sweden) Biotech system consisting of the following components: LCC-500 chromatography controller, two P-500 pumps, MV-7 motor valve, UV-M monitor. A Waters high-pressure liquid chromatography (HPLC) system was also used for protein purification. This system consisted of a Waters 600S Controller, Waters 626 Pump amd the2996 Photodiode Array detector. The Empower™ software suite was used for data collection and chromatogram generation with this system.

2.5.5 Preparative Isoelectric Focusing

The Rotofor® preparative isoelectric focusing apparatus from Bio-Rad (Missisauga, ON, Canada) was used for the preparation of apo-GlxI enzymes from *E. coli* and GloA2 of *P. aeruginosa*.

2.5.6 Incubators

Either a Gyrotory® Model G76 (New Brunswick Scientific, Edison, NJ) water bath shaker at a speed setting of 5, or a Series 25 (also New Brunswick Scientific) controlled environment incubator shaker at 200 rpm was employed for growing bacterial broth cultures. Standing broth cultures or plated bacterial cultures were grown in a Precision® gravity convection incubator from Precision Scientific, Inc. (Chicago, IL).

2.5.7 Protein Concentration and Buffer Exchange

Concentration of purified protein and exchange into storage buffer was achieved using either Centricon® YM10 centrifugal concentrators (0.5 mL – 2 mL volumes), Vivaspin 10 (Sartorius, Gottingen, Germany) centrifugal concentrators (0.5 mL – 2 mL volumes), Nanosep microcentrifugal concentrators (10 kDa cutoff membrane for 40 μL – 400 μL volumes) (Pall Life Sciences, , Ann

Arbor, MI, U.S.A.), Amicon® ultrafiltration cells (50mL or 10mL volume), using Millipore YM10 membranes (Millipore, Billerica, MA).

2.5.8 Spectrophotometry

Protein quantitation and spectrophotometric assays of GlxI activity were performed using a Varian Cary 3 (Mississauga, ON) spectrophotometer, using the Cary WinUv software, version 3 (Varian Instruments Walnut Creek, CA, USA) for instrument control and data collection.

2.6 General Methods for GlxI Characterization

This section describes methods that have been used in the isolation and characterization of GlxI enzymes for several of the studies described within this thesis. The use of methods in this section will be referred to accordingly.

2.6.1 Assay for GlxI Enzymatic Activity

The glyoxalase I enzyme assay employed in these studies was performed according to the procedure documented by (109). A solution of the hemithioacetal substrate at a given concentration was made by the addition of methylglyoxal (MG) and GSH to degassed 50 mM potassium phosphate buffer, pH 6.6. The mixture was equilibrated after mixing at room temperature for 15 minutes prior to ensure hemithioacetal formation to occur. The free GSH was maintained at 0.1 mM to prevent enzyme inhibition (110). Hemithioacetal concentrations were calculated using the dissociation constant for the species at pH 6.6, such that $K_{diss} = 3.1$ mM (111).

The equilibrium equation for hemithioacetal concentration used in these calculations is as follows:

$$K_{diss} = \frac{[MG_{total} - MG_{complex}]\, [GSH_{total} - GSH_{complex}]}{MG\text{-}GSH_{complex}]}$$

Note: $[GSH_{free}] = [GSH_{total} - GSH_{complex}] = 0.1$ mM

Enzyme activity was measure spectrophotometrically by observing formation of S-D-lactoylglutathione at 240 nm (112). The reaction was monitored in quartz cuvettes with a pathlength of 10 mm, and the rate of thioester formation was calculated using the extinction coeffecient of 2860 $M^{-1}cm^{-1}$ (112). Initial rate data was fitted by non-linear regression analysis using the software GraFit version 3.01 (Erithacus Software).

2.6.2 Methylglyoxal (MG): Distillation and Concentration Determination

Distillation of aliquots MG (40% aqueous solution) was performed prior to usage as a working stock to remove polymers and other contaminants. The MG was distilled at atmospheric pressure, and the distillate was collected between 92 – 96 °C (Vince *et al.* 1971). This purified stock was stored at 4 °C for up to six months.

The concentration of the distilled MG was determined on a periodic basis (once a month during useful lifetime) utilizing a method based on the spectrophotometric glyoxalase I assay (113). Essentially the enzyme assay was run in triplicate using a sufficiently dilute MG concentration and excessive GSH concentration, ensuring all MG was consumed during the reaction. The MG stock concentration was subsequently determined from the amount of S-D-lactoylglutathione detected by ΔA_{240} using the extinction coefficient 2860 M^{-1} cm^{-1}.

The procedure for MG calibration is as follows. Matched 1 mL cuvettes were filled with 100 mM potassium phosphate buffer, pH 6.8. To this buffer, GSH was added to a final concentration of 0.5-1.0 mM and approximately 0.1 units of purified *E. coli* GlxI or yeast GlxI grade IV from Sigma was also added (where one unit of enzyme = enzyme quantity producing 1 mmol of *S*-D-lactoylglutathione per minute). The initiation of the GlxI reaction was achieved by addition of distilled MG that was diluted 150-fold, such that the final concentration of this substrate constituent was 0.2-1.0 mM.

2.6.4 Determination of Glutathione (GSH) Concentration

A precise determination of GSH concentration is required for quantitative preparation of MG-GSH hemithioacetal solutions. GSH titration with 5,5'dithio-bis(2-nitrobenzoic acid) (DTNB) was used for [GSH] determination by the method of Ellman (114). As for other assays a 50 mg/mL GSH working stock was prepared in assay buffer (degassed). An aliquot of this stock was diluted 60-fold in 100 mM potassium phosphate buffer pH 7.4, and basified with sodium carbonate to pH 7.5-8.0. In a sample cuvette the diluted, basified GSH was added to 100 mM potassium phosphate buffer pH 7.4 for a final volume of 1 mL, such that the final GSH concentration was around 0.05 mM. DTNB as a 1-2 mg/mL stock in HPLC grade methanol, was titrated into sample and reference cuvettes while monitoring the absorbance at 412 nm until no further increase in absorbance was observed. The overall change in absorbance was used to calculate the GSH stock concentration, based on the molar extinction coefficient of the DTNB-GSH disulfide complex (14 150 M^{-1} cm^{-1}) (115).

2.6.5 Removal of Activating Metals from Buffers and Plasticware

To store purified apoGlxI storage buffers and plastic containers should be free of re-activating metal ions. Such buffers and containers should also be used for the preparation of metal chloride stock solutions and for preparations of metal-reconstituted GlxI. Divalent metals were removed from

buffers and/or water with a cation exchange resin. Specifically, 5-6 grams of Chelex 100 resin was used to treat approximately one liter of solution. Plastic containers were treated to remove metal ions by soaking in 10% HNO_3 (v/v) for 15-20 minutes, followed by numerous rinses with distilled deionized water, and several rinses of Chelex treated water, or rinsing of a buffer storage vessel with aliquots of Chelex treated buffer.

2.6.6 Preparation of Protein Samples for Mass Spectrometry

Purified GlxI samples were desalted prior to injection into an electrospray ionization mass spectrometer. Protein samples were dialyzed to exchange buffer for Milli-Q grade water, with one change of solution between three and six hour periods of stirring respectively. Each dialysis chamber was scaled to permit approximately a 10 000-fold dilution of the buffer constituents in the GlxI sample, i.e 50 μL of purified GlxI in 50 mM MOPS pH 7.0 against 500 mL water.

2.6.7 Microbiological Media

All microbiological media was prepared using deionized-distilled water.

Luria-Bertani (LB) media was used for the growth of *E. coli* except where indicated. The composition of this medium consists of 10g tryptone (EMD Biosciences, Gibbstown, NJ, USA), 10g NaCl (EMD Biosciences, Gibbstown, NJ, USA) and 5g yeast extract (EMD Biosciences, Gibbstown, NJ, USA) per liter of media. The media is adjusted to pH 7.0 with NaOH. LB media was also used as a solid growth medium by adding agar (EMD Biosciences, Gibbstown, NJ, USA) to the prepared broth for a final concentration of 3% w/v.

Terrific Broth (TB) was also used as a growth medium for *E. coli* where indicated. The composition of TB per liter of media is 12g tryptone (EMD Biosciences, Gibbstown, NJ, USA), 24g yeast extract (EMD Biosciences, Gibbstown, NJ, USA), 4mL glycerol (EMD Biosciences,

Gibbstown, NJ, USA), 17mM KH_2PO_4 (from EMD Biosciences, Gibbstown, NJ, USA) and 7.2 mM

K_2HPO_4 (EMD Biosciences, Gibbstown, NJ, USA). The potassium salts are added as a 100 mL

solution of 0.17M KH_2PO_4 and 0.72M K_2HPO_4 to the other media constituents, which have been

dissolved in 900 mL of water.

M9 minimal salts media was used to grow *E. coli* in liquid cultures where indicated. The

concentrated M9 minimal salts solution consists, per liter of: 64g Na_2HPO_4-$7H_2O$ (Bioshop Canada,

Burlington, ON, Canada), 15g KH_2PO_4, 2.5g NaCl and 5.0g NH_4Cl (BDH, Toronto, ON, Canada).

One liter of prepared M9 minimal salts medium consists of:

- 200 mL of M9 salts
- 2 mL of 1M $MgSO_4$ (sterile)
- 20 mL of 20% glucose (v/v) (Fisher, Nepean, ON, Canada)
- 100 µL of 1M $CaCl_2$ (sterile)
- 100 µL of 0.5% thiamine HCl (v/v) (Sigma, Oakville, ON, Canada)

2.7 Isolation and Characterization of GloA2 and GloA3

2.7.1 Bacterial Strains and Sources of Template DNA

E. coli strains BL21(λDE3) (F-, *omp*T, *hsd*S(r-B, m-B), *gal*, *dcm*, λDE3(*lac*I, *lac*UV5-T7 gene 1,

*ind*1, *sam*7, *nin*5) and DH5α (φ80d*lac*ZΔM15, *recA*1, *endA*1, *gyr*AB, *thi*-1, *hsdR*17(r_K-, m_K+),

*supE*44, *relA*1, *deo*R, Δ*(lacZYA-arg*F) U169, *pho*A) were used as GlxI overexpression and plasmid

propagation hosts respectively. Genomic DNA was isolated from wild-type *P. aeruginosa* strain

PAO1 (wild type strain). This strain was obtained as a gift from Dr J. Lam of the University of

Guelph (Ontario, Canada). *Oligonucleotides and DNA sequencing* - DNA primers for isolating *gloA2*

and *gloA3* were obtained from Sigma Genosys (Oakville, Ontario, Canada). Sequencing of the

59

plasmid constructs for overexpression was performed by MOBIX (McMaster University, Hamilton, Ontario, Canada).

2.7.2 Cloning of *P. aeruginosa* Genes *gloA2* and *gloA3*

The putative GlxI DNA sequences used to design oligonucleotide primers were based upon the nucleotide sequences for the gloA2- and gloA3-encoding genes as indexed in the *Pseudomonas* Genome database at (www.pseudomonas.com). The *gloA2* gene was amplified from the aforementioned template DNA by PCR, using the following primer pair:

(+)5′CCAGTCGACCATATGCGAATCCTGCACAGCATGC3′,

(−)5'CGTGGATCCTCAATCGAACTGGGTGCCCTTCTGG3′ . The *gloA3* gene was amplified from the aforementioned template DNA by PCR, using the following primer pair:

(+)5′ CCAGAATTCCATATGAGTTTCAACACCGAAGTACAGC3′,

(−)5′CCAGAATTCTCTCAGCCGCGTCCCATCTCGCCG 3′.

The thermal cycle profile used for amplification of *gloA2* and *gloA3* was as follows:

1) Initial denaturation @ 95°C for 30 s

2) Hot start @ 85°C

3) 10 cycles of:

Denaturation @ 95°C for 30 s

Primer annealing @ 59°C (for *gloa3* amplification) or 63°C (for *gloA2* amplification)

Extension @ 72°C for 45 s

4) 15 cycles of:

Denaturation @ 95°C for 30 s

Primer annealing @ 59°C (for *gloa3* amplification) or 63°C (for *gloA2* amplification)

Extension @ 72°C for 45 s with 5 s time extension per cycle

60

5) Final Extension @ 72°C for 10 min

For both *gloA2* and *gloA3* amplification, primer concentration used was 300nM, the dinucleotide triphosphate concentration was 0.2 mM and the amount of template DNA was 300ng in a 100 µL reaction. Optimal $MgSO_4$ concentrations were 2.0 mM and 2.5 mM for *gloA3* amplification and 1.5 mM for *gloA2* amplification.

The *gloA2* amplification product was ligated into the pET22b expression vector (amp[R], T7 *lac* promoter, *f1* origin of replication; Novagen, Madison, WI, USA), which was prepared by restriction endonuclease digestion with *Nde*I and *Bam*HI. The digestion products were subsequently ligated to generate the over-expression constructs designated pPAG4. The *gloA3* amplification product was ligated into pET22b following restriction endonuclease digestion with *Nde*I and *Eco*RI, which generated the overexpression plasmid called pPAG3. All three plasmid constructs were transformed into *E. coli* BL21(λDE3) cells, yielding the final overexpression systems for these GlxI enzymes.

2.7.3 Growth and Induction of *gloA2*- and *gloA3*-overexpressing *E. coli* Cells

The protocol for induction of GloA2 (using *E. coli* BL21-(λDE3)/pPAG4) was similar to that used for induction of the *E. coli* GlxI-overexpression system, except that no $NiCl_2$ was added to the growth medium and the cells were induced with 0.5 mM isopropyl β-D-thiogalactoside (IPTG) for 4 hours as opposed to the 6 hour induction for *E. coli* MG1655/pGL10(51). For overproduction of GloA3, *E. coli* BL21-(λDE3)/pPAG3 was grown in 0.5 or 1 L of Terrific Broth (TB) containing a range of 0 - 1 mM $ZnSO_4$. The absence or presence of $ZnSO_4$ in the media did not appear to alter the activity of the isolated holoenzyme. At an optical density of 0.5 at 600 nm, induction of protein production was initiated with 0.5 mM IPTG and allowed to proceed for 4 hours before harvesting of cells by centrifugation.

61

2.7.4 Purification of GloA2 and GloA3

BL21(λDE3)/pPAG3 or BL21(λDE3)/pPAG4 cells were re-suspended in 20 mM Tris pH 7.5, and disrupted by sonication. For GloA3 purification, 15 mM DL-methionine or 10 mM dithiothreitol (DTT) was present in purification buffers to attenuate methionine and cysteine oxidation. Glycerol and phenylmethylsulphonyl fluoride PMSF (1M stock in HPLC-grade acetone) were added to the lysates so that the final concentrations were 10% v/v and 1 mM respectively. The lysates were clarified by centrifugation at 48 434 x g for 15 minutes at 4 ºC. Lysates were filtered through a 0.2 μm filter and loaded onto a 10/30 Q-Sepharose Fast Flow column (Amersham Biosciences) at 1 mL/min. The protein was eluted from the column using a 100 minute gradient with a 1%/min change in percent salt concentration [from: 20 mM Tris/HCl, 10% (v/v) glycerol, pH 7.5; to: buffer + 1 M KCl]. The GlxI-containing fractions were pooled and dialysed against 20 mM Tris, pH 8.0 for GloA2, and against 20 mM Tris, pH 7.5 for GloA3, then applied to a Mono-Q (Amersham Biosciences) column. A similar KCl gradient to that used on the Q-Sepharose column was applied for this purification step using the Tris buffers at their respective pH's. GloA2-containing fractions were pooled and dialyzed into 20 mM MOPS, 150 mM KCl, pH 7.0 and applied to a 10/30 Superdex 75 gel filtration column for purification.

The GloA2-containing fractions from this chromatographic step were pooled and dialyzed into 10% glycerol prior to loading into the Rotofor (Bio-Rad, Hercules, CA) preparative isoelectric focusing cell for preparation of apoenzyme at 12 W constant power for 4-6 hours. The cell was maintained with constant cooling by a re-circulating water bath at 4 °C. The focusing medium used in this preparation was the ampholyte solution indicated in the materials section at the specified concentration. Purified apo-GloA2 was concentrated and stored in 50 mM Chelex-treated MOPS, pH 7.0, in acid-treated plasticware at 4 °C. GloA3-containing MonoQ fractions were dialyzed into 50 mM potassium phosphate buffer, pH 6.6 and solid $(NH_4)_2SO_4$ was added to the dialysed sample to a

final concentration of 1.7 M. The sample was filtered with a 0.2 μm filter and loaded onto a 1 mL

Phenyl HP High Sub column (Amersham Biosciences) at 1 mL/min with 50 mM potassium

phosphate, 1.7 M $(NH_4)_2SO_4$, pH 6.6. The protein was eluted with a decreasing gradient of $(NH_4)_2SO_4$

and purified GloA3 was collected as a single peak. The protein was exchanged into 50 mM MOPS,

pH 7.0 (Chelex-treated) and stored at 4 °C.

2.7.5 Molecular-Mass Determination

Electrospray ionization mass spectrometry (ESMS) was used to confirm the molecular mass of the

overproduced bacterial GlxI enzymes in purified samples. Analysis was performed on protein

samples using a Micromass quadrupole time-of-flight (Q-TOF) Ultima Global (Manchester, U.K.)

mass spectrometer at the Waterloo Chemical Analysis Facility, University of Waterloo. Samples

made up in Milli-Q grade water were introduced using eluants consisting of 1:1 water/acetonitrile

plus 0.2% formic acid. Electrospray ionization was performed in positive ion mode.

2.7.6 Sodium Dodecyl Sulfate Polyacrylamide Gel Electrophoresis (SDS/PAGE)

SDS/PAGE was employed to select for GloA2 and GloA3-containing fractions during

chromatographic purification. Separation (using pre-cast gels with acrylamide gradients ranging from

10-15%, or 8-25%) and visualization (Coomassie Brilliant Blue staining) of protein samples by

SDS/PAGE was performed using a PhastSystem™ (Amersham Biosciences).

2.7.8 Metal Analysis

Metal-free water was prepared by passing Milli-Q grade water through Chelex 100 resin (Bio-Rad,

Mississauga, ON, Canada). Purified GloA3 was exchanged into metal-free water by using a

Vivaspin10 centrifugal ulttrafiltration device. Approximately 0.38 - 2 mg of GloA3 was submitted for

metal quantitation in a nitric acid treated plastic tube. The final volume of the sample was 20mL.

Metal content was determined at EnviroTest (now ALS Laboratories Waterloo, ON, Canada) by Inductively Coupled Plasma Mass Spectrometry (ICP-MS). The following elements were quantitated in the sample: Al, Sb, As, Ba, Be, Bi, B, Cd, Ca, Cr, Co, Cu, Fe, Pb, Mg, Mn, Mo, Ni, P, K, Se, Si, Ag, Na, Sr, Tl, Sn, Ti, W, U, V, Zn, Zr. Quantitation of metal in GloA3 was based on three replicates of metal analysis on purified enzyme.

2.7.9 Gel-Filtration Chromatography

Purified GloA2 or GloA3 in 50 mM MOPS, 150 mM KCl, pH 7.0 were applied to a Superdex 75 10/30 column equilibrated with the same buffer at 0.4 mL/min. The column was calibrated using protein standards from Bio-Rad (ovalbumin, myoglobin, and vitamin B12) and Sigma (bovine albumin and carbonic anhydrase). The void volume of the column was determined by injections of Blue Dextran (Sigma) solution. All injections were performed in triplicate using GlxI samples

2.7.10 GlxI Enzyme Assay

The assays and assay conditions used for quantification of GlxI activity were identical with those described for the characterization of *E. coli* GlxI (51).

2.7.11 Metal Activation Profile for GloA2

The purified *GloA2* enzyme was confirmed to be active as a homodimer by gel-filtration chromatography (results not shown). Profiles for metal activation GloA2 with various divalent metal chlorides were assessed by means of the GlxI spectrophotometric assay (51). Samples of a particular apo-GlxI were diluted in 50 mM Chelex-treated MOPS, pH 7.0, and pre-incubated at ambient temperature with 2.5 molar equivalents of metal chloride per dimeric enzyme for at least 10 minutes prior to assay. Enzyme activity was assayed at a 0.5 mM MG-GSH concentration in triplicate.

Amounts of GlxI used per assay were 0.15 µg. Activation was assessed using the following metal chlorides: Mg^{2+}, Ca^{2+}, Zn^{2+}, Cd^{2+}, Mn^{2+}, Co^{2+} and Ni^{2+}.

2.7.12 Determination of Kinetic Parameters

The Michaelis–Menten constants (K_m) and maximal enzyme velocities (V_{max}) for GloA2 and GloA3 enzymes were determined experimentally by measurement of initial reaction rate. Rate data was collected at 11 substrate concentrations between the range of 0.01 and 0.5 mM of MG-GSH. For GloA2, stock enzyme was diluted with 50 mM Chelex-treated MOPS pH 7.0 and 2.5 molar equivalents of $NiCl_2$ or $CoCl_2$, per dimeric enzyme. Enzyme activity at each concentration was measured in triplicate. The entire set of triplicates was measured twice, and the values from the duplicate experiments were averaged to obtain the final parameter values. For GloA3, the purified holoenzyme was diluted to 0.1 mg per mL and assayed under the same conditions as for GloA2, with rate data collected at 11 substrate concentrations ranging between 0.1 to 2 mM MG-GSH. The same number of replicates was used to calculate kinetic parameter values for GloA3 as for GloA2.

2.7.13 Metal Reconstitution of GloA3

Purified GloA3 (1.9 mg) was incubated in 50 mM MOPS containing 50 mM dipicolinic acid (DPA) (final dimeric enzyme concentration of 31.9 µM) with stirring for 4 hrs at 4 °C. DPA was removed from the protein sample by passage through a Nanosep centrifugal ultrafiltration device (molecular mass cut-off of 10 kDa) so that the GloA3 sample was changed over to Chelex-treated MOPS, 50 mM, pH 7.0. The final concentration of the GloA3 sample obtained following ultrafiltration was 19.7 µM dimeric enzyme. To reconstitute the demetallated enzyme, metal chloride (final concentration 25 µM) was added to a dilution of GloA3 (final concentration 5 µM, 5 equivalents of metal chloride per dimeric enzyme) in Chelex treated MOPS pH 7.0. The enzyme was incubated with metal for 48 hours

at 4 °C. Samples were then assayed in 1 mL of 0.5 mM MG-GSH in 50 mM KPB pH 6.6 to obtain relative activation levels.

2.8 Results

Cloning of the *gloA2* and *gloA3* genes into the aforementioned expression constructs yielded systems producing soluble enzyme that exhibited robust levels of activity in the lysate as determined by spectrophotometric assay. Electrospray mass spectra obtained for both purified enzymes were in agreement with the predicted molecular mass from ExPASy (Figure 2.4) (http://www.expasy.org/tools/protpar-ref.html; Geneva, Switzerland) (116). Both GloA2 and GloA3 were identified as dimers in solution by gel filtration chromatography on purified enzyme samples (Table 2.1, Figure 2.5). The apparent molecular weights of GloA2 and GloA3 were 28 kDa and 38 kDa respectively. The elution volumes for both enzymes were lower than the observed elution volume for the 17 kDa myoglobin standard (Table 2.1, Figure 2.5). No additional GloA2- or GloA3-containing fractions were collected at elution volumes indicative of monomeric GlxI in solution.
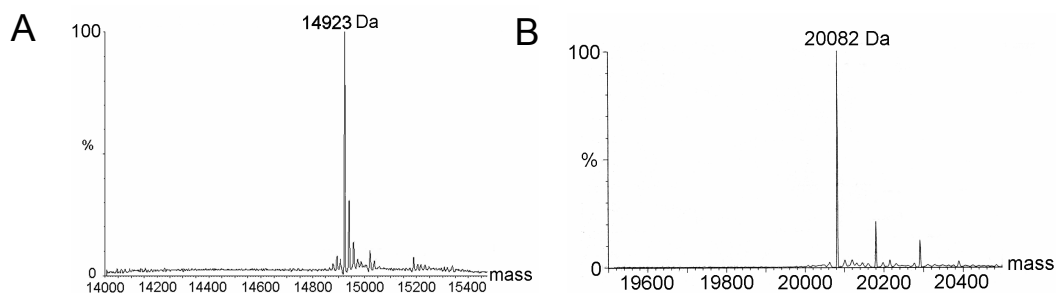
Figure 2.4: Electrospray ionization mass spectra of A) GloA2 and B) GloA3. The observed mass of 14923 Da corresponds well to the calculated mass of 14925 Da for the GloA2 monomer. The observed mass of 20082 Da corresponds with the expected mass of the GloA3 with the N-terminal methionine residue truncated during heterologous production (20084 Da expected for the monomer without N-terminal methionine).

Table 2.1: Molecular Weights of Superdex 75 Standards, GloA2[‡] and GloA3[‡]

Protein	Molecular Weight (MW) (Da)	Log MW	V_e/V_o[*]
A) Bovine Albumin[†]	66000	4.82	1.21
B) Ovalbumin	44000	4.64	1.37
C) Carbonic Anhydrase	29000	4.46	1.50
D) Myoglobin	17000	4.23	1.69
E) Vitamin B-12	1350	3.13	2.53
GloA2	24000[‡]	4.38	1.56
GloA3	38000[‡]	4.58	1.41

[*]V_o was determined by injections of Blue Dextran

[†] Proteins A-E were used to standardize the column

[‡]MW estimates were interpolated from the standard curve below
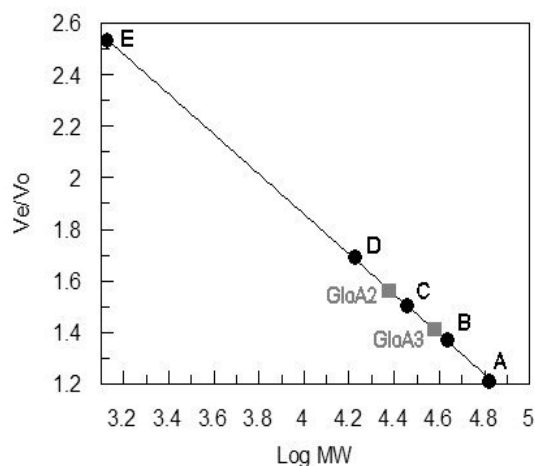
Figure 2.5: Standard curve from Superdex75 chromatography. The lettered data points correspond to the standard proteins in the above table.

Preliminary screens on cell free extracts indicated that GloA2 could convert MG-GSH to *S*-D-lactoylglutathione as indicated by the standard assay (0.5 mM MG-GSH, 50 mM potassium phosphate pH 6.6). This activity was increased with addition of Ni^{2+} and Co^{2+} to the assay buffer, but not increased with addition of Zn^{2+}. Clearly, this initial profile mirrors the characteristic metal activation of the non-Zn^{2+}- activated enzymes from *E. coli*, and *P. aeruginosa* GloA1 . GloA3 extracts by comparison exhibited detectable levels of GlxI activity that was not modifiable by the addition of Ni^{2+}, Co^{2+} or Zn^{2+}. The enzyme activity detected in these lysates did not vary with the presence of $ZnSO_4$ in the growth medium. Differentiation of the activating metal in GloA3 was assessed initially by comparing the second-derivative spectra of 4-(2-pyridylazo)resorcinol-metal (PAR) complexes obtained with denatured enzyme to the spectra of PAR with $NiCl_2$ and $ZnCl_2$ standards indicating the presence of Zn^{2+} (Figure 2.6) (117, 118). Purified, recombinant GloA3 was found to contain Zn^{2+} by inductively coupled plasma mass spectrometry (ICP-MS) with a Zn^{2+}:dimer

68

ratio of 1:1. There is precedent for observed mono-metallation in fully active GlxI enzymes from *E. coli* and *L. major* GlxI enzymes.
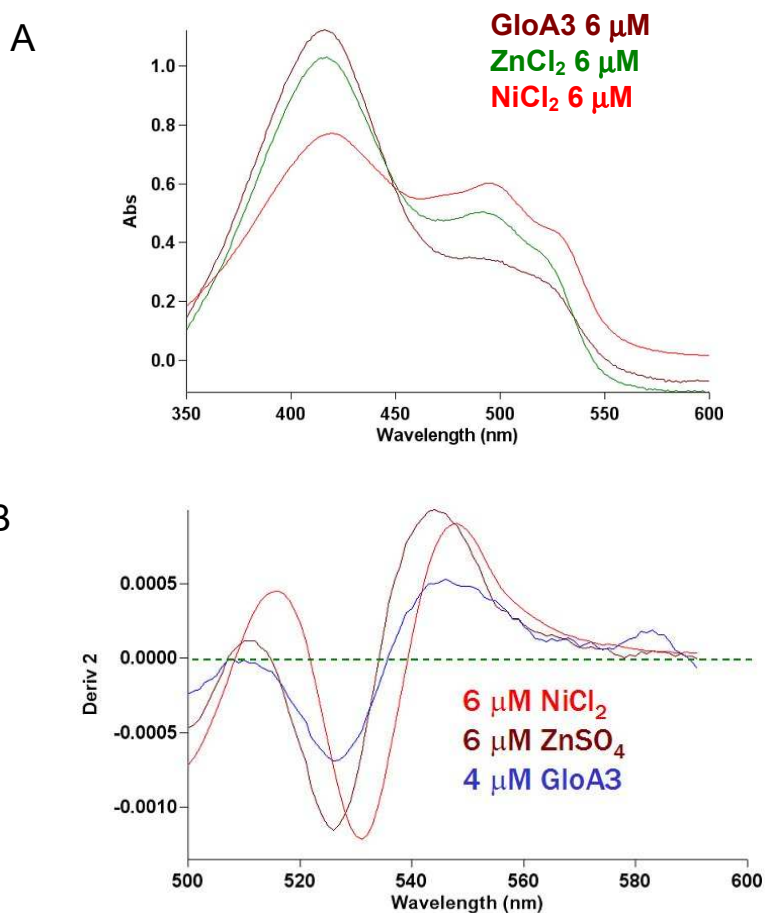
Figure 2.6: A) PAR-metal complex absorption spectra for purified GloA3 and indicated metal standards B) 2nd derivative of the spectra in A)

GloA2 is therefore similar to the non-Zn^{2+}-dependent GlxI enzymes previously characterized based on its metal activation profile and the relative ease with which metal can be removed from the holoform. Isoelectric focusing has been successfully employed demetallating GlxI from *E. coli*, *Y. pestis, N. meningitidis* and *P. aeruginosa* (GloA1)(3, 51). Apo-GloA2 was obtained through this

69

method for kinetic characterization and metal reconstitution studies. For GloA2 and the aforementioned GlxI enzymes, isoelectric focusing produces enzyme with less than 5% specific activity relative to the Ni^{2+}-reconstituted holoform (in the absence of activating metals). These activity levels are highly suggestive of an enzyme preparation that predominantly contains apo-GlxI. GloA2 appears strongly selective for Ni^{2+}- over Co^{2+}-activation compared to the other bacterial GlxI enzymes that we have previously characterized (Figure 2.7).
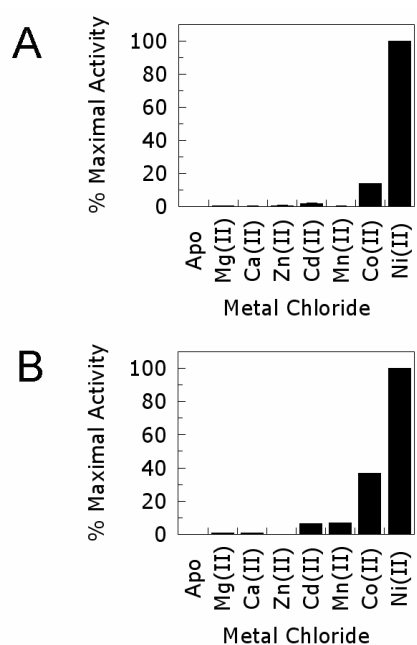
Figure 2.7: A) Metal activation for GloA1 (3) **B) Metal activation for GloA2.** The relative activities shown are normalized by subtraction of the residual specific activity (1.4% of the Ni^{2+}-GloA2 specific activity) observed for the apo-control. Relative activity levels for the Co^{2+}- and Ni^{2+}-substituted enzyme were obtained from the experimental V_{max} values determined for Ni^{2+}-GloA2. The activity of the Ni^{2+}-bound GloA2 is set as the maximal activity (100%) in the metal activation profile for the GloA2 enzyme. Similarly, the maximal activity of 100% in A) is the V_{max} reported for Ni^{2+}-GloA1 (3).

The metal binding properties of GloA3 are quite different from GloA2. The apo-form of GloA3 could not be obtained by isoelectric focusing, so that fractions isolated from this purification process were still highly active when assayed. Clearly this differs from our observations of non-Zn^{2+}-activated GlxI enzymes to date, wherein isoelectric focusing results in apoenzyme formation. Several attempts were made at removing the activating metal from GloA3 for the purpose of determining metal selectivity. Incubation of the enzyme with 30 mM EDTA in 50 mM MOPS pH 7.0 for 48-72 hours (similar condition for preparation of *P. putida* apo-GlxI (59)), was unsuccessful in deactivating this enzyme. Partial denaturation at pH 3.8 along with EDTA present at 100 mM in sodium acetate has been used to generate apo-superoxide dismutase previously. However subjecting GloA3 to similar conditions only resulted in aggregation and precipitation of the enzyme, which could not be reversed by dialysis into 50 mM MOPS pH 7.0. The chelator 1,10-phenanthroline could produce a detectable decrease in enzyme activity with short-term incubation (20 minutes) but 2,6-pyridinedicarboxylic acid (dipicolinic acid, DPA) produced the greatest loss of activity under the same conditions. Preparations of partially demetallated enzyme were prepared by removing the chelator with a centrifugal ultrafiltration device, generating GloA3 that could be re-metallated with different metal chlorides. The 4-hour incubation in DPA reduced activity to 16% of that observed for non-treated enzyme. Partial reactivation of GloA3 was observed with Mg^{2+}, Zn^{2+} and Cd^{2+} reconstitution (26%, 76% and 87% activity of untreated enzyme, respectively) while apparent hyper-reactivation was observed with Co^{2+}, Ni^{2+} and Mn^{2+} re-constitution (115%, 146% and 146% activity of untreated enzyme, respectively) (Figure 2.8).
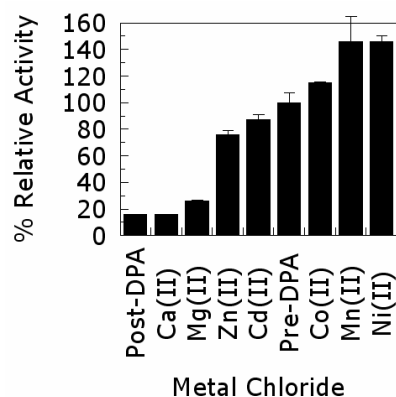
Figure 2.8: Metal activation of DPA-treated GloA3. Percentage of observed enzyme activity relative to non-DPA treated GloA3 (100%) is shown ± standard deviation. GloA3 was de-metallated and reconstituted as described in Experimental Procedures.

Kinetic parameters of GloA2 are very similar to those of *P. aeruginosa* GloA1 and *E. coli* GlxI (Table 2.2). The catalytic efficiency of GloA2 approaches the value observed for the *E. coli* enzyme but the selectivity of Ni^{2+} activation over Co^{2+} re-constitution is much more pronounced for GloA2 compared to the non-Zn^{2+}-dependent bacterial GlxI enzymes characterized previously (*E. coli*, *P. aeruginosa* GloA1, *N. meningitidis*, *Y. pestis*). GloA3 is comparable in efficiency to the other GlxI enzymes in *P. aeruginosa*, confirming that all three homologs are fully functional GlxI enzymes with wild type activity levels (Table 2.2). In comparison to dimeric *P. putida* GlxI, GloA3 has a higher rate for substrate turnover (k_{cat} for GloA3 $\approx$ 787 s^{-1}, k_{cat} for *P. putida* GlxI $\approx$ 115 s^{-1} and the catalytic efficiency differs threefold (2.6 x 10^6 M^{-1}s^{-1} for GloA3, 8.2 x 10^5 M^{-1}s^{-1} for *P. putida* GlxI) .

72

Table 2.2: Kinetic Parameters for *P. aeruginosa* GlxI Enzymes

Enzyme	K_m (μM)	V_{max} (μmol/min/mg)	k_{cat} (s^{-1})	k_{cat}/K_m (M^{-1}s^{-1})
GloA1[*]	Ni^{2+} : 32 ± 2	Ni^{2+}: 571 ± 28	Ni^{2+}: 271	Ni^{2+}: 8.5×10^6
	Co^{2+}: 16 ± 3	Co^{2+}: 180 ± 7	Co^{2+}: 86	Co^{2+}: 5.4×10^6
GloA2	Ni^{2+}: 21 ± 0	Ni^{2+}: 497 ± 8	Ni^{2+}: 247	Ni^{2+}: 1.2 x 10^7
	Co^{2+}: 24 ± 11	Co^{2+}: 75 ± 1	Co^{2+}: 37	Co^{2+}: 1.6 x 10^6
GloA3	287 ± 47	1176 ± 4	787	2.8 x 10^6

[*]Kinetic parameters for GloA1 are as described previously (3).

2.9 Discussion

Previous research has determined the existence of two biochemically distinct classes of GlxI

enzymes, a Zn^{2+}-activated and a non-Zn^{2+}-activated (but Ni^{2+}/Co^{2+} activated) class (3). Two distinct

classes of GlxI have now been identified and investigated in *P. aeruginosa*. The GlxI homologs

encoded in the *P. aeruginosa* genome provided an opportunity to investigate both metal activation

classes of this enzyme. GloA2 mirrors the kinetic characteristics and metal selectivity of previously

characterized non-Zn^{2+}-dependent GlxI enzymes very closely. Not only are the holoforms in this class

very similar, but the relative ease of obtaining apoenzyme preparations of the non-Zn^{2+}-dependent

GlxI enzymes is also observed. GloA3 in contrast, is expressed as a highly active Zn^{2+}-holoenzyme

from which the activating metal is quite difficult to remove. Difficulty in demetallating the

Zn^{2+}dependent GlxI enzymes has been observed with other GlxI in this metal activation class. For

example *P. putida* GlxI as characterized by St. Jean *et al.* required dialysis against 30 mM EDTA for 96 hours in order to obtain inactive enzyme. In addition the yeast GlxI enzyme cannot be re-constituted following extraction of its active site metal ion . In contrast to non-Zn^{2+}-activated GlxI enzymes, GloA3 can be reconstituted with Ni^{2+} as well as Zn^{2+} which has been observed with rat liver and sheep liver GlxI (also Zn^{2+}-dependent). Another observable characteristic of the Zn^{2+}-activated enzymes is that Mg^{2+} reconstitution is possible with the Zn^{2+}-dependent class members including GloA3, but is not a characteristic of non-Zn^{2+}-dependent GlxI enzymes (119).

An alignment comparison of all three *P. aeruginosa* GlxI enzymes indicates several interstitial regions present in the extended enzymes, but systematically absent in the shorter non-Zn^{2+}-dependent forms (Figure 2.9). The additional structural elements in the Zn^{2+}-dependent GlxI enzymes may also account for the observed recalcitrance of GloA3 to metal removal. For example, region A in Figure 2.8 corresponds to an α-helix turn proximal to the metal ligands as observed in the crystal structure for the human GlxI enzyme, a member of the Zn^{2+}-dependent class of this enzyme. It is possible that the active site of the Zn^{2+}-dependent GlxI enzymes is less open and more tightly assembled so that commonly used chelating agents are not useful for demetallation.

```
                                  20                      40                      60
                                   |                       |                       |
E. coli     - - - - - - - - - -  - - - - - - - - - -  - - - - - - - - - M  RLLHTMLRVG  DLQRSIDFYT  KVLGMKLLRT 31
GloA1       - - - - - - - - - -  - - - - - - - - - -  - - - - - - - - - M  RILHTMIRVG  NIDRSIDFYT  RVLGMTLLRK 31
GloA2       - - - - - - - - - -  - - - - - - - - - -  - - - - - - - - - M  RILHSMLRVA  DLEAALEFYT  RALDMRLLRR 31
GloA3       MSFNT- - - - -  - - -EVQPGIC  MEPDAITQEY  VFNHTMLRVK  DPKRSLDFYS  RVLGMRLLRR 52
P. putida   MSLHD- - - - -  - -LQTLPGVT  AQPDAATAQF  VFNHTMLRVK  DIEKSLDFYT  RVLGFRLVDK 53
H. sapiens  MAEPQPPSGG  LTDEAALSCC  SDADPSTKDF  LLQQTMLRVK  DPKKSLDFYT  RVLGMTLIQK 60
                                                                   *
                                  80         A            100         B           120
                                   |                       |                       |
E. coli     SENPEYKYSL  AFVGYGPETE  - - - - - - - - - -  - - - - -EAVIE  LTYNWG- - - -  -VDKYELGT- 70
GloA1       NDYPDGQFTL  AFVGYGNEAD  - - - - - - - - - -  - - - - -SAVIE  LTHNWG- - - -  -VDAYEIGT- 70
GloA2       RDYPEGRFTL  AFVGYQDERA  - - - - - - - - - -  - - - - -AAALE  LTHNWD- - - -  -RDGYTQGD- 70
GloA3       LDFEEGRFSL  YFLAMTRGEE  VPDAVDERQR  YTFGRQSVLE  LTHNWGSESD  DSQ-YHNGNQ 111
P. putida   RDFPEAAFSL  YFLALVDPAQ  IPADDTARHQ  WMKSIPGVLE  LTHNHGTEND  ADFAYHNGNT 113
H. sapiens  CDFPIMKFSL  YFLAYEDKND  IPKEKDEKIA  WALSRKATLE  LTHNWGTEDD  ATQSYHNGNS 120
                                                                   *
                  C                        140                     160                     180
                                            |                       |                       |
E. coli     - - -AYGHIAL  SVDNAAEACE  KIRQNGGNVT  REAGPVKGGT  TVIAFVEDPD  GYKIELIEEK 127
GloA1       - - -GYGHIAI  EVDDAYQACD  DIRYNGGQVT  REAGPMKHGT  TVIAFVTDPD  GYKIELIQKS 127
GloA2       - - -GYGHLAI  EVEDAAVTCA  RARALGYRVT  REAGLMQHGR  SVIAFLEDPD  GYKVELIQKG 127
GloA3       DPRGFGHICF  SVPDLVAACE  RFETLGVNFV  K- - -PLDRGM  KNVAFISDPD  GYWVEIVQAS 168
P. putida   DPRGFGHICI  SVPDVRAACA  RFEELEVPFQ  KR- -LQDGRM  NHLAFVKDPD  GYWVEIQPT 171
H. sapiens  DPRGFGHIGI  AVPDVYSACK  RFEELGVKFV  KK- -PDDGKM  KGLAFIQDPD  GYWIEILNPN 178
                  *                                                                 *

E. coli     DAGRGLGN- -  - 135
GloA1       S- - - - - - - - -  - 128
GloA2       TQFD- - - - - -  - 131
GloA3       LNGEMGRG- -  - 176
P. putida   ELEG- - - - - -  - 175
H. sapiens  KMATLM- - - -  - 184
```

Figure 2.9: Sequence alignment of *P. aeruginosa* GlxI enzymes (GloA1, GloA2 and GloA3; Accession Numbers are: AAG06912, AAG04099 and AAG08496 respectively) with other representative enzymes from both metal activation classes. Regions A-C are sequences that are not found in Ni^{2+}-activated GlxI enzyme.

P. aeruginosa as a multihost pathogen may be better endowed for successful colonization and propagation due to the presence of several MG detoxifying enzymes. A hypothetical basis for enhanced virulence could be functional under a broader set of divalent metal limiting conditions in *vivo*. Based on our own previous work with respect to Ni^{2+} activation of the *E. coli* enzyme and previously reported work (by Mannervik *et al.*) on the human Glx I which is Zn^{2+} activated, each of these metals are found by X-ray crystallography and by enzyme activity assays, that their importance lies in their active site binding and enzyme activation, as opposed to a structural role (50, 51, 52, 53, 60, 61, 120). In fact the current mechanism appears to indicate that the interaction of the substrate

with the active site metal is critical for catalysis (121, 122, 123). All the GlxI enzymes listed above are inactive when there is no metal ion in the active site. Additionally the *E. coli* enzyme shows no structural change in the protein in the absence of metal, indicating that the metal does not appear to control solely structural aspects of the enzymes (51, 52). Further characterization of GlxI expression in *P. aeruginosa* and the effect metal availability has on expression would be valuable for quantitating the proportion of each homolog as a contributor to MG detoxification in this bacterial species.

2.9.1 Putatative GlxI Homologs in *Salmonella typhimurium*

Campos-Bermudez *et al.*'s have reported the presence of three GlxI-encoding genes in the genome of *Salmonella typhimurium* (4, 124). Therefore it was of interest to determine how related each of the *S. typhimurium* GlxI homologs were to canonical GlxI sequences. The lactoylglutathione lyase-encoding gene *gloA* from this organism, designated STM1435 encodes a GlxI enzyme sharing 91% amino acid identity to *E. coli* GlxI (124). This gene likely encodes a GlxI enzyme for MG detoxification in *S. typhimurium*. The additional GlxI-like sequences are encoded by STM0235 (*yaeR*) and STM3117 (124). The STM3117 locus has been identified in previous studies as a gene that is upregulated in murine macrophage infections with *S. typhimurium* (43). Colonization of these host immune cells involves the formation of a *Salmonella*-containing vacuole that provides a hospitable environment for establishing infection although it is a nutrient limited compartment (43). STM3117 is subject to upregulation as part of the gene expression profile for *S. typhimurium* during macrophage colonization (43).

The protein encoded by *yaeR* aligns with glyoxalase family proteins in a BLASTP search of the non-redundant protein database at NCBI. Alignment with confirmed GlxI sequences from *E. coli* and *P. aeruginosa* indicates that all of the putative metal ligands are conserved in the *yaeR* gene

product. In fact the *S. typhimurium yaeR* gene product shares 88% identity with the same gene product in *E. coli*. The *yaeR* genes share 78% sequence identity at the nucleotide level. Additionally the chromosomal location of the *yaeR* locus appears conserved between *E. coli*, *S. typhimurium* and *Shigella flexneri* where it is situated between a lysine decarboxyalase encoding gene and a cell cycle control locus in all three genomic contexts. An alignment of the YaeR protein against *E. coli* GlxI reveals that all four metal ligands are conserved and given the presence of a *yaeR* gene in *E. coli* there is the potential for at least two functional GlxI enzymes in this species as well as *S. typhimurium*.

Based on genomic analysis the locus designated STM1435 is likely to encode a GlxI-enzyme. However phenotypic analyses of mutants for STM3117 and *yaeR* would be interesting to determine whether abolishing expression of these gene products enhances MG (Figure 2.9).

```
 E. coli  (AAC27133)       M--------------------------------RLLHTMLRVGDLQRSIDFYTKVLGM
STM1435                    M--------------------------------RLLHTMLRVGDLQRSIAFYTNVLGM
 Y. pestis  (CAL21009)     M--------------------------------RLLHTMLRVGDLQRSIDFYTKVLGM
GLOA1                      M--------------------------------RILHTMIRVGNIDRSIDFYTRVLGM
 GLOA2                     M--------------------------------RILHSMLRVADLEAALEFYTRALDM
 L. major  (AY604654)      M------------------------------PSRRMLHTMIRVGDLDRSIKFYTERLGM
GLOA3                      M--------SFNTEVQPGICMEPDAITQEYV-----FNHTMLRVKDPKRSLDFYSRVLGM
 P. putida  (NP_745896)    M-------SLHDLQTLPGVTAQPDAATAQFV-----FNHTMLRVKDIEKSLDFYTRVLGF
 H. sapiens  (NP_006699)   MAEPQPPSGGLTDEAALSCCSDADPSTKDFL-----LQQTMLRVKDPKKSLDFYTRVLGM
STM0235                    M---------------------------LGLKQVHHIAIIATDYAVSKAFYCDILGF
 STM3117                   M------------LFFNVASLKYKHHESIQMIIDRIDHLVLTVSDISTTIRFYEEVLGF


 E. coli                   KLLRTSENPEY---KYSLAFVGYGPETE--------------EAVIELTYNWGVDK---
 STM1435                   KLLRTSENPEY---KYSLAFVGYGPETE--------------EAVIELTYNWGVES---
 Y. pestis                 RLLRTSENTEY---KYSLAFVGYSDESK--------------GSVIELTYNWGVDQ---
GLOA1                      TLLRKNDYPDG---QFTLAFVGYGNEAD--------------SAVIELTHNWGVDA---
GLOA2                      RLLRRRDYPEG---RFTLAFVGYQDERA--------------AAALELTHNWDRDG---
 L. major                 KLLSRKDFEEA---KFSLYFLSF-PKDDIPKNKNGEPD-VFSAHGVLELTHNWGTEKNPD
GLOA3                      KLLSRKDFEEA---KYTLVFLGYGPEMS-------------STVLELTYNYGVTS---
 P. putida                RLVDKRDFPEA---AFSLYFLALVDPAQIPADDTARHQWMKSIPGVLELTHNHGTENDAD
 H. sapiens               TLIQKCDFPIM---KFSLYFLAYEDKNDIPKEKDEKIAWALSRKATLELTHNWGTEDDET
STM0235                   DLLSEVWREERDSWKGDLALNG-------------------QYVIELFS---------
STM3117                   SAVT---FKQN---RKALIFGAQKINLH--------------QQEME-----------


 E. coli                  --YELGT---------AYGHIAL-SVDNAAEACEKIRQNGGNVTREAGPVKG----GTTV
STM1435                   --YDMGN---------AYGHIAL-SVDNAAEACERIRQNGGNVTREAGPVKG----GSTI
 Y. pestis                --YDMGT---------AFGHLAL-GVDDVAATCDQIRQAGGKVTREAGPVKG----GNTI
GLOA1                     --YEIGT---------GYGHIAI-EVDDAYQACDDIRYNGGQVTREAGPMKH----GTTV
GLOA2                     --YTQGD---------GYGHLAI-EVEDAAVTCARARALGYRVTREAGLMQH----GRSV
 L. major                --YKHDE---------AYGHIAI-GVEDVKELVADMRKHDVPIDYE-----D----ESGF
GLOA3                     SQYHNGNQDP-R----GFGHICF-SVPDLVAACERFETLGVNFVK---PLDR----GMKN
 P. putida               FAYHNGNTDP-R----GFGHICI-SVPDVRAACARFEELEVPFQKR--LQDG----RMNH
 H. sapiens              QSYHNGNSDP-R----GFGHIGI-AVPDVYSACKRFEELGVKFVKK--PDDG----KMKG
STM0235                  --FPFPPARPSRPEACGLRHLAF-SVENVENAVAHLEKHQVKCE----PIRIDPY-TGKR
STM3117                  --FEPKASRPTP----GSADLCFITSTPINDVVSEILQAGISIVEG--PVERTGATGEIM


 E. coli                  IAFVEDPDGYKIELIEEKDAGRGLGN--------------------------------
STM1435                   IAFVEDPDGYKIELIEAKDAGRGLGN--------------------------------
 Y. pestis                IAFVEDPDGYKIELIENKSAGDCLGN--------------------------------
GLOA1                     IAFVTDPDGYKIELIQKSS-----------------------------------------
GLOA2                     IAFLEDPDGYKVELIQKGTQFD-------------------------------------
 L. major                MAFVVDPDGYYIELLNEKTMMEKAEAD---------------------------------
GLOA3                     VAFISDPDGYWVEIVQASLNGEMGRG----------------------------------
 P. putida               LAFVKDPDGYWVEVIQPTELEG-------------------------------------
 H. sapiens              LAFIQDPDGYWIEILNPNKMATLM-----------------------------------
STM0235                  FTFFNDPDGLPLELYEQ------------------------------------------
STM3117                  SIYIRDPDGNLIEISQYV----------------------------------------
```

Figure 2.10: Alignment of *S. typhimurium* GlxI homologs. STM numbers identify the GlxI homologs from *S. typhimurium* as indexed in The Insitiute for Genomic Research (TIGR) microbial database. NCBI accession numbers for for *E. coli*, *Y. pestis*, *L. major*, *P. putida* and *H. sapiens* GlxI sequences are indicated above. GloA1, GloA2 and GloA3 designate the three GlxI homologs in *P. aeruginosa*.

78

Chapter 3 Characterization of *Escherichia coli* Glyoxalase II

Escherichia coli GlxI is the first non-Zn^{2+}-activated GlxI enzyme reported upon in the biochemical literature (51). Non-Zn^{2+}-dependent GlxI enzymes constitute a second metal activation class of this enzyme (the first being Zn^{2+}-dependent GlxI enzymes), based on the prevalence of this metal activation profile amongst GlxI enzymes from bacteria and parasites (Leishmanial and Trypanosomal) (3, 67, 69).

For organisms with non-Zn^{2+}-dependent GlxI, it is worth investigating whether the GlxII enzyme in this system mirrors the metal activation requirements of the first enzyme. If both proteins in a given Glx system have the same metal ion requirement, the system could be subject to regulation based on availability of the activating metal. It is also possible that the upregulation of Glx system enzymes may in turn affect the regulation of systems that affect the transport of metal ions required to assemble these proteins in their fully functional states. Firstly it is important to test that both GlxI and GlxII in a given organism require the same metal ion for activation.

Most of the GlxII enzymes characterized to date have been obtained from eukaryotic organisms, notably *Homo sapiens* and *Arabidopsis thaliana*. Chapter One outlines structural features of this enzyme in detail that are briefly summarized here. GlxII enzymes are monomers that are members of the Zn^{2+}-metallohydrolase family with a conserved fold that is observed in metallo-β-lactamase enzymes (77). Crystal structures indicate that the active sites of both GlxII and metallo-β-lactamase enzymes indicate that the active sites typically contain a binuclear metal centre (77). Initial characterization of *A. thaliana* GlxII led Ridderstrom and Mannervik to conclude that the enzyme was metal-independent because the activity was unchanged with the addition of Zn^{2+} or Mg^{2+} ions to the growth medium during expression (75). However the Zn^{2+} activation of cytoplasmic *A. thaliana* GlxII was finally confirmed based on inductively coupled plasma atomic emission spectroscopy

(ICP-AES) analysis by Crowder *et al* (76). Active forms of the *A. thaliana* GlxII have been isolated with heterogeneously metallated active sites (79, 80). The cytoplasmic GlxII enzyme from *A. thaliana* is produced in *E. coli* with a binuclear iron/zinc active site (79, 80). The metal content of recombinant *A. thaliana* GlxII metal content can be biased depending on the metal chloride supplied to the host *E. coli* cells during growth in minimal medium (80). The kinetic parameters are comparabable for *A. thaliana* GlxII loaded with Mn^{2+}, Fe^{2+} or Zn^{2+} by metal supplementation in minimal medium during growth and induction (80).The GlxI- and GlxII-encoding genes in *E. coli* are designated *gloA* and *gloB* respectively. These genes are not clustered in an operon, but are situated at discrete locations on the *E. coli* chromosome. The map position of the *gloA* is 1,725,861-1,726,268 nucleotides while *gloB* is encoded between nucleotides 234,027-234,782 as indicated in the EcoCyc database (125). Therefore there is no evidence of coordinated gene expression for these two enzymes. As mentioned previously, the GlxI enzyme from *E. coli* is not Zn^{2+}-activated. However the GlxII enzyme from an organism with a non-Zn^{2+}-dependent GlxI enzyme has not been characterized previously. In this chapter the isolation and biochemical characterization of *E. coli* GlxII is described (126). The bulk of this research was conducted by Jason O'Young, who was an undergraduate member of the Honek laboratory at the time (126). This work demonstrates that GlxII has been conserved as a binuclear monomeric Zn^{2+}-metallohydrolase, possessing the conserved active site consensus sequence for metal binding (126).

3.1 Materials and Methods

3.1.1 Materials

See Chapter 2, section 2.5 for materials referred to in the described methods.

3.1.2 Theoretical Calculations

Calculations to determine theoretical molecular mass and pI were performed using ProtParam on the ExPASy Proteomics Server (http://www.expasy.org/tools/protpar-ref.html; Geneva, Switzerland) (116).

3.1.3 DNA Manipulation and Plasmid Construction

All manipulation of DNA and plasmid isolation was performed according to the protocols of Sambrook and Russell (127). The putative Glyoxalase II gene sequence (GeneID 944902) was amplified from an *E. coli* K-12 (strain MG1655) genomic template by PCR using the following primer pair:

GloBF: 5′-CCAGTCGACCATATGAATCTTAACAGTATTCCCGCC-3′

GloBR: 5′-CCAGGATCCTCAGAACCTATCTTTCTTTGACC-3′

Primers were obtained from Sigma Genosys (Oakville, ON, Canada). Thermal cycling was performed on a thermal cycler from Techne (Staffordshire, UK). The desired PCR products were excised from a 1.5% agarose gel following electrophoretic analysis and purified using an ELU-QUIK DNA purification kit from Scheleicher and Schuell (Keene, NH, USA) and subjected to *Nde*I and *Bam*HI (New England Biolabs, Ipswich, MA, USA) restriction endonuclease digestion. The digestion products were subsequently ligated into a pET22b expression vector (amp^r, T7 *lac* promoter, f1 origin of replication; Novagen, Madison, WI, USA), which had also been digested with the above restriction endonucleases to generate construct pGloB. Sequencing of plasmid constructs was performed by

81

MOBIX (Hamilton, Ontario, Canada). The cloned *gloB* gene was sequenced in the 5' to 3' and 3' to

5' directions using the T7 forward and reverses primers respectively. pGloB was propagated in *E.*

coli strain DH5α, isolated, and transformed by heat shock into CaCl$_2$-treated *E. coli* BL21(λDE3)

competent cells for recombinant protein production.

3.1.4 Expression and Purification of *E. coli* GlxII

A one liter LB culture of BL21(λDE3)/pGloB supplemented with 50 mg/L of carbenicillin was grown

to an optical density (OD$_{600nm}$) of 0.7 before induction of *gloB* expression with IPTG at a final

concentration of 0.5 mM. Induction of the culture was allowed to proceed for 4 h before recovery of

the cells by centrifugation at 6000*g* for 15 min. The cells were resuspended in 50 mM Tris buffer, pH

8.0, and re-pelleted at 6000*g* for 15 min and flash frozen in liquid N$_2$ for storage at −80 °C.

Frozen BL21(λDE3)/pGloB cells (1 g) were suspended in 50 mM Tris, pH 8.0, buffer (5 mL)

and the suspension was disrupted by sonication followed by the addition of phenylmethylsulfonyl

fluoride (PMSF) to 1 mM final concentration (added from a 1 M stock), and glycerol to 10% (v/v).

Cellular debris was removed by centrifugation at 48,300*g* for 15 min at 4 °C. The recovered

supernatant was filtered through a 0.2 μM filter (Acrodisc Ion Chromatography filter, Pall Life

Sciences, Ann Arbor, MI) then loaded onto a 10/30 Q-Sepharose column (Amersham Biosciences,

Uppsala, Sweden) with elution utilizing a gradient of 0–1 M KCl (in 50 mM Tris, pH 8.0) over a

100 min interval (flow rate of 0.8 mL/min). Fractions identified by SDS–PAGE analysis and kinetic

assay (corresponding to 50–60% KCl) were pooled and dialyzed against 50 mM Tris, pH 6.5,

overnight at 4 °C. The dialyzed sample was diluted to 5 mL and filtered using a 0.2 μm filter prior to

loading onto a 5/5 Mono-Q column. Elution was accomplished by applying a gradient of 0–1 M KCl

(in 50 mM Tris, pH 6.5) over a 100 min interval (flow rate of 0.5 mL/min). Fractions identified by

SDS–PAGE analysis and kinetic assay (corresponding to 25–30% KCl) were pooled and dialyzed at 4 °C against 50 mM phosphate buffer, pH 6.5, overnight.

Solid $(NH_4)_2SO_4$ was added to the dialyzed sample, for a final concentration of 1.7 M and the resulting solution after filtration (0.2 μm filter, Pall,) was loaded onto a Phenyl HP Hi Sub column (1 mL). The sample was loaded onto the column with 1.7 M $(NH_4)_2SO_4$ in 50 mM potassium phosphate buffer (pH 6.5). Elution was accomplished utilizing a gradient of 1.1–0 M ammonium sulfate in 50 mM potassium phosphate buffer (pH 6.5) applied over a 20 min period (flow rate of 0.5 mL/min). Fractions identified by SDS–PAGE analysis and kinetic assay (corresponding to approximately 0.25–0.5 M $(NH_4)_2SO_4$) were pooled and dialyzed at 4 °C against 50 mM Tris, 100 mM KCl, pH 7.5, overnight. The dialyzed sample was filtered (0.2 μm) and loaded onto a Superdex 75 column utilizing 50 mM Tris, 100 mM KCl, pH 7.5, as eluting buffer. Fractions were analyzed by SDS–PAGE, where *E. coli* GlxII was identified as a band migrating approximately the same distance as the 30 kDa marker (carbonic anhydrase) in the size standard. The enzyme was stored in 50 mM Tris, pH 7.5, at 4 °C. The enzyme appeared homogeneous in purity after gel filtration as determined by SDS–PAGE with Coomassie brilliant blue staining of protein (data not shown).

3.1.5 Molecular Mass Determination and Mass Determination for Native GlxII

The molecular mass of the recombinant *E. coli* GlxII was determined utilizing electrospray ionization mass spectrometry. Samples were introduced into a Micromass Q-TOF Global Ultima mass spectrometer using an eluant of 50:50 H_2O:acetonitrile plus 0.2% formic acid. Samples were run in positive ion mode and *m/z* ratios were deconvoluted using the MaxEnt1 algorithm in the MassLynx (V4.0, Micromass Limited/Waters, Milford, MA) software. SDS–PAGE was utilized to screen for GlxII during purification. Separation of purification fractions was performed on a PhastSystem electrophoresis unit using 10–15% gradient gels (Amersham Biosciences, Uppsala, Sweden). Proteins

were visualized on the gels by Coomassie brilliant blue staining. The quaternary structure of GlxII was determined by gel filtration using a 10/30 Superdex 75 (Amersham Biosciences, Uppsala, Sweden) column as described above, employing the appropriate protein standards. Injections were performed in triplicate for native molecular mass determination.

3.1.6 Glx II Enzyme Assay

Glyoxalase II enzymatic activity was determined as previously reported by Marasinghe *et al.* in 50 mM MOPS, pH 7.1 buffer (based upon pH optimization for activity assay) (2). S-lactoylglutathione (SLG) was utilized as the substrate in these assays. The decrease in absorbance due to hydrolysis of the SLG ($\varepsilon = 3.1 \text{ mM}^{-1} \text{ cm}^{-1}$) was monitored at 240 nm (2). The activity assay for identification of column fractions was performed at a substrate concentration of 500 µM. All activity assays for *E. coli* GlxII were performed using a Cary 3 UV–vis spectrophotometer (Varian, Mississauga, ON) with assays conducted at 25 °C (Pelletier cooling), and data were collected using the Kinetics module of CaryWinUV version 3.0 (Varian, Mississauga, ON).

3.1.7 Kinetic Analysis

Determination of the Michaelis constant, K_m, and the maximal enzyme velocity, V_{max}, for *E. coli* GlxII involved measurement of the initial reaction rate utilizing 10 substrate concentrations ranging between 50 and 500 µM. Assays were performed in 1 mL of substrate with 0.002 mg of GlxII added per replicate. The enzyme stock was diluted with 50 mM MOPS, pH 7.1. Data were fitted by least squares linear regression using GraFit version 3.01 (Erithacus Software).

3.1.8 Metal Analysis

Metal-free water was prepared by passing Milli-Q grade water through Chelex 100 resin obtained from Bio-Rad (Mississauga, Ontario, Canada). Purified enzyme solution was exchanged into metal-

free water by utilizing a Centricon® (Millipore) ultrafiltration device with a 10 kDa cut off membrane,. All plastic containers were presoaked with nitric acid (10% v/v) and rinsed with Chelex-treated water. Metal content of purified GlxII was determined using Inductively Coupled Plasma Mass Spectrometry (ICP-MS). This analysis was performed at the EnviroTest Laboratory, which is now the Waterloo branch of ALS Laboratories (Waterloo, Canada) The following elements were analyzed for using this method: Al, Sb, As, Ba, Be, Bi, B, Cd, Ca, Cr, Co, Cu, Fe, Pb, Mg, Mn, Mo, Ni, P, K, Se, Si, Ag, Na, Sr, Tl, Sn, Ti, W, U, V, Zn, and Zr.

3.1.9 Metal activation Studies

Purified *E. coli* GlxII was incubated (final concentration of 27.8 μM) with 50 mM dipicolinic acid DPA in 50 mM MOPS, pH 7.0, for 4 h at 4 °C. The DPA was removed from the GlxII sample by centrifugal ultrafiltration with a 10 kDa cut-off Nanosep device (Pall Life Sciences, Ann Arbor, MI, USA). This ultrafiltration step was used to change the GlxII buffer to 50 mM MOPS, pH 7.0. The MOPS buffer was treated prior to usage with Chelex 100 (Bio-Rad, Mississauga, Ontario, Canada) resin to remove any potentially contaminating and re-activating divalent metal ions. The final concentration of DPA-treated GlxII was determined by the method of Bradford to be 36.9 μM ($\approx$ 1.04 mg/mL which is within the range of detection by this protein quantitation method). This enzyme stock was used to set up metal reconstitution incubations containing 5 μM GlxII, 6 equivalents of $MnCl_2$, $NiCl_2$, $ZnCl_2$, and $CoCl_2$ (final concentration 30 μM), in 50 mM MOPS, pH 7.0 (Chelex-treated). The enzyme was incubated with metal for 16 h prior to assay in 0.5 mM SLG (dissolved in 50 mM MOPS, pH 7.1). The assay was performed in triplicate using 500 μL of substrate, using 0.71 μg GlxII per replicate.

3.2 Results

The *gloB* gene in *E. coli* codes for a GlxII enzyme 251 amino acids in length with a predicted

molecular mass of 28434 Da. Sequence alignment of the *E. coli* GlxII enzyme with other

characterized GlxII sequences reveals that it possesses the typical conserved residues associated with

Zn^{2+}-binding including the T-H-X-H-X-D-H motif (Figure 4.1) (77). The cloning of *E. coli gloB* into

pET22b generated an expression vector (named pGloB) for GlxII production in *E. coli* Bl21(λDE3)

cells.

```
                                              20                   40                   60
                                              |                    |                    |
                         E. coli  - - - - - - - - - -  - - - - - - - - - -  - - - - - - - - - -  - - - - - - - - - -  - - - - - - - - - -  - - - - - - - - - -
                      H. sapiens  - - - - - - - - - -  - - - - - - - - - -  - - - - - - - - - -  - - - - - - - - - -  - - - - - - - - - -  - - - - - - - - - -
         A. thaliana cytoplasmic  - - - - - - - - - -  - - - - - - - - - -  - - - - - - - - - -  - - - - - - - - - -  - - - - - - - - - -  - - - - - - - - - -
A. thaliana mitochondrial precursor  MPVISKASST  TTNSSIPSCS  RIGGQLCVWP  GLRQLCLRKS  LLYGVMWLLS  MPLKTLRGAR 60
           P. falciparum targeted  - - - - - - - - - -  - - - - - - - - - -  MRFLKTLFSL  NCLASVGFYK  KFACKNLFFE  NSFIRKDLHT 40
               S. cerevisiae GLO4  - - - - - - - - - -  - - - - - - - - - -  - - - - - - - - - -  - - - - - - - - - -  - - - - - - - - - -  - - - - - - - - - -
               S. cerevisiae GLO2  - - - - - - - - - -  - - - - - - - - - -  - - - - - - - - - -  - - - - - - - - - -  - - - - - - - - - -  - - - - - - - - - -

                                              80                  100                  120
                                              |                    |                    |
                         E. coli  - - - - - - - - - -  - - - - - - -MNL  NSIPAFDD- -  - -NYIW-VLN  DEAGRCLIVD  PGDAEPVLNA 38
                      H. sapiens  - - - - - - - - - -  - - - - - - -MKV  EVLPALTD- -  - -NYMYLVID  DETKEAAIVD  PVQPQKVVDA 39
         A. thaliana cytoplasmic  - - - - - - - - - -  - - - - - - -MKI  FHVPCLQD- -  - -NYSYLIID  ESTGDAAVVD  PVDPEKVIAS 39
A. thaliana mitochondrial precursor  KTLKITHFCS  ISNMPSSLKI  ELVPCSKD- -  - -NYAYLLHD  EDTGTVGVVD  PSEAAPVIEA 116
           P. falciparum targeted  YFIDKRKYFH  LNKKDICTNT  IIIPFYKD- -  - -NYSYIFYD  DKE-EGIVVD  PAD-YNIIND 94
               S. cerevisiae GLO4  - - - - - - -MKF  LLQQIRNMHV  KPIKMRWLTG  GVNYSYLLST  EDRRNSWLID  PAEPLEVSPK 53
               S. cerevisiae GLO2  - - - - - - - - - -  - - - - - - -MQV  KSIKMRWESG  GVNYCYLLSD  SKNKKSWLID  PAEPPEVLPE 43

                                             140                  160                  180
                                              |                    |                    |
                         E. coli  IAA-NNWQPE  AIFL[THHHHD  H]VGGVKELVE  KF- - - - - -PQ  IVVYGP- -QE  TQDKGTTQVV 89
                      H. sapiens  ARK-HGVKLT  TVLT THHHWD  H]AGGNEKLVK  LE- - - - - -SG  LKVYGG- -D-  DRIGALTHKI 89
         A. thaliana cytoplasmic  AEK-HQAKIK  FVLT THHHWD  H]AGGNEKIKQ  LV- - - - - -PD  IKVYGG- -SL  DKVKGCTDAV 90
A. thaliana mitochondrial precursor  LSR-KNWNLT  YILN THHHDD  H]IGGNAELKE  RY- - - - - - -G  AKVIGSAVDK  DRIPGIDILL 168
           P. falciparum targeted  ISKKENIKIK  HVLC THKHSD  H]NNGNQYYYE  K- - - - - - - -N  INVYGIKEYD  NKYINQDI- - 144
               S. cerevisiae GLO4  LSAEEKKSID  AIVN THHHYD  H]SGGNLALYS  ILCQENSGHD  IKIIGGSKSS  PGVT- - - -EV 109
               S. cerevisiae GLO2  LTEDEKISVE  AIVN[THHHYD  H]ADGNADILK  YLKEKNPTSK  VEVIGGSKDC  PKVT- - - -II 99

                                             200                  220                  240
                                              |                    |                    |
                         E. coli  KDGETAFVLG  HEFSV- -IAT  PGHTLGHICY  F- - - - - - -SK  PYLF-CGDTL  FSGGCGRLFE 139
                      H. sapiens  THLST-LQVG  S-LNVKCLAT  PCHTSGHICY  FVSKPGGSEP  PAVF-TGDTL  FVAGCGKFYE 146
         A. thaliana cytoplasmic  DNGDK-LTLG  QDINILALHT  PCHTKGHISY  YVNGKEG-EN  PAVF-TGDTL  FVAGCGKFFE 147
A. thaliana mitochondrial precursor  KDSDKWMFAG  HEVRI- -LDT  PGHTQGHISF  YFPG- - - - -S  ATIF-TGDLI  YSLSCGTLSE 220
           P. falciparum targeted  -SNLTHFQIN  -NFKINIFLS  NFHSKNQVSY  LIENDNNKSK  KNIFFTGDFL  FISGIGKNFE 202
               S. cerevisiae GLO4  PDNLQQYHLG  -NLRVTCIRT  PCHTKDSICY  YIKDLETGEQ  -CIF-TGDTL  FIAGCGRFFE 166
               S. cerevisiae GLO2  PENLKKLHLG  -DLEITCIRT  PCHTRDSICY  YVKDPTTDER  -CIF-TGDTL  FTAGCGRFFE 156
                                                                          *

                                             260                  280                  300
                                              |                    |                    |
                         E. coli  GTASQMYQSL  -KKLSALP- -  - - -DDTLVCC  AHEYTLSNMK  FALSILPHDL  SINDYYRKVK 193
                      H. sapiens  GTADEMCKAL  LEVLGRLP- -  - - -PDTRVYC  GHEYTINNLK  FARHVEPGNA  AIREKLAWAK 201
         A. thaliana cytoplasmic  GTAEQMYQSL  CVTLAALP- -  - - -KPTQVYC  GHEYTVKNLE  FALTVEPNNG  KIQQKLAWAR 202
A. thaliana mitochondrial precursor  GTPEQMLSSL  -QKIVSLP- -  - - -DDTNIYC  GRENTAGNLK  FALSVEPKNE  TLQSYATRVA 274
           P. falciparum targeted  QDNEDLYNSI  NKLKL- - - - -  LDKQNIYIFC  GHEYTLDNLK  FALTVDSTNK  NLLSFYDHVV 257
               S. cerevisiae GLO4  GTGRDMDMAL  NQIMLRAVGE  TNWNKVKIYP  GHEYTKGNVS  FIRAKIYSDI  GQNKEFDALE 226
               S. cerevisiae GLO2  GTGEEMDIAL  NNSILETVGR  QNWSKTRVYP  GHEYTSDNVK  FVR-KIYPQV  GENKALDELE 215
                                                                          *

                                             320                  340                  360
                                              |                    |                    |
                         E. coli  ELRAKNQITL  PV-ILKNERQ  INVFLRTEDI  DLINVIN- - -  - -EETLLQQP  EERFAWLRSK 247
                      H. sapiens  EKYSIGEPTV  PS-TLAEEFT  YNPFMRVRE-  - - -KTVQ- - -  - -QHAGETDP  VTTMRAVRRE 251
         A. thaliana cytoplasmic  QQRQADLPTI  PS-TLEEELE  TNPFMRVDK-  - - -PEIQ- - -  - -EKLGCKSP  IDTMREVRNK 252
A. thaliana mitochondrial precursor  HLRSQGLPSI  PT-TVKVEKA  CNPFLRISSK  DIRKSLS- - -  - -IPDSATE-  AEALRRIQRA 327
           P. falciparum targeted  N-SNKNYPTV  PT-LLEHEYL  YNPFLRCDQN  DVRKSIDLYA  KKKNIKIQQE  SDYIVILRLM 315
               S. cerevisiae GLO4  QYCKSNECTT  GHFTLRDELG  YNPFMRLDDR  AVRLAVG- - -  - -DTAGTYPR  SVVMQELRKL 281
               S. cerevisiae GLO2  QFCSKHEVTA  GRFTLKDEVE  FNPFMRLEDP  KVQKAAG- - -  - -DTNNSWDR  AQIMDKLRAM 270


                         E. coli  KDRF - - - - -  251
                      H. sapiens  KDQFKMPRD   260
         A. thaliana cytoplasmic  KDQWRG - - -  258
A. thaliana mitochondrial precursor  RDRF - - - - -  331
           P. falciparum targeted  KDNFKAS - -  322
               S. cerevisiae GLO4  KNAM - - - - -  285
               S. cerevisiae GLO2  KNRM - - - - -  274
```

Figure 3.1: Alignment of GlxII amino acid sequences. *E. coli* GlxII is indexed with the NCBI accession number: AAC73317. The other GlxII sequences include *H. sapiens*, *A. thaliana* cytoplasmic and mitochondrial (pre-protein sequence shown), *P. falciparum* GlxII pre-protein, and *S. cerevisiae* isoforms of GlxII (NCBI Accession numbers are: CAA62483, NP_187696, NP_565999, AAQ05976, CAA58065, CAA71335 respectively). The % identity of these GlxII relative to the *E. coli* enzyme are 34%, 36%, 38%, 28%, 30% and 33%, respectively. The box indicates the THxHxDH active site motif and asterisks indicate other metal binding histidine residues. The alignment was created in CLC Free Workbench (CLC bio A/S) version 3.0.1 using the accurate alignment algorithm.

87

IPTG-induced cultures of BL21(λDE3)/pGloB produce significant levels of soluble GlxII within four hours of induction. Active holo-GlxII could be recovered from lysates of induced cells following anion exchange, hydrophobic interaction and gel filtration chromatographic steps respectively. The molecular mass of the recombinant protein is in accordance with the predicted mass as assessed by ESMS (Figure 3.2). The purified enzyme from these enrichment steps is approximately 85% pure as assessed from SDS-PAGE with Coomassie Brilliant Blue staining (Figure 3.3). ICP-MS analysis of purified *E. coli* GlxII indicates the presence of Zn^{2+} in the protein at a ratio of 1.7 equivalents per mol monomeric enzyme (native protein size confirmed by analytical size exclusion chromatography). The metal:enzyme ratio was also confirmed by subjecting the GlxII to a denaturing colorimetric PAR assay (118). These two methods of metal analysis are in agreement with recombinant *E. coli* GlxII being produced as a binuclear zinc holoenzyme.
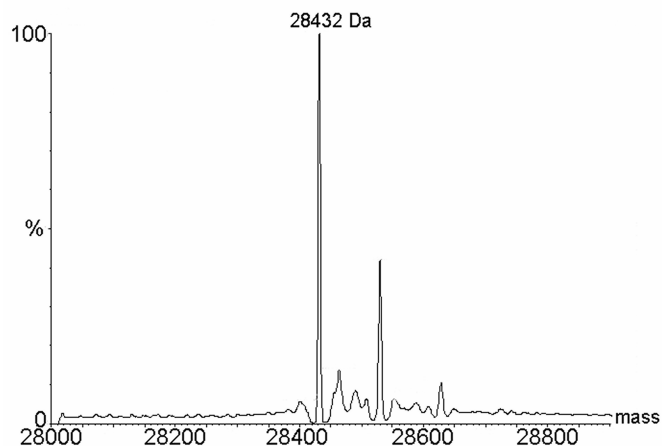
Figure 3.2: ESMS for purified *E. coli* GlxII. The peak for GlxII is labelled with the observed molecular mass which compares favourably to the predicted value of 28434 Da.
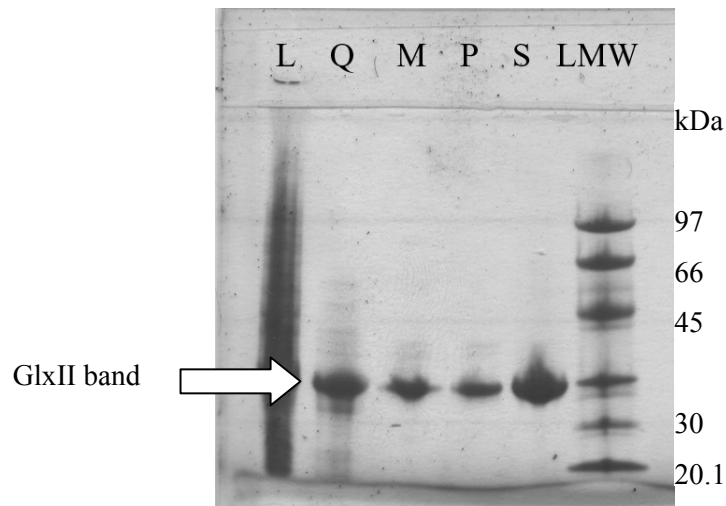
Figure 3.3: SDS-PAGE purification summary for *E. coli* GlxII. L = lysate, Q = fractions from Q-Sepharose Fast Flow, M = fractions from MonoQ, P = fractions from Phenyl HP High Sub, LMW= low molecular weight marker. Marker sizes are indicated to the right of the figure and the arrow points to the band identifiable as *E. coli* GlxII.

Prior to kinetic characterization of *E. coli* GlxII, an initial pH profile (pH range surveyed was 5.5-9.5) was constructed by assaying for activity at concentrations of SLG exceeding typical K_m values for the enzyme. From this profile it was established that kinetic parameters for *E. coli* GlxII would be obtained at a pH of 7.1.

The kinetic parameters obtained for the overproduced Zn^{2+}-GlxII are comparable to the values for previously characterized enzymes from other sources. Kinetic constants determined on the purified protein using SLG are listed in Table 3.1. Catalytic efficiency of *E. coli* GlxII most closely resembles that of the *Plasmodium falciparum* tGloII and *C. albicans* enzymes (Table 3.1) (128, 129). The *E. coli* GlxII falls well within the range of catalytic efficiencies for other GlxII enzymes such as the bovine liver and *Saccharomyces cerevisiae* cytoplasmic forms (Table 3.1) (11, 130).

Table 3.1: Kinetic Parameters for Various GlxII Enzymes[*]

[*]Parameters in bold are those that are close in magnitude to those obtained for *E. coli* GlxII

GlxII Source	k_{cat} (s^{-1})	K_m (μM)	k_{cat}/K_m (M^{-1}s^{-1})
E. coli **(126)**	**53 ± 11**	**184 ± 22**	**4.7 × 10^5**
P. falciparum **(tGloII) (128)**	**64.3**	**225**	**2.9 x 10^5**
P. falciparum (cGloII) **(128)**	119.6	100	1.19 x 10^6
Human liver (147)	780	187	4.17 x 10^6
Yeast Glo-2 (130)	979	112	8.7 x 10^6
YeastGlo-4 (130)	723	72.2	10x10^6
A. thaliana Glx2-2 (80)	408	220	1.9 x 10^6
A. thaliana **Glx2-5 (mitochondrial) (3)**	**129**	**391**	**3.3 x 10^5**
Bovine liver (11)	ND	190	0.023x10^6
S. typhimurium **(4)**	**168.8**	**408**	**3.5 x 10^5**
C. albicans **(129)**	**142**	**177**	**8.0 x 10^5**

Human GlxII has been studied to characterize refolding and zinc activation after guanidinium HCl denaturation of the enzyme in the presence of EDTA (131). This approach was attempted in our lab for preparation of apo-*E. coli* GlxII. The unfolding/refolding protocol developed for *Pseudomonas aeruginosa* alkaline protease in the Honek laboratory was adapted to *E. coli* GlxII for this purpose (132). Unfortunately, the final yield of protein was insufficient for quantitation and in some cases was so poor that no measurable GlxII activity was detected in the prepared samples. For a survey of metal specificity, a demetallated *E. coli* GlxII preparation was obtained by incubating the enzyme with 2,6-pyridinedicarboxylic acid (DPA). The chelator was removed from the protein sample by ultrafiltration. Several equivalents of the metal chloride were added to the DPA-treated GlxII and activity was screened for in 0.5 mM *S*-lactoylglutathione in 50 mM MOPS pH 7.0.

Interestingly, reconstitution with $ZnCl_2$ did not enhance the activity of the DPA-treated enzyme (Figure 3.4). Addition of $ZnCl_2$ to the active holoenzyme has no additive or detrimental effect on the observed catalytic activity of *E. coli* GlxII (data not shown). This is intriguing since the recombinant holoenzyme was found to contain Zn^{2+}. Analysis of the *E. coli* GlxII sequence revealed the presence of several cysteine residues. It is possible that the DPA-demetallated GlxII is rendered inactive by Zn^{2+} mismetallation that occludes the active site of the enzyme (which may or may not be appropriately metallated). It is also possible that the mismetallated GlxII has assumed an inactive conformation. Importantly adding Ni^{2+} ions to the DPA-treated enzyme does not increase activity (Figure 3.4). This together with the metal analysis confirms that the *E. coli* GlxII is conserved in nature as a Zn^{2+}-activated metallohydrolase. Furthermore this finding clarifies that the Glx system in *E. coli* does not have a uniform Ni^{2+} ion requirement. It is only the first enzyme of the pathway that has diverged in metal selectivity. The reconstitution of DPA-treated GlxII with Mn^{2+} and Co^{2+} was particularly efficacious indicating the relaxed metal selectivity of *E. coli* GlxII in contrast to the GlxI enzyme from the same organism (Figure 3.4).
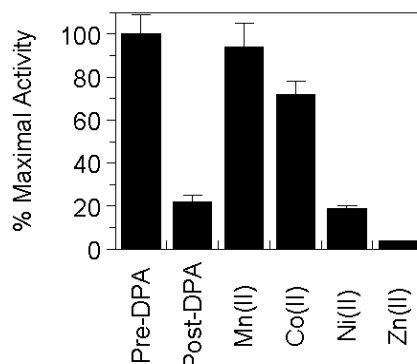
Figure 3.4: Relative re-activation of DPA-treated *E. coli* GlxII with various divalent metal ions. The bar labeled Pre-DPA denotes the activity of the recombinant GlxII holoenzyme after purification. This activity represents the maximal activity (100%) observable for the native enzyme. All other enzyme activity percentages in this figure are relative to this holoenzyme activity. The bar labeled Post-DPA denotes the activity of DPA-treated GlxII without the addition of any re-activating metal chlorides. The bars labeled Mn(II), Co(II), Ni(II), and Zn(II), represent relative activities of DPA-treated enzyme following addition of activating metal chlorides as indicated in the experimental procedure. The error bars represent the standard deviation for the activity of the triplicate assays.

3.3   Discussion

The characterization of *E. coli* GlxII described herein is sufficient to confirm that it is a Zn^{2+}-dependent hydrolase. Our investigation did not examine how the metal content of the enzyme can be changed with different supplemental metals during growth as with the studies of *A. thaliana* GlxII. Differential metal incorporation into *E. coli* GlxII was not part of the scope of research for this investigation, but should be revisited in light of the various holoforms recently characterized for the highly related *Salmonella typhimurium* GlxII.

This recent report of promiscuous metal selectivity in GlxII comes from the published characterization of the enzyme from *Salmonella typhimurium* (4), published subsequent to our

92

reported findings on the GlxII enzyme from *E. coli* (126). The GlxII from this Gram-negative species is 78% identical and 89% similar to the *E. coli* enzyme at the amino acid level.

The recombinant *S. typhimurium* GlxII as expressed in *E. coli* contains 1.15 equivalents of metal per monomeric enzyme, with Mn^{2+}, Fe^{2+} and Zn^{2+} as the contributing metal ions in the sample (4). When *S. typhimurium* GlxII is produced in *E. coli* under minimal medium growth conditions with specific metal supplementation (Mn^{2+}, Fe^{2+} and Zn^{2+}) the metal content of the enzyme reflects the ions present during overproduction (4). This is similar to the results obtained for differential metal loading of recombinant *A. thaliana* GlxII under minimal medium growth conditions as described in Chapter 1 (80).

Sub-stoichiometric amounts of metal are present in the *S. typhimurium* GlxII enzyme whether it is produced in rich medium or minimal medium with metal supplementation (4). The reason for this < 2 metal per monomer ratio is attributed to loss of metal ions from the active site during purification (4). Catalytic efficiency values for the enzyme either from rich media or loaded with Mn^{2+}, Fe^{2+} and Zn^{2+} are comparable reflecting a relaxed stringency for metal utilization in GlxII, which has been observed with the *A. thaliana* enzyme (4).

Electron paramagnetic resonance (EPR) studies have been conducted on the *S. typhimurium* GlxII enzyme, revealing that a range of metal centres can be observed for this enzyme including magnetically coupled Fe(III) and magnetically uncoupled Fe(II)/Fe(III) (4). The observation of mixed metallation in *A. thaliana* and *S. typhimurium* GlxII enzymes contrasts significantly with other enzymes of the Zn-metallohydrolase superfamily, including human GlxII which have been observed to be exclusively dinuclear Zn^{2+}-holoenzymes (4, 77, 81).

The crystal structure of *S. typhimurium* GlxII has been solved to 1.4 Å resolution (Figure 3.5) (4). Given the conservation of sequence and metal binding motifs, it is not surprising that the overall topology mirrors other GlxII enzymes and the metallo-β-lactamases (Figure 3.5).
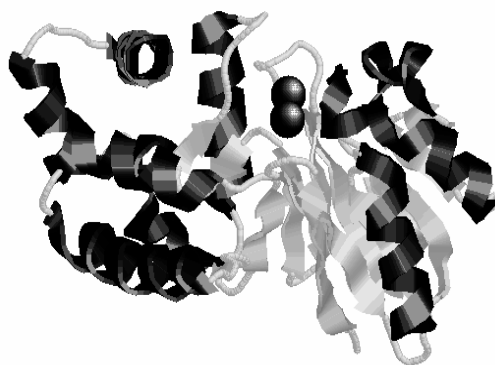
Figure 3.5: Structure of *S. typhimurium* GlxII. The black spheres indicate the metal ions bound to the holoenzyme (PDB ID: 2QED) (4).

Binuclear metallation of the enzyme is observed in the crystal structure, although the identity of the metals was not assigned in the crystal structure (Figure 3.5). The active site residues that ligate to both metal ions are well conserved also. Metal site 1 contains the ligands His53, His55, and His110. The ligands associated with metal site 2 are Asp57, His58, and His165 (Figure 3.6) (4). The metal ligands listed are conserved in the *E. coli* GlxII sequence (Figure 3.7).

Second sphere ligands play a role in the positioning of the primary metal ligands in *S. typhimurium* as has been observed previously in human GlxII and *A. thaliana* GLX2-5. The positioning of active site histidines is influenced by hydrogen bonds with the non-ligating nitrogen atoms in the His imidazole rings (Figure 3.6) (4). Given the overt structural similarity to the aforementioned GlxII enzymes, it is also not surprising that second sphere interactions are also

94

conserved in the *S. typhimurium* hydrolase. For example the Thr52→Asp28→His58 hydrogen

bonding interaction is analogous to the Thr53 → Asp29 → His59 interaction in *A. thaliana* GLX2-5

(Figure 3.6) (4). The second sphere interaction of Thr52 with His53 is also analogous to the Thr53

hydrogen bonding interaction with His54 in *A. thaliana* GLX2-5 (Figure 3.6) (4). Other conserved

His ligand interactions include Arg136 carbonyl→ His110 (conserved GLX2-5 as Lys140 carbonyl

→ His110), Glu139 → H_2O → His55 (conserved human GlxII as Glu146 → H_2O → His56) and

Asp11→His165 (conserved in GLX2-5 as Asp11→His169) (Figure 3.6) (4). All of the

aforementioned second sphere ligands are conserved in the *E. coli* GlxII sequence (Figure 3.7).
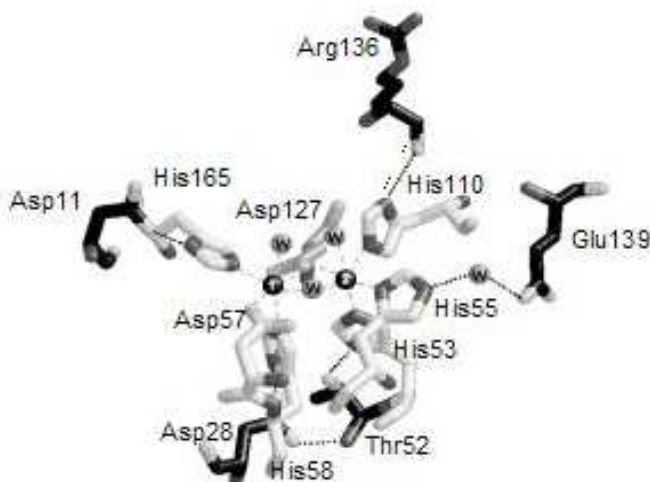
Figure 3.6: Active site of *S. typhimurium* GlxII. Grey stick forms represent inner sphere metal ligands and second sphere ligands are depicted as black stick forms. The numbered black spheres indicate the metal ions and water ligands are designated with the letter "W." The grey dashed lines indicate coordination to the metal ions and the second sphere hydrogen-bonding interactions are indicated as black dashed lines. This diagram was created in RasWin version 2.6 using PDB file 2QED (4).

```
EC    MNLNSIPAFDDNYIWVLNDEAGRCLIVDPGDAEPVLNAIAANNWQPEAIFLTHHHHDHVG    60

ST    MNLNSIPAFQDNYIWVLTNDEGRCVIVDPGEAAPVLKAIAEHKWMPEAIFLTHHHHDHVG    60


EC    GVKELVEKFPQIVVYGPQETQDKGTTQVVKDGETAFVLGHEFSVIATPGHTLGHICYFSK    120

ST    GVKELLQHFPQMTVYGPAETQDKGATHLVGDGDTIRVLGEKFTLFATPGHTLGHVCYFSR    120


EC    PYLFCGDTLFSGGCGRLFEGTASQMYQSLKKLSALPDDTLVCCAHEYTLSNMKFALSILP    180

ST    PYLFCGDTLFSGGCGRLFEGTPSQMYQSLMKINSLPDDTLICCAHEYTLANIKFALSILP    180


EC    HDLSINDYYRKVKELRAKNQITLPVILKNERQINVFLRTEDIDLINVINEETLLQQPEER    240

ST    HDSFINEYYRKVKELRVKKQMTLPVILKNERKINLFLRTEDIDLINEINKETILQQPEAR    240


EC    FAWLRSKKDRF    251

ST    FAWLRSKKDTF    251
```

Figure 3.7: Amino acid sequence alignment of *E. coli* (EC, NCBI accession number U57363) and *S. typhimurium* (ST, NCBI accession number NP_459259) GlxII enzymes. Residues highlighted in grey are metal ligands. Second sphere ligands are highlighted in black. The conserved T-H-X-H-X-D-H motif is underlined in the alignment.

In contrast to the *S. typhimurium* GlxII enzyme, the *E. coli* GlxII has been characterized and isolated from rich media propagated host cells as a binuclear Zn enzyme, as inferred from containing 1.7 equivalents zinc per monomer. The *S. typhimurium* GlxII produced in *E. coli* grown in LB medium contained 0.21 equivalents zinc, 0.64 equivalents iron and 0.30 equivalents manganese for a total metal content of 1.15 equivalents per monomer (4). Possible reasons for the difference in metallation of the enzyme may include the difference in endogenous metallochaperones involved in

assembling GlxII in *E. coli* versus *S. typhimurium*. Also the *E. coli* enzyme may have been in the presence of more exogenous zinc during the stages of purification such that the second site may have obtained metal occupancy as a consequence of different buffer exchanges. Further metal analyses of *E. coli* GlxII recombinantly expressed in rich media or metal supplemented minimal media would be valuable in providing an assessment as to whether this bacterial GlxII parallels the *S. typhimurium* enzyme for promiscuity of active site metal occupancy.

Chapter 4

Kinetics of Phenylglyoxal-Glutathione Isomerization and Determination of Deuterium Isotope Effects in *E. coli* Glyoxalase I

The mechanistic details of the GlxI-catalyzed reaction have been a subject of investigation since the 1950's (133, 134, 135). This enzyme catalyzes a 1,2-proton transfer via a *cis*-enediolate intermediate analogous to the reaction catalyzed by triosephosphate isomerase (122). There is continued interest in examining the mechanistic intricacies of the GlxI-catalyzed isomerization because it will improve our understanding of metalloenzyme-catalyzed 1,2-proton transfers (122). Several other metal-dependent enzymes are thought to catalyze similar reactions via the *cis*-enediol intermediate. These include fucose isomerase, fuculose-1-phosphate aldolase (class II), phosphoglucose isomerase and uronate isomerase (136, 137, 138, 139).

Molecular dynamics and density functional theory approaches have been used to evaluate the proposed GlxI mechanism and the energetics of the rate-limiting proton transfer step. The proposed role of the Zn^{2+} centre, based upon the modeling study of Himo *et al.* was to increase the C1 proton's acidity via coordination of the substrate to the active site metal (140). The calculated energy barrier for proton transfer (14.4 kcal/mol) from their model corresponds well with the value calculated (14 kcal/mol) from the observed reaction rate (kcat ≈ 1500 s-[1] for human GlxI (140). The Lewis acid properties of divalent transition metal ions such as Zn2+ or Ni2+, may be a preferred element in enzyme active sites to facilitate proton transfer in the aforementioned isomerases.

The currently accepted proton transfer mechanism for GlxI is based on data from several experimental approaches. Initial attempts at postulating the nature of enzymatic MG-GSH hemithioacetal isomerization were put forth in the 1950's, by means of detecting solvent deuterium incorporation into the substrate by NMR methods. NMR screening of the yeast GlxI reaction in ^2H_2O

and ^3H_2O solvent systems supported a hydride transfer mechanism (Figure 4.1) (133, 134, 135). This mechanism was proposed because no deuterated or tritiated lactic acid product (from GlxII-catalyzed thioester hydrolysis) could be detected (133, 134, 135). This mechanism was re-evaluated using the same experimental methodology by Hall, Doweyko and Jordan (141). They concluded that the observed 15% deuterium incorporation into the product at 25°C in ^2H_2O and 22% incorporation at 35°C were both indicative of a proton transfer (Figure 4.2) (141).
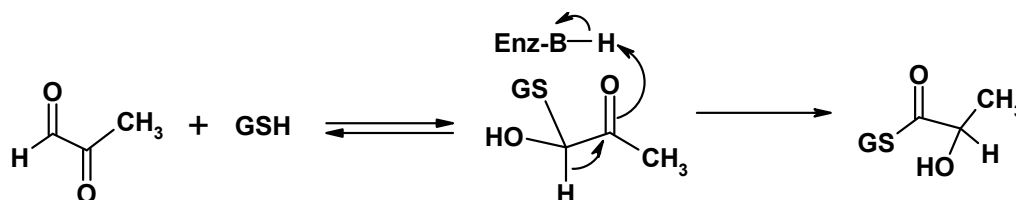

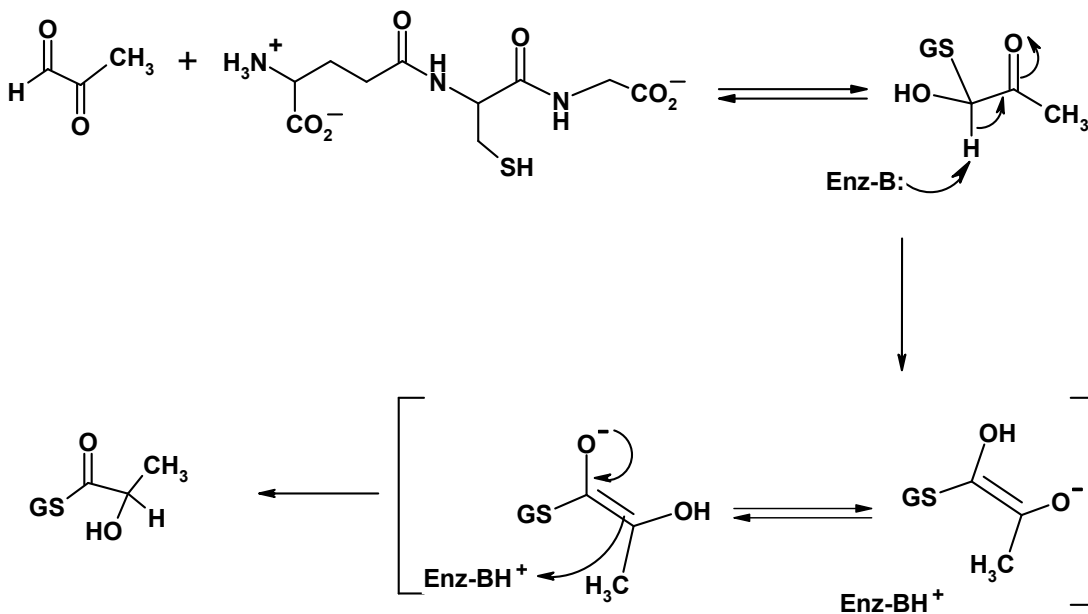**Figure 4.1: Hydride mechanism for GlxI-catalyzed reaction**

Figure 4.2: Enediol mechanism (proton transfer) for GlxI-catalyzed reaction

99

Partition analysis of the yeast GlxI-catalyzed isomerization of fluoromethylglyoxal (fluoroMG) has been performed and also produced data supporting a proton transfer mechanism. GlxI isomerization of the fluoroMG-GSH hemithioacetal partitions products into *S*-fluorolactoylGSH and *S*-pyruvylGSH accompanied by fluoride elimination.
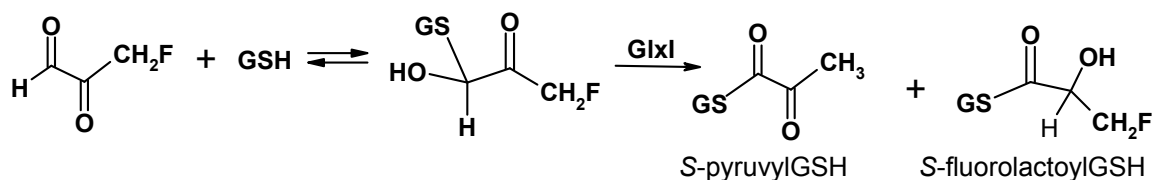
Figure 4.3: Products of GlxI-catalyzed reaction with fluoroMG

The ratio of partitioning can be influenced by the presence of deuterium on C_1 of fluoroMG. Chari and Kozarich were able to use the ratio of fluorinated thioester versus fluoride elimination product (Figure 4.3) as a diagnostic for the likelihood of proton transfer by considering the effect of the deuterium on the substrate (87). This is required because the observation of deuterium incorporation into substrate as well as fluoroMG partitioning can be explained as a hydride migration accompanied by a non-catalytic base-dependent exchange of fluoride or proton (87). In either case the rate of product release should remain constant. Chari and Kozarich observed a deuterium isotope effect that influenced the partitioning ratio, such that fluoride elimination was increased when deuterated (H-atom on C1 substituted) fluoroMG was used as a substrate for GlxI (87). If the reaction were to proceed via a proton transfer then the rate of fluoride elimination would be re-protonation of the substrate (Figure 4.4) (87). The corresponding decrease in fluorothioester formation (Figure 4.5) would increase the partitioning towards fluoride elimination as observed in this study (87). Therefore a proton transfer contribution to GlxI catalysis does support hemithioacetal to thioester conversion via an enediol intermediate. The alternative result that would support a hydride transfer mechanism is

100

that deuteride migration would decrease fluoride elimination via an isotope effect for this process, subsequently suppressing the partitioning of product towards *S*-pyruvylglutathione (Figure 4.6) (87).

Figure 4.4: Enediol mechanism for GlxI catalyzed fluoro-MG-GSH isomerization with fluoride elimination

Figure 4.5: Enediol mechanism for GlxI catalyzed fluoro-MG-GSH isomerization without fluoride elimination
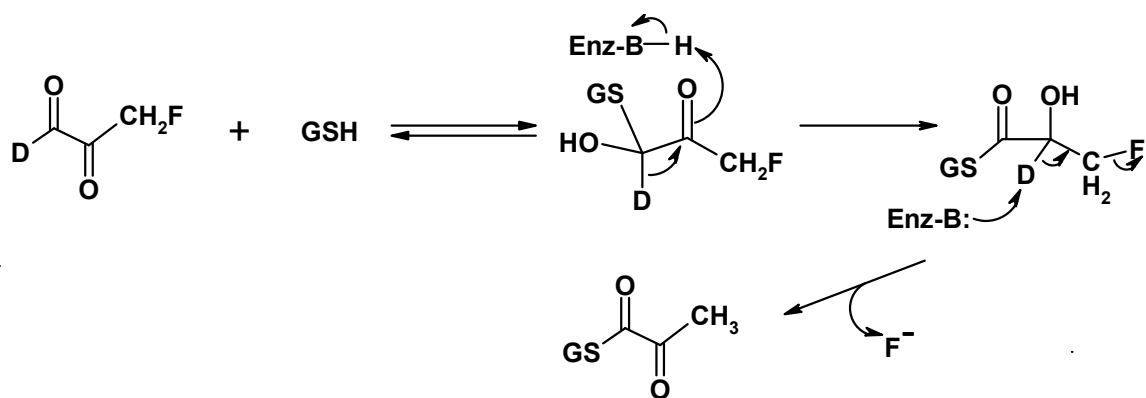
Figure 4.6: Hydride transfer mechanism for GlxI-catalyzed fluoro-MG-GSH isomerization with fluoride elimination
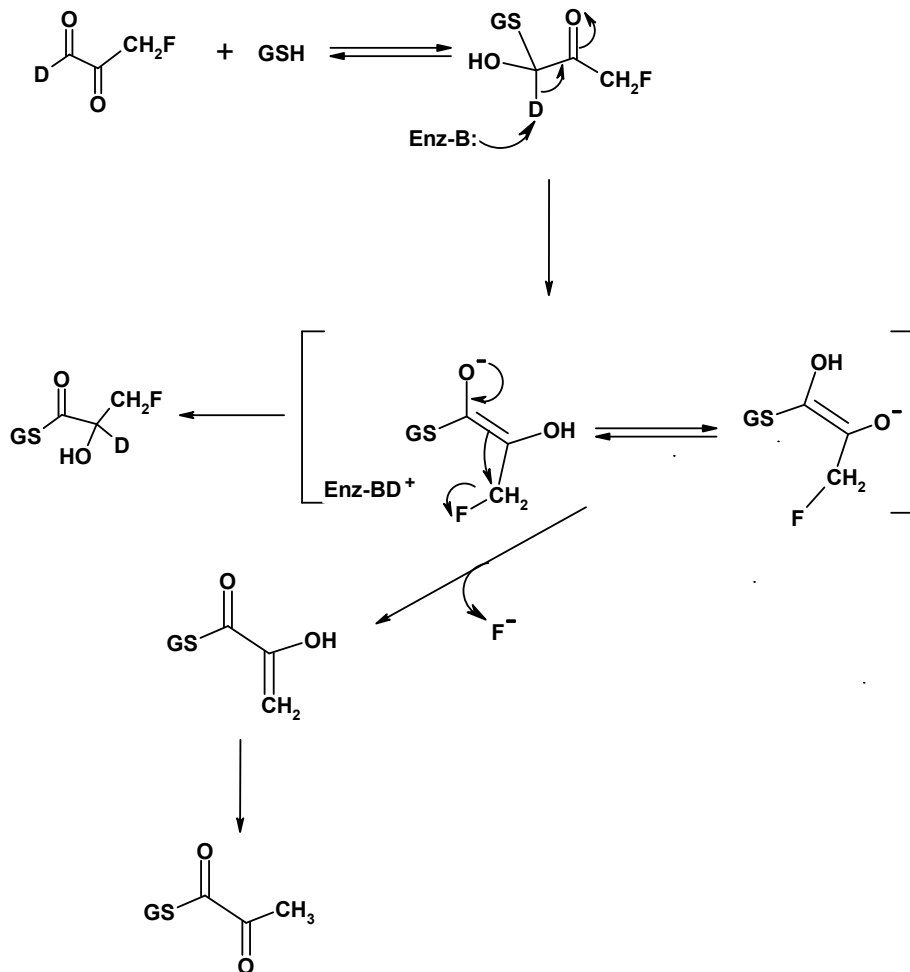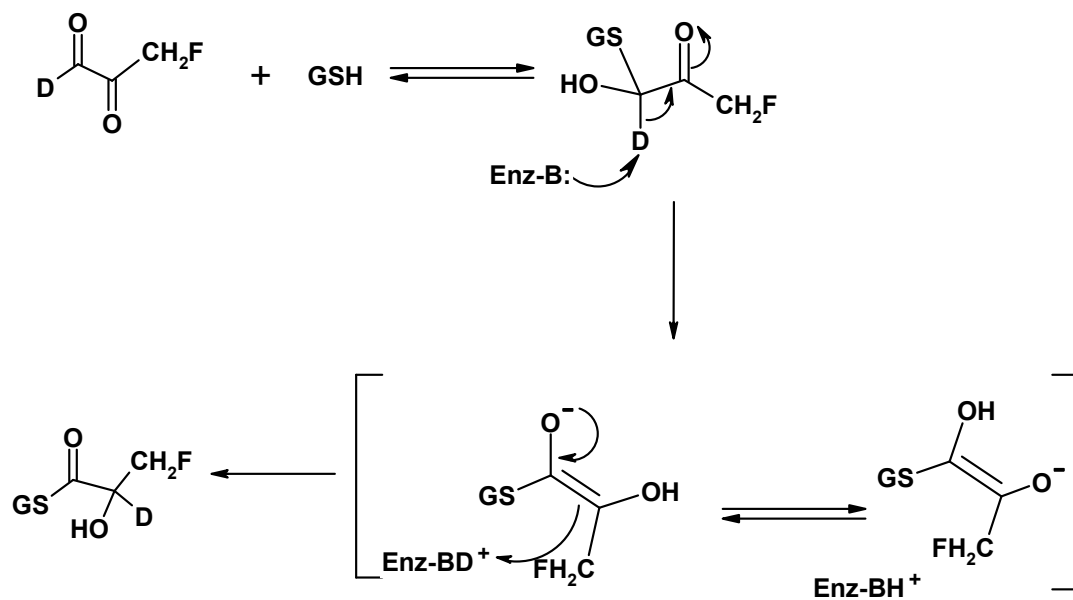
The rate of deuterated substrate turnover by GlxI has been examined using the yeast enzyme to assess the degree of rate dependence on the proton transfer step during catalysis (86). These deuterium isotope effect experiments rely on the observable perturbation of a reaction rate as a consequence of chemical bond energy being changed by isotopic substitution. In turn the isotope-dependent effect on reaction rate can aid in determining whether a particular enzymatic step is a contributor to the overall rate of the enzymatic reaction. Although a single covalent bond-breaking/forming event is unlikely to be the sole rate-determining step, isotope effects are useful tools in formulating plausible mechanisms for enzymatic reactions particularly for fundamental processes such as proton transfer. To this end, the kinetic isotope effect experiment can at the very least indicate whether a chemical step is partially rate limiting. The interpretation of isotope effects on reactions (both enzymatic and non-enzymatic) has been discussed at length in the chemical and biochemical literature (5, 142, 143, 144). The theory behind occurrence of an isotope effect, aspects of experimental set up and interpretation of results will be briefly reviewed in the following section.

4.1 Theory of Kinetic Isotope Effects

The physical basis for an observed isotope effect on a chemical reaction lies in the difference in zero-point vibrational energy for the chemical bond at which the isotopic substitution is occurring (143). The simple harmonic oscillator comprises the model on which comparisons of C-H versus C-D bond energies can be based. If the harmonic oscillator is defined by Hooke's law, the reduced mass of the system will proportionally affect the vibrational energy of the system (143). In the case of the deuterium experiment the zero-point vibrational energy for a C-^{1}H bond is 4.15 kcal/mol (17.4 kJ/mole) and for C-^{2}H is 3.0 kcal/mol (12.6 kJ/mole) (Figure 4.7) (143). For an enzymatic reaction where the C-^{1}H or C-^{2}H bond is broken, the same transition state is formed. However, the activation

energy for breaking the C-^{2}H bond will be higher because it is deeper in the potential energy well compared to the C-^{1}H bond (143).
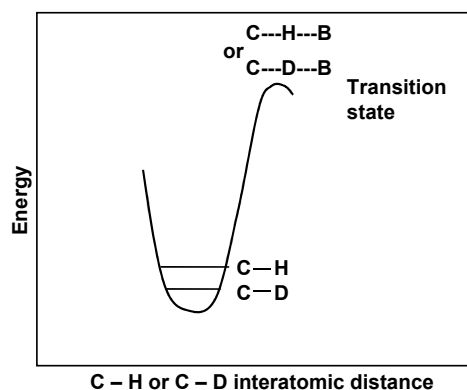
Figure 4.7: Difference in zero-point vibrational energies for C-H versus C-D bonds (adapted from (5)**)**

The kinetic isotope effect experiment requires availability of a selectively deuterated substrate that can be used to characterize reaction rates for an isolated enzyme, in anticipation of comparing these data to that acquired with the protio-substrate (143). The acidity of the deuteron of interest must be taken into consideration as it may be subject to exchange with solvent protons (143). In the case of isotope effect studies on GlxI, the substrates utilized have been α-deuteriophenylglyoxal and perdeuteriomethylglyoxal.

The simplest analysis of a kinetic isotope effect (KIE) is the ratio of reaction rate with the deuterated substrate to that with the non-deuterated substrate, to obtain $k_{(H)}/k_{(D)}$ (143). A ratio with a value between 2-15 indicates that the isotope effect for proton transfer occurs in the transition state for the enzymatic reaction (143). Low, but real isotope effects are assigned when the ratio has a value of less than two (143). These values are interpreted such that the proton transfer step is considered partially rate limiting for the mechanism under consideration. Typically observed KIE values are 1.5

to 2 (143). Pronounced KIE where values $\approx$ 8 have been observed in a few enzymatic reactions

(143). An important warning before proceeding to determine isotope effect data, particularly

concerning the absence of a detectable rate difference, is that another step in the mechanism may have

a rate comparable to that of the step being investigated (143). This other process may mask an

apparent isotope effect, particularly if it is more rate limiting than the proton transfers that might

occur during the reaction. The simplest interpretation of the absence of a kinetic isotope effect is that

the step involving hydrogen transfer is not the slowest of mechanistic events (143). Generally the

first empirical indicator of a kinetic isotope effect on an enzymatic reaction is the reduction of the

apparent V_{max} value (143). The V_{max} term is a composite that includes rate constants for bond

breaking/reformation steps. In the context of hydrogen atom transfer, the presence of a substituted

deuterium generally does not affect substrate binding to the enzyme, so kinetic isotope effects on K_m

where $K_m = K_S$ are typically not observed (143).

The methodology of Northrop is widely employed for the interpretation of kinetic isotope effects in the context of rate limiting steps (142). Northrop's methodology of kinetic isotope effect analysis involves assessing whether the rate perturbation affects V_{max} or V_{max}/K_m (142). Recall under the assumption of Michaelis-Menten kinetics that:

$V = (V_{max}/K_m)[S]$ at low concentrations of S

$V = V_{max}$ at high concentrations of S

Both V_{max} and V_{max}/K_m are composites of various rate constants pertinent to the catalytic cycle of the enzyme under consideration. Therefore the magnitude of effect on each of these composites will vary for a given isotope effect. Northrop's scheme for interpretation was based on the following model of an enzyme-catalyzed reaction:
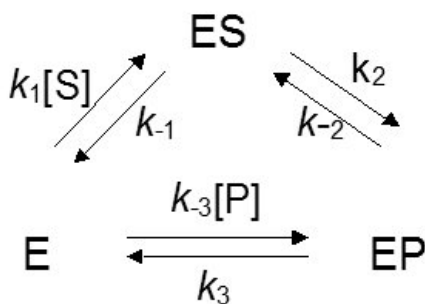
The catalytic step rate constant would be k_2 and would be subject to the isotope effect. Using this scheme several equations can be constructed to describe the enzymatic reaction velocity under different conditions.

For instance, the initial velocity conditions where k_{-2} and $k_{-3}[P]$ are insignificant would have a v term where:

$$V = \frac{k_1 k_2 k_3}{k_3(k_{-1}+k_2) + k_1(k_2 + k_3)[S]}$$

So the expressions for kinetic parameters will be:

$$V_{max} = \{k_2 k_3/(k_2+k_3)\}[ET]$$

$$K_m = \frac{\{k_3(k_{-1} + k_2)\}}{\{k_1(k_2 + k_3)\}}$$

$$V_{max}/K_m = \{k_1 k_2/(k_{-1} + k_2)\}[ET]$$

[ET] is the concentration of all enzyme, that is, the sum of free enzyme and of enzyme in a Michaelis complex.

The intrinsic isotope effect can be defined as that principally affecting k_2, the constant associated with substrate conversion (142). The amount to which the intrinsic isotope effect modifies V_{max} is governed by the ratio of k_2 to k_3 (142). So the relative magnitudes of the chemical step rate versus the rate of product release are being compared in this analysis. If $k_2/k_3 \ll 1$, then the intrinsic isotope effect will markedly diminish the apparent V_{max} (142). If $k_2/k_3 \gg 1$ then the rate of product release is limiting and the intrinsic isotope effect will be obscured by this mechanistic step (142).

107

$$\frac{V_{max\ (H)}}{V_{max\ (D)}} = \left(\frac{k_{2(H)}}{k_{2(D)}}\right) \left\{\frac{(k_{2(D)} + k_3)}{(k_{2(H)} + k_3)}\right\}$$

$$\frac{V_{max\ (H)}}{V_{max\ (D)}} = 1 \text{ when } k_2 >> k_3$$

$$\frac{V_{max\ (H)}}{V_{max\ (D)}} = \frac{k_{2(H)}}{k_{2(D)}} \quad \text{when } k_3 >> k_2$$

Whether the intrinsic isotope effect is influential on V_{max}/K_m depends on the ratio of k_2 to k_{-1}; essentially a comparison of the off rates from the ES complex (142). The isotope effect on V_{max}/K_m is inversely proportional to the ratio of k_2/k_{-1}, such that the effect is attenuated when $k_2 >> k_{-1}$ but is fully apparent when $k_{-1} >> k_2$.

$$\frac{(V_{max}/K_m)_H}{(V_{max}/K_m)_D} = \frac{\left\{\left(\frac{k_{2(H)}}{k_{2(D)}}\right) + \left(\frac{k_2}{k_{-1\ (H)}}\right)\right\}}{\left(\frac{k_2}{k_{-1(H)}}\right) + 1}$$

The "commitment to catalysis" of the enzymatic reaction refers to how frequently ES decomposition to EP occurs relative to ES dissociating into E and S (142). Therefore if ES is converted to EP many more times than the breakdown of ES to enzyme and substrate the commitment to catalysis is high (142). Logically, it follows that a low commitment to catalysis will be reflected by a relatively higher rate of non-productive decomposition of the Michaelis complex (142).

108

The yeast GlxI enzyme has been used to obtain deuterium isotope effect values for MG-GSH and PG-GSH isomerization using perdeuteriomethylglyoxal and α-deuteriophenylglyoxal respectively (86). Base catalyzed isomerization of methylglyoxal-GSH versus perdeuteriomethylglyoxal-GSH results in a measured $k_{(H)}/k_{(D)}$ value of 3.8 (86). The $k_{(H)}/k_{(D)}$ value for base catalyzed isomerization of phenylglyoxal-GSH versus α-deuteriophenylglyoxal is approximately 5.0 (86). These values are considered indicative of the deprotonation of PG-GSH as rate-determining for this reaction (86).

For the GlxI-catalyzed reaction the $k_{(H)}/k_{(D)}$ with methylglyoxal and perdeuteriomethylglyoxal was approximately 2.9 (86). The $V_{\max(H)}/V_{\max(D)}$ with phenylglyoxal and α-deuteriophenylglyoxal for yeast GlxI is 3.2 (86). The value obtained for both sets of substrates is indicative of the proposed proton transfer in the reaction being a rate-determing step (86). This is interesting also since yeast GlxI also exhibits little variation in $V_{\max}$ when it acts upon α-ketoaldehydes with different side chains (86).

The KIE on the K_m values for yeast GlxI require a more discerning approach to interpretation. Recorded $K_{m(H)}/K_{m(D)}$ values for methylglyoxal/perdeuteriomethylglyoxal and phenylglyoxal/α-deuteriophenylglyoxal are 1.7 and 3.3, respectively (86). The difference in the magnitude of these KIE raises the question as to whether secondary isotope effects have arisen in the former situation on account of perdeuteriomethylglyoxal having multiple sites of deuteration (86). In contrast, interpretation of the K_m KIE on phenylglyoxal is less ambiguous because the deuterated substrate is only substituted at the alpha position. So considering this case in isolation it is apparent that the isotope effects on K_m and $V_{\max}$ are approximately the same in the case of yeast GlxI turnover of phenylglyoxal versus α-deuteriophenylglyoxal. These results can be interpreted such that the isotope effect is predominantly manifested as an effect on the rate constant governing conversion of substrate

109

to product (86). This means that the Michaelis constant significantly exceeds the value of the dissociation constant for the ES complex (86).

Recently Feierberg *et al.* investigated the primary kinetic isotope effects of the GlxI-catalyzed reaction and the potential effects of quantum dynamics on the reaction (145). In particular the effects of zero-point energies and tunneling on GlxI-catalysis were analyzed using computational simulations. Their calculated deuterium isotope effect for the GlxI-catalyzed reaction was 5.0 ± 1.3 which is comparable to the above values determined experimentally with yeast GlxI (145). The free energy profiles from using classical trajectories as well as including quantum mechanical nuclear motion converged to the extent that quantum mechanical attributes of the hydrogen translocation contributed little to the observed isotope effect (145). Kinetic isotope effects from this study also included a value of 3.6 ± 0.7 for the uncatalyzed proton transfer in solution and a value of 4.9 for the gas phase reaction (145). The comparable magnitude of all three results indicates that the kinetic isotope effect for the GlxI-catalyzed reaction is an inherent feature of this proton transfer via enediol formation (145). The kinetic isotope effects observed from yeast GlxI studies and the computational study are consistent with isotope effects indexed for mechanistically similar enzymes including triosephosphate isomerase, mandelate racemase and enolase (145).

4.2 Rationale for Investigating Deuterium Isotope Effects in *E. coli* GlxI

The mechanistic attributes of enzyme-catalyzed isomerization are repeatedly observed in different protein systems involved with similar chemical reactions. Although isotope effects in GlxI do not directly indicate the role of the metal ion in catalysis, it is important to ascertain whether the divergence in metal activation has affected mechanistic attributes identified in yeast GlxI. The yeast GlxI enzyme is a Zn^{2+}-activated system, and as such the characterization of kinetic isotope effects is a portion of the comparably larger body of data on the biochemical properties of Zn^{2+}-activated GlxI

enzymes. The quantitation of kinetic isotope effects (if any) for the *E. coli* GlxI-catalyzed reaction

constitutes an enhancement of our understanding of Ni^{2+}-catalyzed endiol proton-transfer

mechanisms. Additionally the ease of metal substitution in the *E. coli* GlxI enzyme permits the

probing of potential metal-dependent effects on the observed isotope effects for the reaction in this

system.

The characterization of *E. coli* GlxI deuterium isotope effects using the substrates

phenylglyoxal (PG) and α-deuteriophenylglyoxal (α-deuterioPG) is outlined in this chapter. The

mono-substituted phenylglyoxal (PG) was selected as the substrate of interest to avoid the potential

difficulties associated with studying a substrate deuterated at multiple sites, such as

perdeuteriomethylglyoxal.

4.3 Materials and Methods

4.3.1 Reagents

See Chapter 2, section 2.5 for materials referred to in the described methods.

4.3.2 Growth and Induction of MG1655/pGL10 for Production of *E. coli* GlxI

The cell line MG1655/pGL10 was used for overproduction of *E. coli* GlxI. A 20 mL Luria-Bertani

(LB) static culture with ampicillin or carbenicillin at 30-50 mg/L was grown overnight at 37ºC. 10

mL of the starter culture was used to inoculate 1L pre-warmed LB media containing carbenicillin at a

final concentration of 50 mg/L. The culture was incubated with shaking at 37ºC until the OD_{600} was

approximately 0.5. At this optical density heterologous GlxI production was initiated with IPTG at

0.5 mM final concentration. The culture was incubated for an additional 6 hours prior to harvesting

cells.

4.3.3 Cell Lysis/Disruption

The preparation of crude *E. coli* cell lysates for protein purification was as follows. Frozen cells were

resuspended in 20 mM Tris buffer pH 7.5 using 10 mL buffer per gram of frozen cells. Crude cell

extracts were prepared using a Sonicator™ cell disruptor model W225, converter model #2 and a

standard tapered microtip, with the output control set at 5, from Heat Systems-Ultrasonics, Inc.

(Plainview, NY). Cells were lysed using 30 pulses of a 10 second duration with intermittent cooling

on ice for 30 seconds. Following disruption, phenylmethylsulfonyl fluoride (PMSF) was added to the

lysate at a 1 mM final concentration, and glycerol was also added at 30% v/v concentration and

thoroughly mixed. The cell debris was pelleted by centrifugation in a JA-25.50 rotor at 20 000 rpm

(48 300 g) for fifteen minutes at 4°C. The supernatant was re-spun several more times under these conditions until no visible cell debris was observed in suspension.

4.3.4 Purification of *E. coli* GlxI

The cell lysate was initially purified by application to a Unosphere-Q (Bio-Rad, Mississauga, ON) anion exchange column (1 mL bed volume) at 1 mL/min. The column was equilibrated with 20 mM Tris pH 7.5, 10% glycerol and protein was eluted at 1 ml/min using a KCl gradient of 0M-1M over 100 min. GlxI-containing fractions were identified by SDS-PAGE, pooled and dialyzed against 2 x 1L 10% glycerol at 4°C. The dialysate was contained in SPECTRA/POR® dialysis tubing with a molecular weight cutoff of 12000-14000. PMSF was added to the dialysis solution at the start of this desalting process to 1.5 mM final concentration, followed by addition at 1.0 mM after three hours. Eight hours into dialysis, the dialysate was placed in a fresh 1L quantity of 10% glycerol and PMSF was added to 1.5 mM final concentration. This exchange was allowed to continue overnight. After PMSF additions the glycerol solution was adjusted to a pH of 7-9 using KOH.

The dialyzed protein was concentrated by ultrafiltration to less than 15 mL in volume for loading into the Rotofor® preparative isoelectric focusing apparatus (Bio-Rad, Missisauga, ON). The focusing chamber was purged of contaminating ions before sample injection by running at 2W constant power for 20 min. The GlxI-containing dialysate was injected into the cell with BioLyte 4-6 ampholyte solution. The final concentration of Biolyte in the cell was 1% v/v. Running conditions for the cell were 12W constant power for 6 hours. Fractions were harvest and GlxI-containing samples were identified by SDS-PAGE. Pooled fractions were concentrated by ultrafiltration and the buffer was concurrently exchanged to Chelex-treated 50 mM MOPS pH 7.0. Purified *E. coli* Apo-GlxI was stored at 4°C for at least 4 months.

4.3.5 Preparation of PG-GSH Hemithioacetal Solutions

PG monohydrate was obtained from Sigma Chemical Company. Stocks of this reagent were prepared at 20 mM concentration in 50 mM potassium phosphate buffer, pH 6.6 for use in enzyme assays. Reduced glutathione was used in the GlxI assay also and its concentration quantitated by DTNB titration as described in (114). Varying concentrations of the PG-GSH hemithioacetal were made in 50 mM potassium phosphate buffer so that the final desired concentration of hemithioacetal was based on the dissociation constant:

$$K_{diss} = \frac{[\text{total phenylglyoxal}] \, [\text{GSH}]}{[\text{hemithioacetal}]}$$

The dissociation constant for the PG-GSH hemithioacetal was determined previously to be 0.6 mM and this value was used for the preparation of substrate stocks for kinetic assay (86). The spectrophotometric assay for GlxI-catalyzed isomerization of the PG-GSH hemithioacetal monitors the decrease in absorbance at 263 nm, which is the isobestic wavelength for the free PG and the hemithioacetal (86). The slope data obtained therefore represents the rate of disappearance of the hemithioacetal. The molar extinction coefficient used for the calculation of V_{max} values is the difference between the extinction coefficients for the hemithioacetal and the thioester at the assay wavelength (146). In these experiments $\mathfrak{C} = 5690$ $M^{-1}cm^{-1}$ for phenylglyoxal and $\mathfrak{C} = 4740$ $M^{-1}cm^{-1}$ for α-deuteriophenylglyoxal (86). The mixtures of PG/ and GSH, or α-deuterioPG and GSH, were equilibrated for 10 minutes prior to assay and the reaction was initiated by the addition of metal-reconstituted *E. coli* GlxI. The holoforms of *E. coli* GlxI used in this investigation were the Ni^{2+}- and Cd^{2+}-reconstituted forms. The concentration range of α-deuterio and non-deuterated PG-GSH hemithioacetals used in these experiments was 0.01 – 0.5 mM. The assay volume was 1 mL and the

final enzyme concentration during the assay was 16.8 nM. Prior to assay, *E. coli* GlxI was reconstituted with 2.5 molar equivalents (per dimeric enzyme) of the appropriate metal chloride. Assay data was collected in triplicate and the final kinetic parameters were estimated from the average of at least two sets of triplicate data for the ten susbstrate concentrations assayed.

4.3.6 Synthesis of α-deuterioPG

The procedure for synthesis of α-deuterioPG is described in Vander Jagt and Han's report of deuterium isotope effects for yeast GlxI (86). Briefly, acetophenone was treated with NaOD in dioxane-D_2O, which yields acetophenone-d_3. Formation of this product was followed by selenous acid oxidation and distillation. The identity of the final product was verified by chemical ionization mass spectrometry and ^{1}H-NMR (Figure 4.8, Figure 4.9). A wavelength scan of the product was performed to confirm that the isobestic wavelength of the synthesized α-deuterioPG was identical to that of the non-deuterated PG (data not shown). The stock solutions of α-deuterio PG were also prepared in 50 mM potassium phosphate buffer; pH 6.6 for use in kinetic assays and dissolution of the solid was achieved by heating at 60 ℃. The gentle heating of the α-deuterioPG stock was also repeated prior to the preparation of each hemithioacetal stock used in the kinetic assay to ensure complete solubility of the α-ketoaldehyde and disrupt any polymer formation in solution that would lower the concentration of available, free compound. The kinetic assay was performed as specified in the paragraph describing the acquisition of kinetic data for *E. coli* GlxI using PG monohydrate as a substrate.
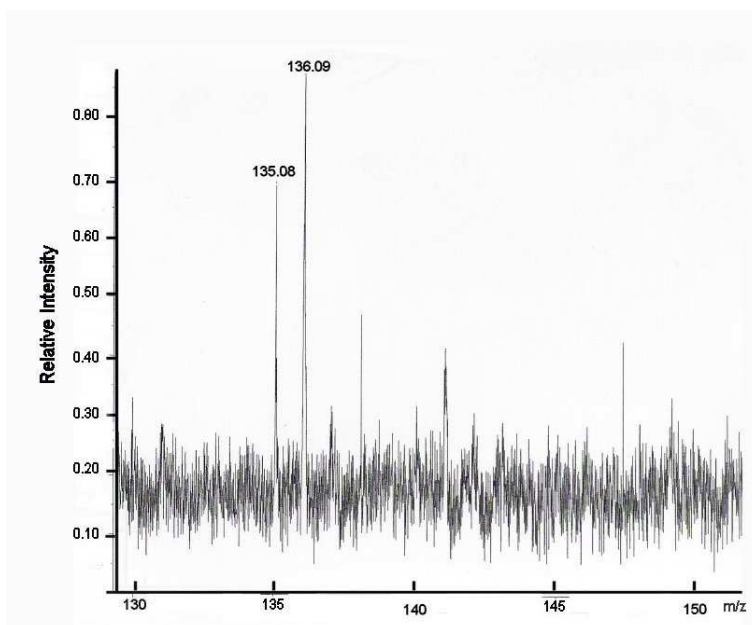
Figure 4.8: Electron ionization mass spectrum of α-deuterioPG. The expected mass of the anhydrous compound is 135.1 amu. The presence of a peak as shown with m/z of 135.08 indicates the presence of deuterated PG. The peak with m/z 136.09 likely represents the M+1 ion of α-deuterioPG.
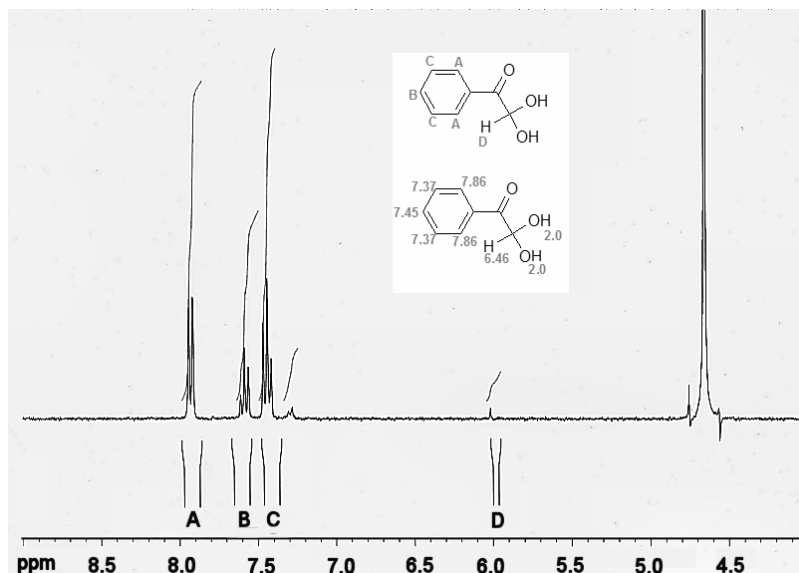
Figure 4.9: ^{1}H NMR spectrum for α-deuterioPG in D$_2$O. The predicted chemical shift values for all protons are shown and the alphabetically labelled protons in the structure correspond to the peaks labelled in the spectrum. A small peak in the region for the α-proton is present (D), indicating that a small percentage of the α-deuterioPG preparation consists of the α-protioPG. Data was not collected in a ppm range that permitted visualation of the hydroxyl proton resonances. Predicted chemical shift values were calculated using ChemNMR (Cambridgesoft®).

4.4 Results

From the aforementioned experiments, Ni^{2+}-substituted *E. coli* GlxI accepts PG-GSH hemithioacetal as a substrate (Figure 4.10). The kinetic parameters for this holoform are as follows: V_{max} = 648 ± 54 μmol/min/mg; K_m = 127 ± 23 μmol; k_{cat} = 322 s^{-1}; k_{cat}/K_m = 2.5 x 10^6 M^{-1}s^{-1} (Table 4.1, Table 4.2). The rate of substrate conversion is similar to that for turnover of MG-GSH by the same holoenzyme, although the catalytic efficiency for PG-GSH is 4.8 times lower than when MG is the α-ketoaldehyde (k_{cat}/K_m = 1.7 x 10^7) (51). The recombinant human enzyme also processes PG-GSH at close to a diffusion-controlled rate of 2.7 x 10^7 M^{-1}s^{-1} (Table 4.1) (147). Therefore it appears that the the *E. coli*

and human GlxI enzymes are comparable in efficiency of processing this bulkier substrate in spite of

the differences in volume of the substrate-binding site between these proteins.
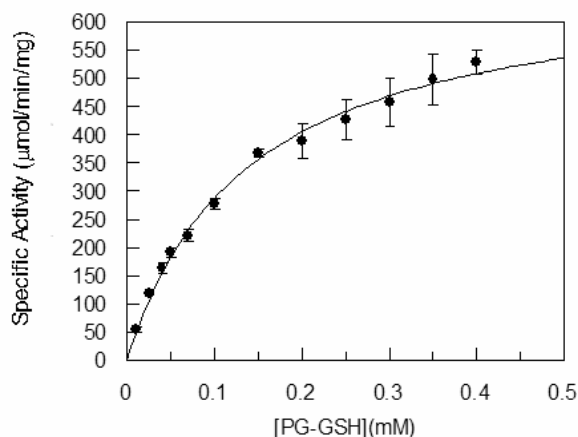
Figure 4.10: Representative plot of PG-GSH concentration versus specific activity for Ni^{2+}-GlxI.
The curve shown is the result of data fitting to the standard Michaelis-Menten equation using Grafit
3.1.

This observation is in accordance with the comparable turnover rates for MG-GSH and PG-

GSH that have been reported previously for yeast GlxI (Table 4.1) (86). PG has been used to

characterize the substrate specificity of several GlxI enzymes from other organisms (Table 4.1)(86).

Table 4.1: Kinetic Parameters for GlxI with PG as the α-ketoaldehyde substrate[*]

GlxI Source	k_{cat} (s^{-1})	K_m (μM)	k_{cat}/K_m (M^{-1}s^{-1})
E. coli (Ni^{2+})	322	127 ± 23	2.5 x 10^6
Yeast	7200	200	3.6 x 10^7
Human	883	34	2.7 x 10^7
Onchocerca volvulus	82	311	2.6 x 10^5
Trypanosoma cruzi (Ni^{2+}) (PG-TSH hemithioacetal)	265	207	1.3 x 10^6

[*]References for the non-*E. coli* GlxI parameters in the table are (86), (147), (146) and (69), respectively.

The human enzyme also processes PG-GSH at close to a diffusion-controlled rate (147). It would appear that the *E. coli* and human GlxI enzymes are comparable for turnover of this bulkier substrate in spite of the notable differences in volume and contours of the substrate-binding site within each protein.

The kinetic parameters for *E. coli* GlxI with α-deuterio-PG-GSH are listed in Table 4.2. The Ni^{2+}-substituted *E. coli* GlxI turns over α-deuterioPG-GSH with a comparable rate and efficiency to that observed when the non-deuterated substrate is used for initial rate determination (Table 4.2). The K_m and V_{max} values for the deuterated substrate are also comparable to that observed with non-deuterated PG. The values for k_{cat} are similar enough to consider the initial velocities of the enzyme almost identical for both substrates. The values for $V_{max(H)}/V_{max(D)}$ (0.85) and $K_{m(H)}/K_{m(D)}$ (0.76) are

indicative of the absence of an observable deuterium isotope effect for proton transfer (Table 4.2).

Recall that the ratios of V_{max} and K_m are equivalent to 1 theoretically if the chemical step under

investigation is not rate limiting. This data is a marked contrast to the effect of α-hydrogen

substitution for the same substrates on yeast GlxI. Yeast GlxI exhibits deuterium isotope effects of

3.3 and 3.2 on K_m and V_{max} respectively, values which suggest that proton-transfer is the rate limiting

step (86). Because yeast GlxI isotope effects are the same magnitude for K_m and V_{max}, the rate of

substrate turnover/conversion seems to be the only mechanistic step affected by the substitution.

Assuming the mechanism Ni^{2+}-substituted *E. coli* GlxI is the same, then the isotope effect could be

obscured by another step in the catalytic mechanism. This step would not be detectable by the

experiments typically used to evaluate the contribution of the proton transfer to substrate conversion.

Table 4.2 Kinetic Parameters and KIE Values for Ni^{2+}-Substituted *E. coli* GlxI

Substrate	V_{max}(μmol/min/mg)	K_m(μmol)	k_{cat}(s^{-1})	k_{cat}/K_m ($M^{-1}s^{-1}$)	$\dfrac{V_{max(H)}}{V_{max(D)}}$	$\dfrac{K_{m(H)}}{K_{m(D)}}$	$\dfrac{V_{max(H)}/K_{m(H)}}{V_{max(D)}/K_{m(D)}}$
PG-GSH	648 ± 54	127 ± 23	322	2.5 x 10^6	0.85	0.76	1.1
α-deuterioPG-GSH	766 ± 69	168 ± 25	381	2.3 x 10^6			

Data obtained for comparing PG-GSH turnover to α-deuterioPG-GSH turnover with Cd^{2+}-

substituted *E. coli* GlxI contrasts markedly with the parameters observed for the Ni^{2+}-holoenzyme.

The rationale behind probing for the deuterium isotope effect with Cd^{2+}-substituted enzyme is based

upon the significant reduction in substrate conversion rate when compared to the value with Ni^{2+}-substitution (Table 4.3) (51, 60). If the proton-transfer step in the Cd^{2+}-holoenzyme is slower than a mechanistic step masking isotope effects in Ni^{2+}-substituted GlxI, then observable deuterium isotope effects might become apparent using Cd^{2+}-substituted GlxI. The results described in the following section support this hypothesis.

Table 4.3 Kinetic Parameters for PG-GSH in Ni^{2+}-and Cd^{2+}-Substituted *E. coli* GlxI

Metal Ion	V_{max}(μmol/min/mg)	K_m(μmol)	k_{cat} (s^{-1})	k_{cat}/K_m (M^{-1}s^{-1})
Ni^{2+} (PG-GSH)	648 ± 54	127 ± 23	322	2.5 x 10^6
(MG-GSH)*	676 ± 17	27 ± 0.4	338	1.2 x 10^7
Cd^{2+} (PG-GSH)	366 ± 59	100 ± 25	182	1.8 x 10^6
(MG-GSH)†	43 ± 5	9 ± 0.4	21.4	2.4 x 10^6

*parameters originally published in (51)
†parameters originally published in (60)

The kinetic parameters obtained for Cd^{2+}-substituted *E. coli* GlxI are summarized in Table 4.3). The Cd^{2+}-substituted *E. coli* GlxI isomerizes PG-GSH hemithioactetal with a comparable efficiency to that reported for the MG-GSH hemithioaceal (Table 4.3, Figure 4.11). In contrast the Ni^{2+}-holoenzyme processes PG-GSH less efficiently by one-order of magnitude relative to the turnover of MG-GSH (Table 4.3). The V_{max} of Cd^{2+}-GlxI is lower with MG than with PG, so the substrate specificity of *E. coli* GlxI may be dependent upon the specific holoform (Table 4.3). Metal activation differences for PG-GSH conversion rates have not been reported for any other Ni^{2+}/Co^{2+}-GlxI enzyme characterized to date.
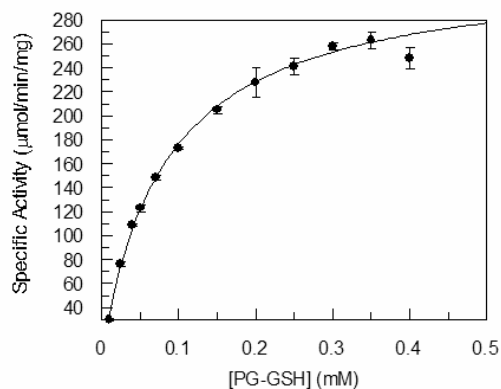
Figure 4.11: Representative plot of PG-GSH concentration versus specific activity for Cd^{2+}-GlxI. The curve shown is the result of data fitting to the standard Michaelis-Menten equation using Grafit 3.1.

The preliminary assessment of Cd^{2+}-GlxI with α-deuterioPG as the α-ketoaldehyde indicates that an isotope effect is observable in this experimental system. The kinetic parameters for this holoform with the deuterated substrate are listed in Table 4.4. The K_m is affected modestly by isotopic replacement in the substrate while the $V_{max(H)}/V_{max(D)}$ value of 2.3 indicates that the α-proton transfer is partially rate-limiting in the reaction (Table 4.4). The effect of deuterium substitution on the ratio V_{max}/K_m is low with a value of 1.7 (Table 4.4). This value does not adequately support the hypothesis that the ES complex off-rate is influencing the value of the intrinsic isotope effect. The KIE on V_{max}/K_m value is small, which reflects a high commitment to catalysis for the GlxI isomerization, which is also apparent from the values observed for k_{cat} (Table 4.4).

Table 4.4 Kinetic Parameters and DIE Values for Cd^{2+}-Substituted *E. coli* GlxI

Substrate	V_{max}(μmol/min/mg)	K_m(μmol)	k_{cat}(s^{-1})	k_{cat}/K_m (M^{-1}s^{-1})	$V_{max(H)}/$ $V_{max(D)}$	$K_{m(H)}/$ $K_{m(D)}$	$V_{max(H)}/K_{m(H)}$ $V_{max(D)}/K_{m(D)}$
PG-GSH	366 ± 59	100 ± 25	182	1.8 x 10^6	2.3	1.6	1.7
α-deuterioPG-GSH	161 ± 5	73 ± 9	80	1.1 x 10^6			

4.5 Discussion

That metals can be removed from the *E. coli* GlxI active site and re-constituted with different divalent cations is advantageous relative to yeast GlxI in the context of kinetic characterization. Yeast GlxI, although well characterized in the biochemical literature, cannot be de-metallated to yield a potentially functional apoenzyme that can easily be reconstituted to an active holoform. Removal of the metal ion from yeast GlxI enzyme actually renders the protein permanently inactive. The *E. coli* GlxI enzyme represents an ideal model system for probing potential metal-ion dependent idiosyncrasies in this lyase/isomerase such as related changes in substrate specificity or substrate binding capacity. The ability to easily use *E. coli* GlxI to detect a potential metal ion-dependent effect is in and of itself novel, since metal replacement as a correlate to isotope effects has not been described previously in the biochemical literature. Comparing the kinetic parameters of Ni^{2+}-substituted and Cd^{2+}-substituted *E. coli* GlxI, it can be seen that the k_{cat} value is reduced 15.8-fold as a consequence of reconstitution with the latter ion (Table 4.3). So it is apparent that the Cd^{2+} metal centre in *E. coli* has the effect of attenuating the rate of catalysis significantly.

The ligand exchange rates for different metal ions may provide a basis for metal-dependent presence/absence of a KIE for the *E. coli* GlxI-catalyzed reaction. The rate of water ligand exchange

123

(i.e. k_{H2O} in s^{-1}) from a Cd^{2+} centre is approximately four orders of magnitude faster ($k_{H2O} \approx 10^{8.5}\,s^{-1}$) than the exchange rate for waters associated with a Ni^{2+} center ($k_{H2O} \approx 10^{4.4}\,s^{-1}$) ((148). Note that these exchange rates are for the first coordination sphere for the metal ion $[M(H_2O)_n^{m+}]$. The impact of water ligand exchange on the rate of the GlxI-catalyzed reaction can be considered under the assumption that substrate binding occurs at the active site metal via vicinal oxygen chelation with concomitant displacement of the resting-state water ligands. If the rate constant for association of the substrate with the active site metal is small relative to the rate constant for the chemical step, the kinetic isotope effect will be suppressed. This is because the chemical step will have occurred regardless of isotopic substitution on the substrate, at a rate exceeding the rate of product release from the enzyme. Conversely if the chemical step occurs at a slower rate relative to the off-rate of the substrate from the active site metal, the isotope effect for the reaction will be manifest in V_{max}. The difference in H_2O exchange rates off Ni^{2+} versus Cd^{2+} centres may imply that substrate binding or release with Ni^{2+} is rate-limiting relative to the catalyzed reaction. In turn, the isomerization itself still proceeds at a faster rate than product release from the Ni^{2+} centre, so the data indicates suppression of the kinetic isotope effect due to the limiting product release. For the Cd^{2+}-substituted GlxI, the isotope effect is therefore apparent because the isomerization occurs at a slower rate compared to the rate of for substrate association/dissociation with the metal ion.

Another possible consequence of the metal-dependent ligand exchange rate is that the catalytic base may be affected in its ability to disengage from metal coordination to facilitate proton abstraction. In this case the deuterium isotope effect for proton transfer is masked because of the decreased propensity for that catalytic residue (or water molecule) to abstract itself from the metal coordination sphere. This "base off-rate" should be distinct from the rate of the substrate to product conversion. Glutamate ligands have been implicated as potential catalytic bases in the enzymatic reaction (63, 65). Consequently it would be useful to determine whether such a ligand has a different

rate of dissociation from a Cd^{2+}-centre versus a Ni^{2+}-centre in *E. coli* GlxI in the presence of substrates or substrate analogs.

The most notable observation from these kinetic experiments is that different metal ions in *E. coli* holoGlxI affect the ability to detect a kinetic isotope effect using α-deutero-substituted substrates. This observation of a kinetic isotope effect was made using Cd^{2+}- substituted *E. coli* GlxI, and was non-detectable with the Ni^{2+}-substituted GlxI enzyme.

Slowing the GlxI k_{cat} by metal ion substitution at the active site may be a potentially useful tool for identifying intermediates from the catalytic cycle. This experimental approach would complement Laue crystallography or other time resolved techniques for resolving short-lived compounds relevant to the enzyme mechanism.

Subtle reconfigurations of *E. coli* GlxI during substrate binding might be different depending on the holoenzyme type. The isotope effects previously described may be indicative of this phenomenon. Slight differences in the outer sphere of *E. coli* GlxI that correlate to the species of bound metal can be determined through highly sensitive methods such as 2-dimensional ^1H-^{15}N-HSQC NMR. Metal dependent changes in the nature of substrate or inhibitor binding can also be observed by this NMR technique.

The *E. coli* GlxI enzyme can efficiently turn over PG-GSH hemithioacetals in the Ni^{2+}- and Cd^{2+}-substituted holoforms. A kinetic isotope effect is not apparent for Ni^{2+}-substituted GlxI when an α-deuterio-substituted PG is supplied as substrate. In contrast deuterium isotope effects on K_m and V_{max} with values of 1.6 and 2.3 respectively are observable with the Cd^{2+}-substituted enzyme. In this case the proton transfer step for hemithioacetal isomerization is at least partially rate limiting. Further replicates of data will be collected to verify the reproducibility of this effect with Cd^{2+}-substituted GlxI. The basis for metal ion-dependent presence of a deuterium isotope effect with this enzyme is

125

not apparent but it is novel since *E. coli* GlxI is the first non-Zn^{2+}-dependent GlxI enzyme characterized by such experimental approaches. The Lewis acidity of Ni^{2+} (pKa ≈ 9.9) versus Cd^{2+} (pKa ≈ 10.1) indicates that α-proton abstraction could be more rate limiting when the latter metal center is present at the GlxI active site, while the hemithioacetal is coordinated to the metal centre via the vicinal oxygen atoms (149). This could account for the apparent KIE with the Cd^{2+}-substituted enzyme in contrast to the results observed with Ni^{2+}-GlxI.

Chapter 5

Investigation of SlyD Involvement in *E. coli* Glyoxalase I Metallocentre Assembly

The earliest reports of transition metals (iron, cobalt, molybdenum) as bacterial growth requirements were published between 1959 and 1965 (150, 151, 152). *Hydrogenomonas* strains were the first bacteria documented to require nickel for growth, this information being reported in 1965 (153). Dixon and co-workers described urease from jack bean in 1975 as the first enzyme requiring Ni^{2+} for catalytic activity (154). Since this time, a number of nickel-dependent enzymes and/or biochemical systems have been characterized in significant detail, greatly enhancing our understanding of biological inorganic chemistry for this particular element. The bacterial Ni^{2+}/Co^{2+}-activated GlxI enzymes are among the relatively small numbers of Ni^{2+}-activated enzymes that have been identified over the last 40 years. These enzymes include urease, NiFe hydrogenase, carbon monoxide dehydrogenase, acetyl-coenzyme A decarbonylase/synthase, methyl-coenzyme M reductase, superoxide dismutase and aci-reductone dioxygenase (155). Two of these well-studied metalloenzymes, urease and the NiFe hydrogenase, require specific metallochaperone systems for nickel atom insertion (155). Proposed schemes for nickel metallocenter assembly have been described in the literature for both urease from *Klebsiella aerogenes* and NiFe hydrogenase-3 from *E. coli* (90, 156, 157, 158, 159, 160). The hydrogenase metallochaperone system is an example of a well-characterized nickel insertion mechanism in *E. coli*.

5.1 The *E. coli* NiFe Hydrogenase Active Site

The NiFe hydrogenase in *E. coli* catalyzes reversible formation of diatomic hydrogen with two electrons and two protons as substrates (161). The protein is heterodimeric with the NiFe metal

centre located on the larger subunit (Figure 5.1) (162). Four cysteine residues coordinate the Ni^{2+} ion and two of these cysteines (Figure 5.2), one CO ligand and two CN ligands coordinate to the iron atom (89). There are three types of NiFe hydrogenase enzymes in *E. coli*, all consisting of a large and small subunit (Figure 5.1) (89). Hyd-3 is the most extensively characterized NiFe hydrogenase from a biochemical perspective (89).
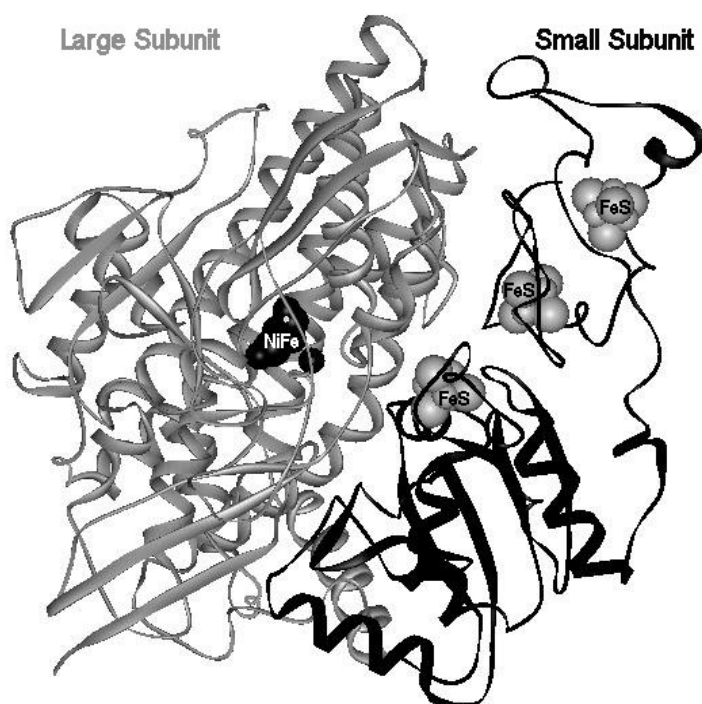
Figure 5.1: Structure of NiFe hydrogenase from *Desulfovibrio vulgaris* (PDB ID:1HR2). The NiFe center is located on the large subunit and indicated in black. The FeS clusters on the small subunit are labelled and shown in grey.
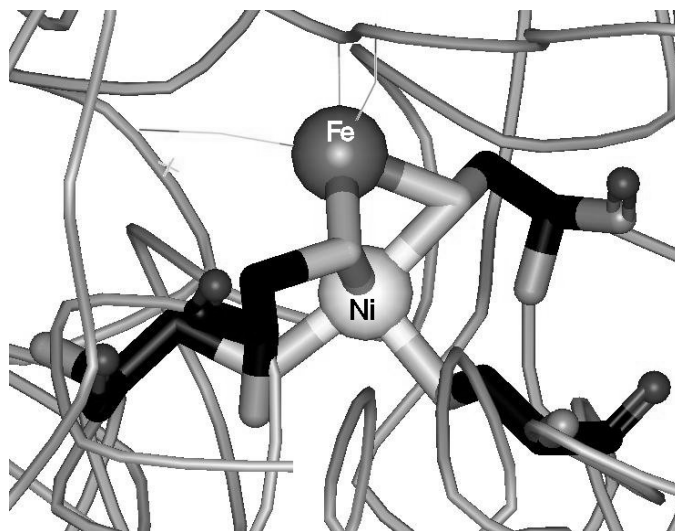
Figure 5.2: The NiFe center of *D. vulgaris* hydrogenase. The coordinating cysteine residues are shown in stick form.

5.2 Nickel Insertion into the Hyd-3 Large Subunit

Two groups of proteins designated Hyp and Hyc are responsible for adding nickel to the Hyd-3 apoenzyme (89). The *hyp* operon encodes five proteins (A-E), and two of them (HypA and HypC) are specific for Hyd-3 maturation (89).

The complex HypCDEF delivers iron and the three diatomic ligands ($Fe(CN)_2CO$) to the Hyd-3 large subunit (LS) (Figure 5.3)(89, 90). The accessory proteins HypB and HypA mediate nickel loading of the LS (Figure 6.3) (89, 90). The peptidyl-prolyl cis/trans-isomerase (PPIase) SlyD has been recently identified as a participant in Ni^{2+} insertion into Ni-Fe hydrogenase; specifically SlyD has been shown to interact with the protein HypB in *E. coli* (Figure 5.3) (7, 163). Intriguingly, SlyD is the only PPIase superfamily member possessing a defined metal-binding region (7). In spite of this other FKBP-type proteins have been implicated in metallocenter assembly for other systems.
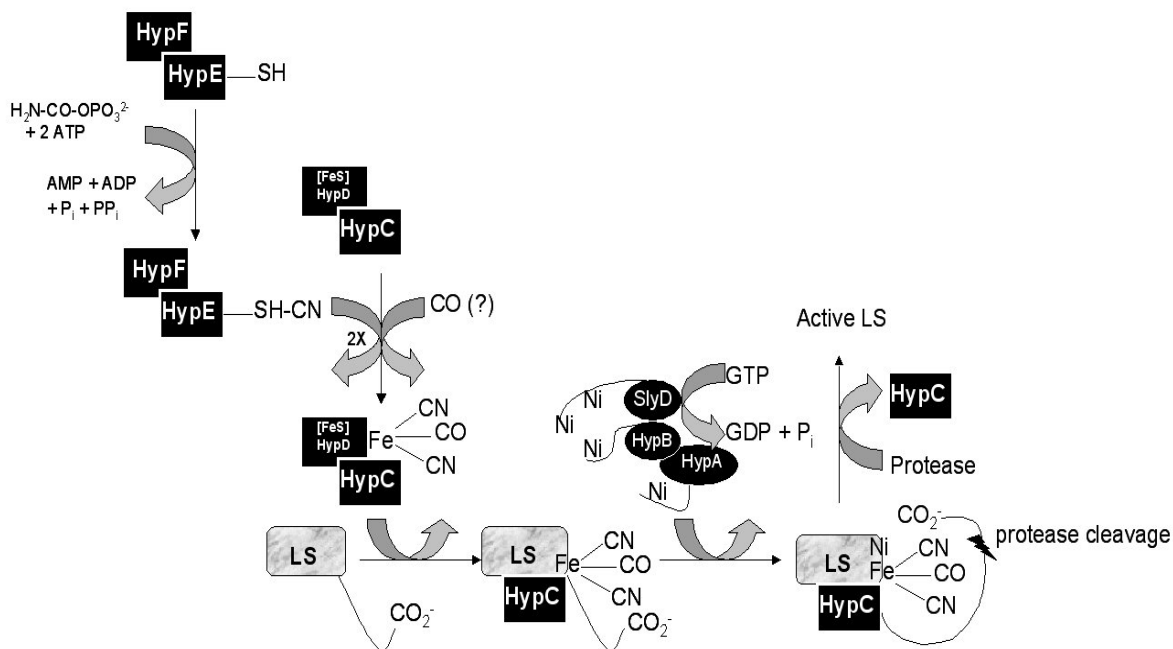
Figure 5.3: Scheme for NiFe insertion into the Hyd-3 large subunit. The abbreviations LS, CN and CO represent the large hydrogenase subunit, the cyanide ligands and the carbon monoxide ligands respectively. HycI cleaves part of the C-terminus of the Hyd-3 large subunit, and Ni2+ must be in the large subunit for this step to occur (Figure 5.3) (89, 90). This scheme was re-drawn from (90)

5.3 SlyD Facilitates Ni Release from HypB into Hyd-3

SlyD was initially assigned a putative nickel loading function in a screen for multiprotein complexes within the *E. coli* proteome (6). The presence of a C-terminal metal-binding domain is relevant to the recently discovered metallochaperone function of SlyD (91). This C-terminal region contains many amino acids that typically function as metal ligands. The SlyD C-terminus contains 15 histidines, 6 cysteines and 7 glutamate/aspartate residues (Figure 5.4) (6).

In the survey of the *E. coli* proteome for SlyD binding partners, no accessory proteins other than HypB were found (6). In *E. coli* strains lacking the SlyD-encoding gene, hydrogenase activity was lower compared to the activity in cells possessing the gene (6). Partial restoration of hydrogenase activity in the deletion mutant could be achieved by the addition of $NiCl_2$ to the growth medium (6). The results of this study indicated that SlyD is involved in Hyd-3 Ni^{2+} insertion and final C-terminal processing of the mature hydrogenase. Hydrogenase activity in *slyD*$^-$ cells could be partially complemented by $NiSO_4$ loading in the growth medium (6).

5.4 Interaction between SlyD and HypB

Two metal binding sites of differing affinities have been identified on the HypB protein (164). The high affinity site binds a single nickel ion at an N-terminal CXXCGC motif with picomolar affinity (Figure 5.4) (164). The low-affinity site binds a single nickel ion with an affinity in the micromolar range using several amino acids in the C-terminal GTPase domain of HypB (Figure 5.4) (164). Whether one or both nickel sites are involved in metallocenter assembly of NiFe hydrogenase remains as yet undetermined.
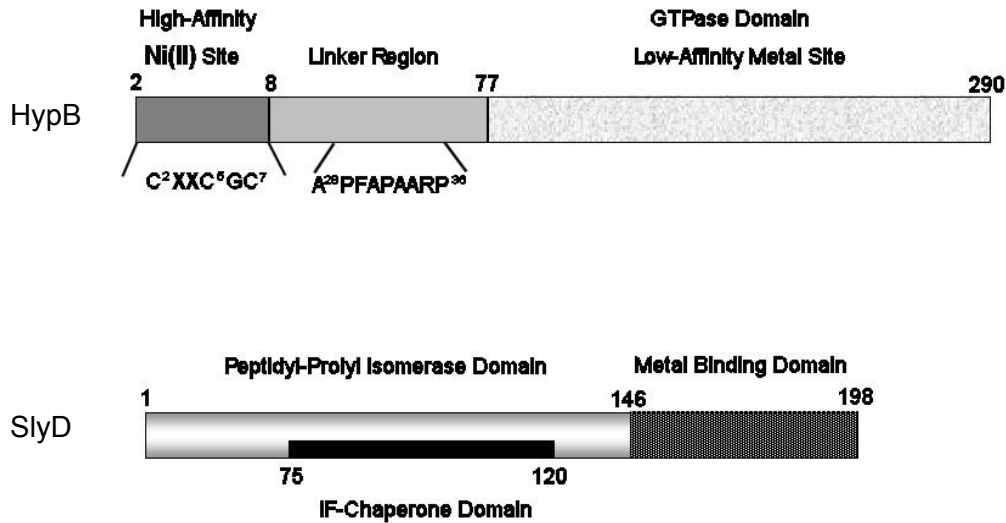
Figure 5.4: Functional domains of hydrogenase accessory proteins HypB and SlyD. This diagram was re-drawn from (7)

The region of HypB that interacts with SlyD is located between the high affinity Ni^{2+} binding site and the GTPase domain (7). A large insert of 41-49 residues in length has recently been identified in FKBP proteins as pertinent to the chaperone activities within this class (165). This region has been designated the "insert in the flap" or IF domain, which has also been identified in SlyD through sequence comparison to related proteins (Figure 5.4) (165). Deletion of amino acids 107-111 in the IF domain impair the chaperone activities of SlyD and the protein is not able to form a non-covalent complex with HypB *in vitro* (7).

The N-terminal region of HypB interacts with SlyD, and the isolated HypB GTPase domains (C-terminal) do not interact with SlyD (7). Both the PPIase and metallochaperone activities of SlyD appear relevant to NiFe Ni^{2+} insertion.

The probable function for these other proteins is to induce metal release from another accessory protein to the site of delivery (7). In the case of SlyD however, there may be a more direct

role with regards to metal sensing, delivery and transfer for creation of functional NiFe hydrogenase *in vivo*.

5.5 SlyD and Ni Insertion into *E. coli* GlxI

This chapter summarizes experimental attempts at determining whether SlyD is a general accessory protein for nickel insertion into multiple metalloproteins including GlxI. These experiments represent a collaborative effort with Dr. Deborah Zamble's research group at the University of Toronto where SlyD was identified as a hydrogenase metallochaperone. This investigation aimed to determine whether SlyD and GlxI can form a stable protein complex, and whether the presence of SlyD in *E. coli* correlated to the level of measureable GlxI activity at basal expression levels.

5.6 Materials and Methods

5.6.1 Reagents

See Chapter 2, section 2.5 for materials referred to in the described methods.

5.6.2 Strains

The *E. coli* strains supplied for the basal level expression tests were a generous gift from the laboratory of Dr. Deborah Zamble at the University of Toronto, Department of Chemistry. The control strain used was *E. coli* DY330 (W3110 ΔlacU169 gal490 lambda cI857 Δ(cro-bioA)), and the isogenic *slyD* deletion mutant was designated Δ*slyD* (6). The strain used for obtaining purified apoGlxI for the protein partner experiment was MG1655/pGL10. Note that this strain was employed previously for the initial characterization of *E. coli* GlxI (51).

5.6.3 Overproduction and Isolation of *E. coli* GlxI for Crosslinking Experiment

Expression and purification of apoGlxI from *E. coli* strain MG1655/pGL10 was performed as described by Clugston *et al.* (51). Apo-GlxI was obtained in sufficient quantities and in appropriate purity for use in the protein partner experiment. The enzyme was supplied in the apo-form based on the assumption that a stable interaction between SlyD and GlxI may not be detectable if the recipient metalloprotein is already metallated. The purified GlxI was supplied as a stock at 0.4 mg/mL in 50 mM MOPS (Chelex-treated, pH adjusted with KOH) pH 7.0.

5.6.4 Conditions for Crosslinking Experiment

Kathleen Zhang, a technician in the laboratory of Dr. D. Zamble (Department of Chemistry, University of Toronto) performed the crosslinking experiment using a purified apo-GlxI preparation from the laboratory of Dr. J. F. Honek. The experimental setup for identifying the aforementioned heterodimeric complexes involves incubation of the two partner proteins followed by the addition of a chemical cross-linking agent to covalently stabilize the dimer. For the incubations, SlyD and HypB were supplied at a final concentration of 16 mM and apo-GlxI was supplied at a final concentration of 12 mM. The proteins were incubated overnight at 4 degrees Celsius followed by treatment with 5mM 1-(3-dimethylaminopropyl)-3-ethylcarbodiimide hydrochloride) (EDC) for one hour at room temperature. This reagent is used to couple primary amines to carboxyl groups, and is commonly employed. The buffer employed for the cross-linking reaction was 25 mM HEPES, 200 mM NaCl, pH 7.5. Samples were analyzed on 12.5% SDS-polyacrylamide gels stained with Coomassie Brilliant Blue. To investigate complex formation in the presence of nickel 100 μM (final concentration) $NiCl_2$ was added to the incubation mixtures. 2.5mM EDTA was used in conditions for identifying complex formation in the presence of a chelating agent.

5.6.5 Conditions for Lysate Preparation: Basal Level GlxI Expression Growth

Broth cultures (20 mL culture volume) of *E. coli* DY330 and DY330Δ*slyD* were grown to stationary phase in LB medium using a 250 mL shake flask at 37 degrees Celsius at 200 rpm. Conditions for growth of DY330 and DY330Δ*slyD* cultures with metal supplementation involved growth under the aforementioned conditions with 0.1 mM NiCl$_2$ present in the media. 10 mL of the cultures was harvested by centrifugation at 3000 g for 15 min and frozen at – 80 °C until required.

Microaerophilic cultures of *E. coli* DY330 and DY330Δ*slyD* were propagated in 200 mL volumetric flasks that were stationary at 37 degrees Celsius to minimize aeration of the culture. The Microaerophilic cultures were grown for 24 hours and harvested as indicated for the aerobic cultures. Cultures were grown with and without NiCl$_2$ supplementation at 0.1 mM final concentration of the metal chloride.

Cultures grown in minimal media were propagated at a 250 mL scale using M9 minimal salts medium with 0.2% glucose and 8μM NiCl$_2$ when metal supplementation was desired. The M9 cultures were grown to stationary phase aerobically using a 1L shake flask incubated at 37 degrees Celsius using 200 rpm agitation. Cultures were harvested as indicated above.

The cell pellets from the growth conditions described above were resuspended in approximately 1 mL/0.5 g cells (wet weight) with 50 mM potassium phosphate buffer, pH 6.6 containing 0.5% v/v Triton-X 100 and 0.15 mg/mL lysozyme. The cells were sonicated on ice for 10 cycles of 10 one-second pulses with intermittent pauses for cooling. The lysates were clarified by centrifugation and the supernatants were used as the source of enzyme for the GlxI assays. The assays were performed as described previously in Clugston *et al.* 1998 in 0.5 mM MG-GSH using 50 mM potassium phosphate pH 6.6 as the assay buffer. Assays were performed in duplicate on a one

mL scale with the addition of 0.1 mM NiCl$_2$ where indicated. Approximately 0.1 mg of total lysate protein was assayed for each growth condition for both the *slyD*$^+$ and *slyD*$^-$ strains.

5.7 Results

5.7.1 SlyD-Apo-GlxI and HypB-Apo-GlxI Cross-linking Experiments

The cross-linking experiments permit the isolation of covalent complexes between partner proteins based on the ability to reactively couple protein partners following formation of a stable non covalent heterodimer. The dimerization should occur with the incubation of the two proteins of interest together for an extended period of time. The SDS-PAGE analysis of any potential complexes will result in loss of the GlxI homodimeric structure. If a complex was formed with either HypB or SlyD however, it should be detectable due to the chemical coupling of the two partner proteins by EDC crosslinking. The SDS-PAGE gel showing the results of the incubation is presented below (Figure 5.5). SlyD from *E. coli* is present in solution with as a dimer of 42 kDa, the monomer being 21 kDa in molecular mass (Figure 5.5). This monomeric weight corresponds well with the observed migration relative to the 25 kDa marker on the gel (Figure 5.5). *E. coli* GlxI is a 30 kDa dimer in solution with the monomer having a predicted mass of approximately 15 kDa. Again the observed migration of *E. coli* GlxI on the SDS-PAGE electrophoretogram is in good agreement with the expected molecular mass. Following incubation of SlyD with the apo-GlxI one would expect a heterodimeric complex of both proteins exceeding the molecular mass of each component independently, if they engage in a physical interaction. Clearly from the results shown below, there is no apparent interaction between SlyD and the GlxI enzyme as both proteins migrate independently following incubation and EDC treatment (Figure 5.5).

136

Similarly there was no detectable interaction between HypB and GlxI based on the SDS-PAGE results. Both proteins migrate independently and no band with a molecular mass indicative of heterodimer formation is observed. The HypB monomer has a predicted molecular mass of 31.6 kDa in agreement with the position of the corresponding protein band on the gel (Figure 5.5). The significance of assaying for an interaction between HypB and GlxI is that the HypB accessory protein may be promiscuous in its function of facilitating nickel metallocenter assembly. HypB may not be exclusively a nickel ion donor for the NiFe hydrogenase. The results of this experiment suggest however that an interaction between this metallochaperone and GlxI does not exist (Figure 5.5).
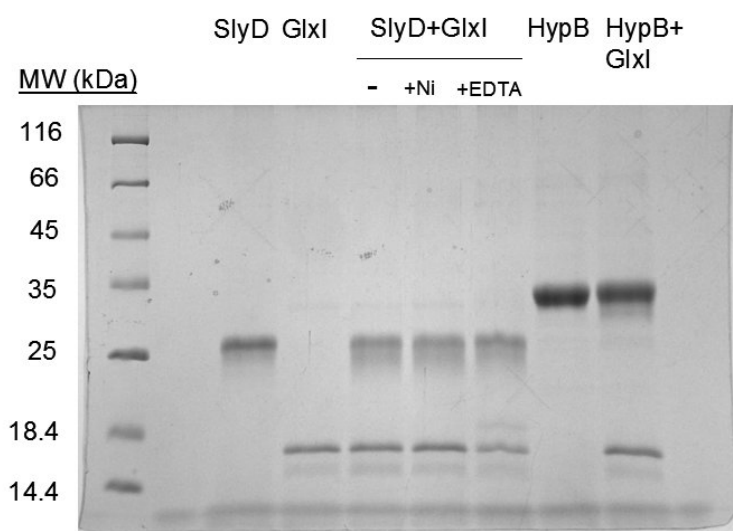
Figure 5.5: SDS-PAGE gel showing results of cross-linking experiment with *E. coli* proteins SlyD, HypB and GlxI.

In vitro cross-linking may not reliably indicate a potential for *in vivo* protein complex. One reason is that the nature of the interaction between the two proteins of interest may be so transient that the complex does not last for the duration of the incubation preceding EDC treatment. Also there

may be an interaction of multiple proteins in addition to the proteins of interest that is necessary for the productive metallochaperone complex to form.

5.7.2 Basal Level GlxI Activity in *E. coli* Strains with and without the *slyD* Gene

Previously, assaying of lysates has been employed to assess the expression level of recombinant *E. coli* GlxI in MG1655/pGL10 (51). The levels of GlxI activity detected in the lysates of this strain are very high because of the copious amounts of recombinant GlxI produced following IPTG induction of the culture (51). The culture experiments with the $slyD^+$ and $slyD^-$ strains involved attempts at detecting basal levels of the enzyme activity at typical expression levels for the chromosomal gene. Glx system components are probably constitutively expressed in *E. coli* yet the level of enzyme present in the lysates was low enough to be undetectable in the presence of MG-GSH with no added $NiCl_2$. Addition of Ni^{2+} ions to the assay buffer permitted measurement of a low level of GlxI activity from the lysates of the strains. The results of the assays in the presence of Ni^{2+} are summarized as follows:

Aerobic Culture - LB Medium

$slyD^+$ strain

+ 0.1 mM $NiCl_2$ 0.73 μmol/min/mg
w/o 0.1 mM $NiCl_2$ 0.81 ± 0.02 μmol/min/mg

Δ$SlyD$ strain

+ 0.1 mM $NiCl_2$ 0.85 ± 0.02 μmol/min/mg
w/o 0.1 mM $NiCl_2$ 1.15 ± 0.30 μmol/min/mg

Microaerophilic Culture - LB Medium

slyD⁺ **strain**

w/ 0.1 mM NiCl$_2$ 0.17 ± 0.01 μmol/min/mg
 w/o 0.1 mM NiCl$_2$ 0.57 μmol/min/mg

Δ*SlyD* **strain**

w/ 0.1 mM NiCl$_2$ 0.12 μmol/min/mg
w/o 0.1 mM NiCl$_2$ 0.67 ± 0.04 μmol/min/mg

Nutrient Limited Culture - M9 Minimal Salts Medium

slyD⁺ **strain**

w/ 8 μM NiCl$_2$ 0.12 μmol/min/mg
 w/o 8 μM NiCl$_2$ 0.06 μmol/min/mg

Δ*SlyD* **strain**

w/ 8 μM NiCl$_2$ 0.10 μmol/min/mg
w/o 8 μM NiCl$_2$ 0.12 ± 0.01 μmol/min/mg

The range of observed GlxI activity in the lysates was from 0.1 μmol/min/mg to 1 μmol/min/mg. The levels of activity measured between the aerobic and microaerophilic cultures with or without NiCl$_2$ supplementation were quite similar when measured with Ni^{2+} added to the assay buffer. Furthermore the absence of the *slyD* gene did not appear to uniformly decrease the amount of measured GlxI activity in the lysates across the various growth conditions. In some cases, the apparent activity of the slyD deletion mutant lysates appeared higher than for the strain with the metallochaperone-encoding gene for a similar condition. This is apparent for the results with the microaerophilically grown cells. A possible explanation for this result is that the growth condition may make both strains susceptible to growth inhibition by Ni^{2+} and so a lower level of GlxI activity is observed.   These results do indicate that the presence of the SlyD metallochaperone-encoding gene in *E. coli* DY330 correlates to higher intracellular levels of GlxI.

5.8 Discussion

5.8.1 Alternative Methods for Detecting a SlyD-GlxI Interaction

This investigation failed to detect interactions of the NiFe hydrogenase accessory proteins SlyD and

HypB with the Ni^{2+}-dependent isomerase/lyase GlxI in *E. coli*. This conclusion is based upon the

failure to observe EDC-stabilized dimerization of either metallochaperone with GlxI following

protracted incubation. Additionally the basal GlxI activity in wild type and *slyD⁻* strains are

comparably low with no siginificant differences. Alternative methods of assessing the formation of

SlyD-GlxI or HypB-GlxI complexes might include a Western blotting approach. The absence of

detectable post-incubation complexes in the aforementioned experiments indicates that such an

interaction may not be observable by Western blot analysis.

The two-hybrid method is a widely used *in vivo* technique that was initially pioneered in

yeast cell hosts (166). Detection of the protein complex *in vivo* relies on transcriptional activation of

a measurable reporter gene that is expressed when the interaction of interest occurs (166). The

components of the two-hybrid system are two fusion proteins. The gene encoding the bait protein is

fused to the gene encoding the reporter's promoter binding domain of the transcription factor on one

plasmid (166). A second plasmid contains a fusion of the gene for the partner protein of interest and

the gene for the transcriptional activation domain of the transcription factor (166). Both plasmids are

expressed in the host cell and the presence of a protein-protein interaction is inferred from increased

expression levels for the reporter gene. This reporter gene allows amplification of the signal

indicating a protein interaction so that this method may be more useful for detecting transient protein-

protein interactions in the host cell (167). However the false positive rate using the two-hybrid

system may be as high as 50%, requiring verification of the complex formation by alternative

strategies (168).

5.8.2 *E. coli* GlxI and Possible Metallochaperone Interactions *in vivo*

A notable aspect of the Ni^{2+}/Co^{2+}-activated GlxI enzymes is the ease of metal removal and reconstitution under experimental conditions. The holoforms from this metal activation class can easily be converted to the apoform by EDTA treatment or preparative isoelectric focusing (51). Reactivation of the purified enzyme requires only short-term incubation in a stoichiometric excess of activating metal ion (51). The metallation of nascent *E. coli* GlxI may not require an additional repertoire of accessory proteins for insertion of the ion into the active site. Given the potential for GlxI activation by different cations ($Ni^{2+,}Co^{2+}$, Cd^{2+}, Mn^{2+}), there may be a sampling of holoenzymes in the *E. coli* cell that are differently metallated depending on the ions available to the apoprotein (51). It is also possible given the nanmolar affinity of *E. coli* GlxI for Ni^{2+} that it may be able to efficiently take up ions from NiFe hydrogenase or SlyD when these proteins are being degraded in the cell (60).

Nickel is a relatively low abundance metal in bacterial cells. Magnesium is the most abundant metal ion with approximately 0.1 M cellular concentration (169). Fe, Zn, and Ca follow Mg for cellular abundance with concentrations of about 10^{-4} M (169). The divalent ions Cu and Mn are present in *E. coli* at concentrations around 10^{-10} μM (169). Nickel and cobalt are at the low and sub-micromolar range in cells respectively (169). Therefore the availability of Ni^{2+} relative to the cellular concentration of GlxI in *E. coli* may provide an indication as to whether it is predominantly Ni^{2+}-activated or otherwise *in vivo*.

Glx system enzymes are likely constitutive elements of the *E. coli* proteome given the potential to form toxic MG from glycolytic triose phosphates. In conjunction with evidence for highly

active GlxI with only half-of-the-sites metallation, the stoichiometric demand for Ni^{2+} by this enzyme is not nearly as great as for the NiFe hydrogenase-3 of *E. coli* (51, 60).

5.8.3 Ni^{2+} Transport in *E. coli* and its Relevance to GlxI

Metal ion transport in *E. coli* is mediated in part by influx systems with broad selectivity for different ions of the same valency. Promiscuity of metal transporters is a beneficial strategy to maintain the ionic requirements of *E. coli* without the metabolic expense of having to synthesize a specific transporter for each required metal ion. In the case of the NiFe hydrogenases the Ni^{2+} requirement is sufficiently great that it is beneficial to have the Nik transporter that is dedicated to Ni^{2+} influx to assemble the protein under microaerophilic conditions. The Nik system employs an ATP-dependent ABC-type transporter called NikABCDE for import of Ni^{2+} ions (160). The repressor protein NikR, which prevents expression of NikABCDE in the presence of nickel, regulates the expression of this transporter (170). The FNR regulator controls expression of the nik operon, which codes for the NikABCDE and NikR, so that increased Ni^{2+} transport into *E. coli* occurs as the organism transition from aerobic to anaerobic respiration (171).

Ni^{2+} and Co^{2+} mobilization into *E. coli* is also possible through the magnesium transporter CorA and the Zn recruitment system ZupT (172, 173, 174).

5.8.4 RcnA is a Ni^{2+}/Co^{2+} Efflux Protein in *E. coli*

The identification of the RcnA/RcnR Ni^{2+}/Co^{2+} efflux system suggests that there is a second pool of nickel available to *E. coli* that may be relevant to Ni^{2+} availability for GlxI *in vivo*. Rodrigues *et al.* identified the RcnA and RcnR gene products (initially denoted YohM and YohL respectively) in 2005 (175). RcnA appears to be a Ni^{2+} and Co^{2+} efflux protein and *rcnR* encodes a divergently transcribed

repressor of *rcnA* expression (175, 176, 177). RcnA is a membrane-associated protein with a histidine rich region located that likely plays a role in metal binding (175).

The *rcnA* gene appears to be strictly induced in the presence of Ni^{2+} and Co^{2+}. The *rcnA* gene is not fully expressed until complete repression of the Nik transporter genes has occurred under anaerobic conditions. *rcnA* expression is unaffected in a *ΔnikR* background, so a different Ni^{2+}/Co^{2+} transport system likely controls regulation of this efflux protein (176). Ni^{2+}-induced *rcnA* expression is similar under anaerobic and aerobic growth conditions (176). This implies a general function for the Ni^{2+}/Co^{2+} efflux even when the cell does not require large quantities of nickel for hydrogenase assembly (176).

Deletion of the *rcnA* gene generates an *E. coli* phenotype of reduced Hyd-3 activity on formate (which induces Hyd-3 activity via the transcription factor FhlA) which is evidence for an RcnA-NikR interaction (176). The deletion of *nikR* restores Hyd-3 activity in the *ΔrcnA* strain. Based upon these results Iwig *et al.* suggest that RcnA might function to maintain the expression of the Nik transporter at lower Ni^{2+} concentrations by exporting excess Ni^{2+} that may inappropriately activate NikR. This ensures that Hyd-3 can be fully activated at lower Ni^{2+} concentrations during anaerobic growth. Iwig *et al.* also proposed that RcnA might be necessary for export of Ni^{2+} following degradation of Hyd-3 when the cell no longer requires this enzyme.

5.8.5 *E. coli* may have Protein-Specific Ni Reserves

Iwig *et al.* have hypothesized that *E. coli* has access to two pools of Ni^{2+} ions based on their studies of the RcnA/RcnR system (Figure 5.6). The first pool is imported by the Nik transporter and provides the main source of Ni^{2+} for assembly of the NiFe hydrogenases (Figure 5.6). The second pool of Ni^{2+} ions has a currently undefined import system but is regulated at least in part by the RcnA and RcnR proteins (Figure 5.5). The proposed function of the second pool is to supply Ni^{2+} to other constituents

of the *E. coli* metalloproteome, which would include GlxI (Figure 5.6) (176). The "Nik" pool is a larger reserve of Ni^{2+} but when *E. coli* does not require hydrogenase enzymes, then the concentration of Ni^{2+} from both pools will be low (176). If the Nik pool is saturated, Ni^{2+} ions can enter the second pool according to the model proposed by Iwig *et al.* (Figure 5.6). The RcnA associated pool of Ni^{2+} exerts some control over the activity of RcnR and NikR for binding their cognate DNA regions (176).

The two Ni^{2+} pools in *E. coli* are "linked" through NikR, because the levels of its activity can be influenced by the ion concentration from both reserves (Figure 5.6) (176). Ni^{2+} from the hydrogenase assembly pool may enter the RcnA-associated pool through degradation of Hyd-3 large subunits so that the excess Ni^{2+} has a route for cellular efflux (Figure 5.6). Also excess nickel from the hydrogenase assembly pool may be re-routed to the second pool for export by RcnA to maintain cellular homeostasis (176).

In the context of *E. coli* GlxI assembly *in vivo*, the RcnA associated Ni^{2+} pool may constitute the source of activating ions for the enzyme as opposed to Ni^{2+} imported by NikABCDE and supplied to Hyd-3 via SlyD. The presence of a histidine rich region on RcnA may function as a site for transient metal binding for transfer to apoenzymes such as nascent GlxI (176). This would imply a dual function for RcnA as metal delivery protein as well as an efflux pump.

E. coli may not use Co^{2+} ions *in vivo* for activation of GlxI given the toxic effects of this metal on the organism.
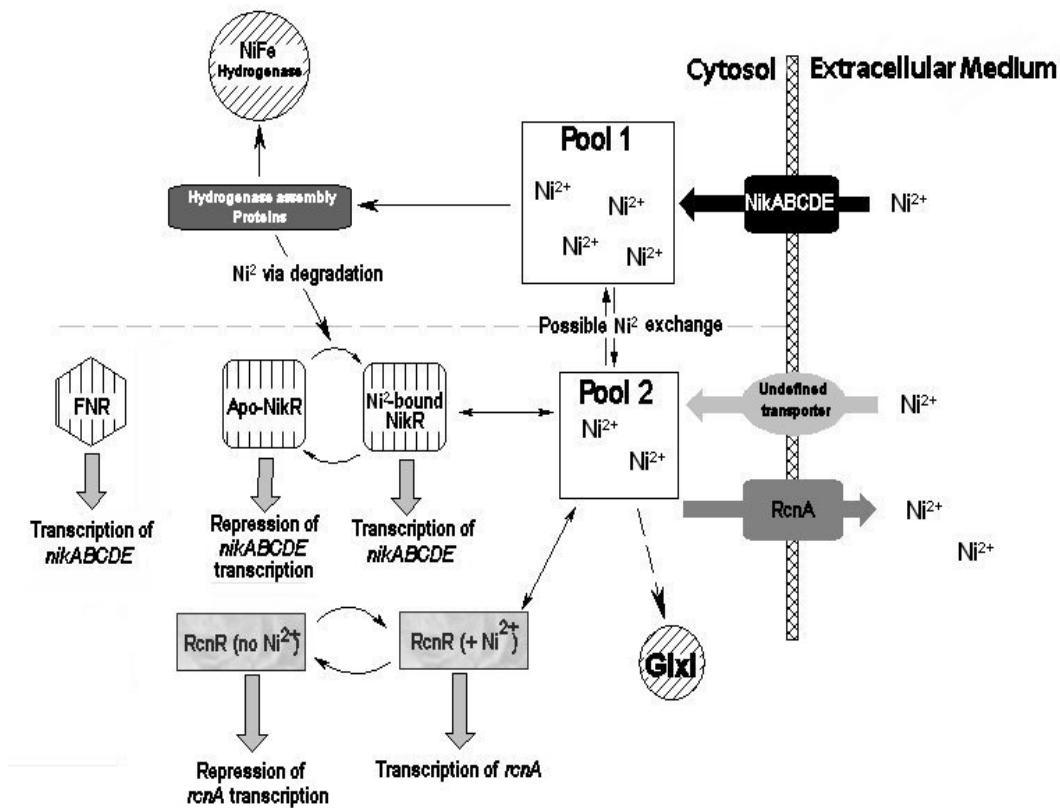
Figure 5.6: Scheme for nickel transport in *E. coli*. Diagram adapted from (176)

6.8.6 Cobalt is not a Likely Contributor to *E. coli* GlxI Activation *in vivo*

Cobalt impairs the growth of *E. coli* significantly at concentrations of 100 μM in minimal medium
(178). The CorA transporter does seem to play a major role in Co^{2+} accumulation as mentioned
previously, and deletion of the encoding gene decreases uptake markedly in medium spiked with
$CoCl_2$ (178). Expression of the Fur (ferric uptake regulator) gene *fhuF* (encodes ferrichrome
reductase) is increased in *E. coli* with exposure to exogenous $CoCl_2$, implying that observed decreases
in iron uptake may be due to cobalt accumulation via iron transport systems (178). This impairs the
activities of several important [Fe-S] enzymes in *E. coli* cells (178). Experimental findings by
Ranquet *et al.* indicate a disruption of iron homeostasis and [Fe-S] cluster synthesis in *E. coli*

145

resulting from the insertion of Co^{2+} into [Fe-S] clusters, leading to protein inactivation. The potential for cellular impairment with Co^{2+} concentrations exceeding 5-10 µM in *E. coli* implies that wild type cells limit Co^{2+} uptake, except for the ions present in vitamin B12. Therefore Co^{2+} may not be a plausible reservoir for activation of *E. coli* GlxI *in vivo*. Assuming that Ni^{2+} is the preferred activating metal *in vivo*, the pool of Ni^{2+} associated with GlxI function in *E. coli* remains as yet undefined.

Chapter 6

Metal Binding and Inhibitor Binding Studies of *E. coli* Glyoxalase I

6.1 Monomeric GlxI Enzymes Exhibit Differential Catalytic Site Activities

Glyoxalase I enzymes can occur as homodimeric or fused dimer structures (Figure 6.1). Examples of homodimeric GlxI enzymes include those from *E. coli*, *H. sapiens*, *L. major* and *P. putida* (51, 59, 67, 147). Fused dimer GlxI enzymes have been isolated primarily from *S. cerevisiae*, *Plasmodium falciparum* and plant sources such as wheat bran (57, 58, 179). The proteins in the βαββ superfamily (including GlxI) are assembled so that the constituent monomers form two identical active sites/binding sites (9, 54).
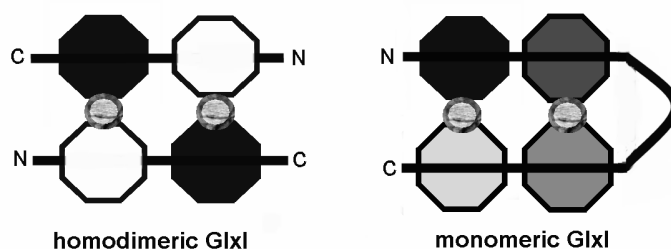

Figure 6.1: Schemes for assembly of homodimeric versus monomeric GlxI enzymes. In the homodimeric model, similarly coloured octagons represent identical domains in the protein. In the monomeric model all βαββ domains are connected sequentially in a contiguous polypeptide sequence. Circles represent bound metal ions. Diagram adapted from (8).

```
P. falcip    -------MAQEISNLVKKYNVTWQQTMLRIYDPKETVEFYEKNFGMINIHTYHFNEYNFS
S. cerev     MSTDSTRYPIQIEKASNDPTLLLNHTCLRVKDPARTVKFYTEHFGMKLLSRKDFEEAKFS
E. coli      ------------------------------------------------------------
H. sapiens   ------------------------------------------------------------

P. falci     LYFLITPPYDEEERKKLPEPNTKESEKYLWNLNTVCLELTYNHNSQEKL----SNGNNEN
S. cerev     LYFLSFPKDD--------IPKNKNGEPDVFSAHGV-LELTHNWGTEKNPDYKINNGNEEP
E. coli      ------------------------------------------------------------
H. sapiens   ----------------------------------------MAEPQP----PSGGLTD

P. falci     DRGFGHIAFNCNDVIEQCDNLFKKNVKFHKLPHETKMKTIGFALDPNNYWIEIVKRSNQV
S. cerev     HRGFGHICFSVSDINKTCEELESQGVKFKKRLSEGRQKDIAFALGPDGYWIELITYSREG
E. coli      ------------------------------------------------------------
H. sapiens   EA-----ALSC------CSD---------------------ADPST------------

P. falci     KWKNYKNIT---NFSQTMIRVKNPEKSLYFYIHILGMKLIHVKHCS----DFSLYFLKSN
S. cerev     --QEYPKGSVGNKFNHTMIRIKNPTRSLEFYQNVLGMKLL--RTSEHESAKFTLYFL---
E. coli      -----------MRLLHTMLRVGDLQRSIDFYTKVLGMKLL--RTSENPEYKYSLAFV---
H. sapiens   --KDFL-------LQQTMLRVKDPKKSLDFYTRVLGMTLI--QKCDFPIMKFSLYFL---

P. falci     YACAENNKEMIEDQSNKNTNEIYDFNSLKNSYQTDEDYENFKQSWEPVLELTHNHGTEDD
S. cerev     ------GYGVPKTDS-------------------------VFSCESVLELTHNWGTEND
E. coli      ------GYG-PETE-----------------------------EAVIELTYNWGVDK-
H. sapiens   --AYEDKNDIPKEKDEKIA-------------------WALSRKATLELTHNWGTEDD

P. falci     DNFSYHNGNTEPRGFGHIGFLVNDLENYCKELETL---NVTFKKKVTEGLMKNIAFIYDP
S. cerev     PNFHYHNGNSEPQGYGHICISCDDAGALCKEIEVKYGDKIQWSPKFNQGRMKNIAFLKDP
E. coli      ----YELGTA----YGHIALSVDNAAEACEKIRQN-GGNVTREAGPVKGGTTVIAFVEDP
H. sapiens   ETQSYHNGNSDPRGFGHIGIAVPDVYSACKRFEEL---GVKFVKKPDDGKMKGLAFIQDP

P. falci     DNYVIELIQRDTSFIAK--
S. cerev     DGYSIEVVPHGLIA-----
E. coli      DGYKIELIEEKDAGRGLGN
H. sapiens   DGYWIEILNPNKMATLM--
```

Figure 6.2: Alignment of sequences of monomeric GlxI enzymes from *P. falciparum* and *S. cerevisiae* (Accession nos. AAQ05975 and CAA67622 respectively) with homodimeric GlxI sequences from *E. coli* and *H. sapiens* (Accession nos. U57363 and NP_006699 respectively). Metal ligands are highlighted in black.

148

Several studies of monomeric GlxI enzymes have allowed some exploration of differential

kinetics of the two active sites in the native protein. The monomeric GlxI enzymes are structurally

"fused dimers" where all βαβββ modules are joined via protein linkers to form both active sites

within a contiguous stretch of polypeptide sequence (Figure 6.2) (9, 57, 58, 179). Analysis of

monomeric GlxI sequences indicates that they were likely formed as a result of two gene duplications

(of a unit of a gene encoding a single βαβββ module) and subsequent fusion events resulting in

assembly of consecutive βαβββ modules (1/2 active site) at the genetic level (Figure 6.3)(9, 54).

Each gene duplication event would have resulted in the formation of an additional βαβββ module

(1/2 active site) or tandem βαβββ module.
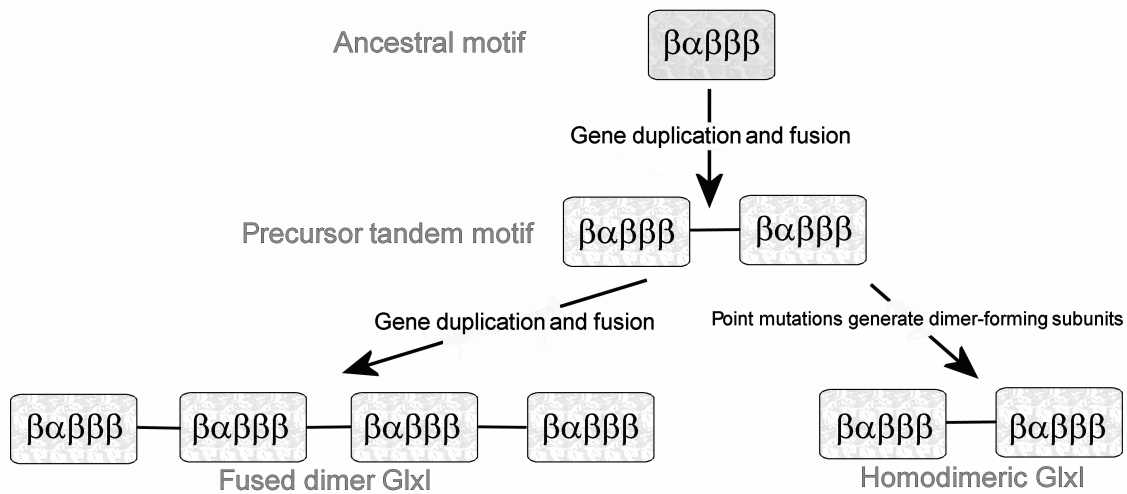

Figure 6.3: Scheme for evolution of homodimeric and fused monomeric GlxI enzymes. Adapted from (9)**.**

6.2 Yeast GlxI has Different Kinetic Parameters for Each Active Site

The yeast (*Saccharomyces cerevisiae*) GlxI displays significantly different kinetic parameters for

turnover of MG-GSH depending on which active site is inactivated (57). Frickel *et al.* created two

yeast GlxI variants with E163Q and E318Q substitutions respectively, selectively disabling the active

sites. Glutamate substitutions in both active sites resulted in a variant with a severely compromised

capacity to isomerize MG-GSH ($k_{cat} \approx 0.31$ s^{-1}) (57). Interestingly, inhibition constants for both of the

single active site variants were found to be comparable in the presence of *S*-hexylglutathione (57).

Frickel *et al.* estimated from their kinetic analysis that the active site containing His25, Glu89, His269

and Glu318 supplies approximately 75% of the total enzyme activity with the remaining 25%

contributed by the site with His185, Glu242, His117 and Glu163. This estimate is conservative, as

the residual enzymatic activities of each single active site variant together do not account for the total

enzyme activity observed for wild type yeast GlxI (57). Furthermore they did not explore any aspect

of potential allosterism between active sites but acknowledged that this phenomenon may apply to the

enzyme under study.

6.3 *P. falciparum* GlxI Active Sites Exhibit Allostery

P. falciparum GlxI is another Zn^{2+}-activated monomeric GlxI enzyme whose characterization was

first reported in 2003 (128, 180). Similar to the yeast GlxI study, Deponte et al. created variants with

a glutamate substitution specific to each active site and characterized the proteins by performing

steady state kinetic measurements (8). Their approach to active site inactivation was to create single

and double E→Q substitutions corresponding to each active site (E91 and E345 are from one active

site, E161 and E272 are in the other) (8). The muteins created were E91Q, E345Q, E91Q/E345Q,

E191Q, E272Q, E161Q/E272Q and E161Q/E345Q (latter variant had both active sites modified) (8).

Biphasic kinetics are observed for the wild type and mutagenized enzymes, so that two apparent K_m

and k_{cat} values can be calculated for each active site (8). The catalytic efficiencies of the E91 and

E345 variants (including the double residue substitution), are equivalent to approximately 7% of that

for the wild type *P. falciparum* GlxI (8). Conversely, the catalytic efficiencies of the E161 and E272

variants (including the double residue substitution), were equivalent to approximately 60% of wild type *P. falciparum* GlxI (8). Furthermore the "relative to wild type" magnitudes of $K_{\text{m}app}$ and k_{cat} app appear to correlate to the active site which was modified (8). The residual enzyme activities in each of the single active site glutamate to glutamine variants did not indicate additive activities contributing to the catalytic proficiency of the *P. falciparum* GlxI as a whole (8).

Additionally Deponte and co-workers observed differential protease susceptibility of *P. falciparum* GlxI (wild type and variant enzyme) in the presence and absence of added substrate (8). These data are complementary in supporting the hypothesis that the active sites of monomeric *P. falciparum* GlxI are allosterically coupled even though the binding affinity of each active site is markedly distinct (8). Whether coupling of active sites in homodimeric GlxI enzymes occurs remains to be determined, but asymmetry of active sites has been documented in *E. coli* GlxI, specifically the different metal stoichiometry between two supposedly identical active sites.

6.4 Evidence for Non-Symmetric Active Sites in *E. coli* GlxI

The metal binding site stoichiometry in *E. coli* GlxI is a property of the enzyme for which there is conflicting data. Titration of the apoenzyme with Ni^{2+}, Co^{2+}, Mn^{2+} and Cd^{2+} results in maximal activation levels achieved at a ratio of approximately one metal per dimer (56). Inductively coupled plasma atomic emission spectroscopy of Ni^{2+}-, Co^{2+}, Mn^{2+}, Cd^{2+} and Zn^{2+} holoGlxI indicates a binding ratio of one metal ion per dimer as well (51, 60). Furthermore these estimates are in agreement with the number of metallation sites determined by isothermal titration calorimetry (ITC) of *E. coli* GlxI with all metals used for ICP-AES analysis (51, 60). However the published crystal structures for Ni^{2+}-, Co^{2+}, Zn^{2+} and Cd^{2+}-bound *E. coli* GlxI indicate that both active sites of the homodimer are occupied by metal ions (52).

Further characterization of metal binding in *E. coli* GlxI is required to resolve whether the enzyme is fully active with metal occupancy at one or both of the active sites. From a structural perspective, metallation of *E. coli* GlxI must be a subtle process. This is apparent from the absence of secondary structure changes between the apo-dimer versus the holo-dimer as shown by circular dichroism spectroscopy (56). Furthermore the root mean-squared deviation when comparing the C-α atoms of the apo-GlxI crystal structure to that of the Ni^{2+}-substituted enzyme is only 0.32 Angstoms (60).

This chapter describes the examination of microscopic structural changes in *E. coli* GlxI accompanying metal binding, using ^{1}H-^{15}N heteronuclear single quantum coherence (HSQC) NMR. This study is pertinent to addressing whether GlxI actually uses both active sites for enzymatic catalysis.

6.5 Materials and Methods

6.5.1 Reagents

See Chapter 2, section 2.5 for materials referred to in the described methods.

6.5.2 Expression and Purification of ^{15}N-labelled *E. coli* GlxI – Wild Type and H74Q

All cultures for overproduction of ^{15}N-labelled protein were grown on a 0.5 L or 1 L scale. Wild type *E. coli* GlxI was overproduced in an *E. coli* BL21(λDE3) host using the plasmid pGL10, which is normally expressed in the MG1655 background for recombinant protein production. The BL21 strain was used in this study as less co-contaminating proteins persisted across purification steps for the protein. Large scale (1L volume) cultures of BL21(λDE3)/pGL10 grown in M9 minimal salts medium containing 18.8 mM ^{15}N-labelled $(NH_4)_2SO_4$ (Cambridge Isotope Laboratories, Andover, MA, USA) 50 mg/L carbenicillin were inoculated with growth from a 20 mL culture of the

bacterium cultivated in M9 minimal salts medium (containing unlabelled $(NH_4)_2SO_4$ as a nitrogen source) with 50 µg/mL carbenicillin. The aforementioned 20 mL culture was initially inoculated with growth from a 10 mL starter culture of BL21(λDE3)/pGL10 grown in LB broth containing 50 µg/mL carbenicillin. Prior to inoculating the intermediate and large-scale cultures, the innoculum was centrifuged at 3000 g and resuspended in sterile M9 salts solution to minimize the carry-over of any secreted β-lactamase. The large-scale culture was grown to an OD_{600} of 1 and then induced with 0.5 mM IPTG for 12 hours. Cells were harvested by centrifugation at 6000 g and frozen in liquid nitrogen until the time of purification.

For overproduction of the H74Q active site variant of *E. coli* GlxI, the MG1655 host strain containing the plasmid pGL13 was used. The protocol described above for overproduction of wild type ^{15}N-labelled *E. coli* GlxI was similarly employed for labelling of H74Q GlxI.

Purification of the cell lysates for wt and H74Q GlxI initially consisted of precipitating contaminating proteins by the addition of $(NH_4)_2SO_4$ to 60% saturation. The majority of recombinant GlxI remains in the supernatant at this salt concentration and this remaining soluble portion of lysates was dialysed into 20 mM Tris pH 8.0 containing 1 mM PMSF for application to the UnosphereQ anion exchange column. The dialysed protein was applied to the column (loaded at 0.8 mL/min) and eluted using a linear gradient of KCl from 0 to 1M over 100 minutes at 0.8 mL/min. The labelled GlxI fractions were eluted between 20 and 40% KCl and pooled for dialysis into 20 mM Tris pH 8.5 and loaded onto a MonoQ 5/5 column at 0.5 mL/min. The enzyme was eluted from the column with a linear gradient of KCl from 0 to 1M over 100 minutes at 0.5 mL/min. GlxI containing fractions were pooled and concentrated. The buffer change and concentration of the purified ^{15}N-labelled GlxI was carried out by ultrafiltration using a Vivaspin 2mL centrifugal concentrator (10000 MWCO) spun at 3000 g in a clinical centrifuge. During the buffer change the protein was exchanged into 50 mM MOPS containing 100 mM DPA pH 7.0 to ensure removal of any bound metal. The protein was then

exchanged (centrifugal ultrafiltration) into 20 mM MOPS pH 6.59 for storage and NMR analysis

using enough buffer solution to ensure that prior buffer components were diluted more than 1000-fold

before storage of the protein at 4 °C. The protein concentration was determined by the method of

Bradford and the absence of any contaminating metal was confirmed by the PAR assay using protein

denatured in 4M Gdn-HCl (118, 181).

For the purification of ^{15}N-labelled H74Q GlxI the lysate was subjected to ammonium sulfate

as described for the wild type enzyme. A significant quantity of H74Q GlxI precipitated following

addition of $(NH_4)_2SO_4$ to 60 % saturation in the lysate. This protein was solubilized and desalted by

dialysis into 20 mM Tris pH 8.5 for application to a UnosphereQ column where the protein was

eluted off using a linear gradient of 1 mL UnosphereQ (flow rate for application was 0.8 mL/min)

column where the protein was eluted with a linear gradient of KCl from 0 to 1M over 100 minutes

(flow rate was 0.8 mL/min). The GlxI containing fractions from this step were dialyzed into 20 mM

Tris pH 7.5 and solid $(NH_4)_2SO_4$ was added to the sample for a final concentration of 1M. The

sample was applied to a Phenyl HP Hi Sub (Amersham Biosciences) column with 20 mM Tris pH 7.5

containing 1 M $(NH_4)_2SO_4$ at 1 mL/ per minute and eluted off the column with a linear decreasing

gradient of $(NH_4)_2SO_4$ (1M to 0M over 15 minutes). A polishing size exclusion step was included

when necessary during purification. Specifically the concentrated H74Q GlxI sample was applied to

and eluted from a Superdex75 column (10/30) at 0.5 mL/min using 20 mM Tris pH 7.5, containing

150 mM $(NH_4)_2SO_4$.   Subsequently these fractions were pooled, the buffer exchanged and

concentrated as described above for wild type *E. coli* GlxI.

6.5.3 ^{1}H-^{15}N NMR Conditions

All NMR spectra were collected at 25°C on a Bruker Avance 600 or 700 MHz spectrometer equipped

with a triple-resonance pulse-field gradient probe. ^{1}H-^{15}N HSQC NMR spectra were recorded in the

States-TPPI mode for quadrature detection (182, 183). All the NMR samples were prepared in the same buffer, (20 mM MOPS pH 6.59 plus 5% D_2O (final concentration)) ^1H-^{15}N HSQC titrations of the Apo-wild type and H74Q *E. coli* GlxI enzymes were performed by stepwise addition of Ni^{2+} or inhibitor (at a high concentration) into the ^{15}N-labeled component (typically at a concentration of 0.1-0.3 mM) to a final 1 to 2-fold excess.

7.5.3 NiCl$_2$ Titration of Wild Type and H74Q Variant *E. coli* GlxI

The step-wise titrations of Ni^{2+} ions into the apo-wild type and H74Q *E. coli* GlxI enzymes were performed on a 600 MHz and 700 MHz NMR machine respectively. NiCl$_2$ stocks were prepared at concentrations so that the wild type dimeric enzyme was exposed to 0.25 equivalents of Ni^{2+} with the addition of 5 mL of metal chloride solution.

6.6 Results

6.6.1 Ni^{2+} Titration of Wild Type and H74Q GlxI

ESMS analysis confirms that ^{15}N-labelling of the amide backbone of wild type (Figure 6.4) and H74Q GlxI is complete when the aforementioned expression systems are used. Thus ^{15}N-labelled wild type and H74Q GlxI was obtained with molecular masses at the expected values for protein produced by BL21(λDE3)/pGL10 and MG1655/pGL13 with ^{15}N-labelled $(NH_4)_2SO_4$ as the sole nitrogen source. Gel filtration chromatography on a Superdex 75 column during purification indicates that the ^{15}N-labelled GlxI is homodimeric. An apparent molecular weight of 24 kDa and a similar elution volume to carbonic anhydrase (30 kDa) were observed during this procedure. No protein-containing fractions indicative of GlxI monomers (14.9 kDa) were observed during separation. Preparations of ^{15}N-labelled GlxI for this investigation approach 85-90% purity as assessed by SDS-PAGE with Coomassie Brilliant Blue Staining. However the yields are quite modest averaging about 1-2 mg of

protein from 4L of culture for wild type and H74Q *E. coli* GlxI under the described growth conditions.
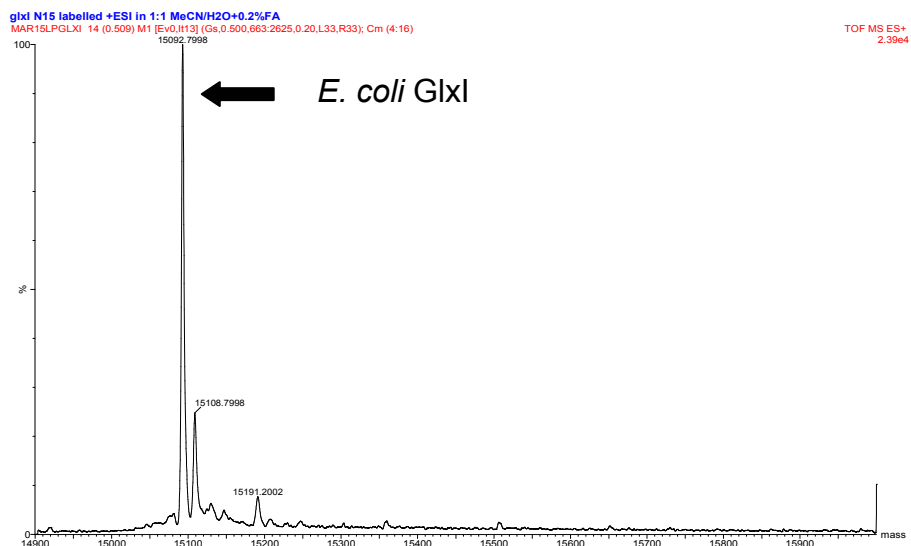
Figure 6.4: Representative electrospray ionization mass spectrum for ^{15}N-labelled wild type *E. coli* GlxI. The peak corresponding to the protein of interest is indicated with an arrow. The calculated molecular mass of the GlxI monomer is 15097 Da and the observed molecular mass is 15093 Da.

During the execution of this project, Dr. Zhengding Su attempted to create a plasmid construct in which the *E. coli gloA* gene was flanked at the 3'-end by a sequence encoding a hexahistidine tag preceded by a thrombin cleavage site. In practice this may have improved recovery of ^{15}N-labelled *E. coli* GlxI, as the enhancement of purity by nickel-nitriloacetic acid affinity chromatography is generally superior and more efficient than the chromatographic methods documented in this section. However the recombinant expression system obtained from this re-cloning exercise generated detectable but insoluble GlxI based on SDS-PAGE analysis of lysates from test inductions.

The initial ^1H-^{15}N HSQC NMR experiment conducted was a Ni^{2+}-titration of wild type *E. coli* with $NiCl_2$. The colorimetric PAR assay was used to confirm that the protein being titrated was in the apo-form following ultrafiltration in the presence of DPA before the NMR experiment was performed. An initial 1D ^1H-NMR spectrum (data not shown) of the apoGlxI revealed a well-defined amide region indicating that the protein was well folded under the solution titration conditions (20 mM MOPS pH 6.59 + 10% D_2O v/v). Theoretically, there would be 132 resonance peaks (135 amino acids in *E. coli* GlxI minus the non-detectable proline residues) corresponding to each residue in the monomer if the homodimer is symmetric or if the protein was monomeric in solution. Alternatively, dimer asymmetry where the residues in each monomer were not chemical shift equivalent would yield a 2D spectrum with 270 peaks. There are approximately 128 detectable resonance peaks in the wild type GlxI spectrum (Figure 6.5). In conjunction with the gel filtration analysis, this shows that the apoGlxI enzyme in solution is dimeric.

Interestingly, the ^1H-^{15}N HSQC spectrum of the apoGlxI reveals an initial asymmetry of the monomeric modules comprising the native protein. Specifically, two peaks were observed in the region of the spectra that correspond to ring ^{15}N resonances of tryptophan residues (Figure 6.5). Examination of the amino acid sequence reveals that the *E. coli* GlxI monomer possesses only one tryptophan residue (Figure 6.5). The presence of two peaks indicates conformational asymmetry of Trp61 in the native GlxI apoenzyme.
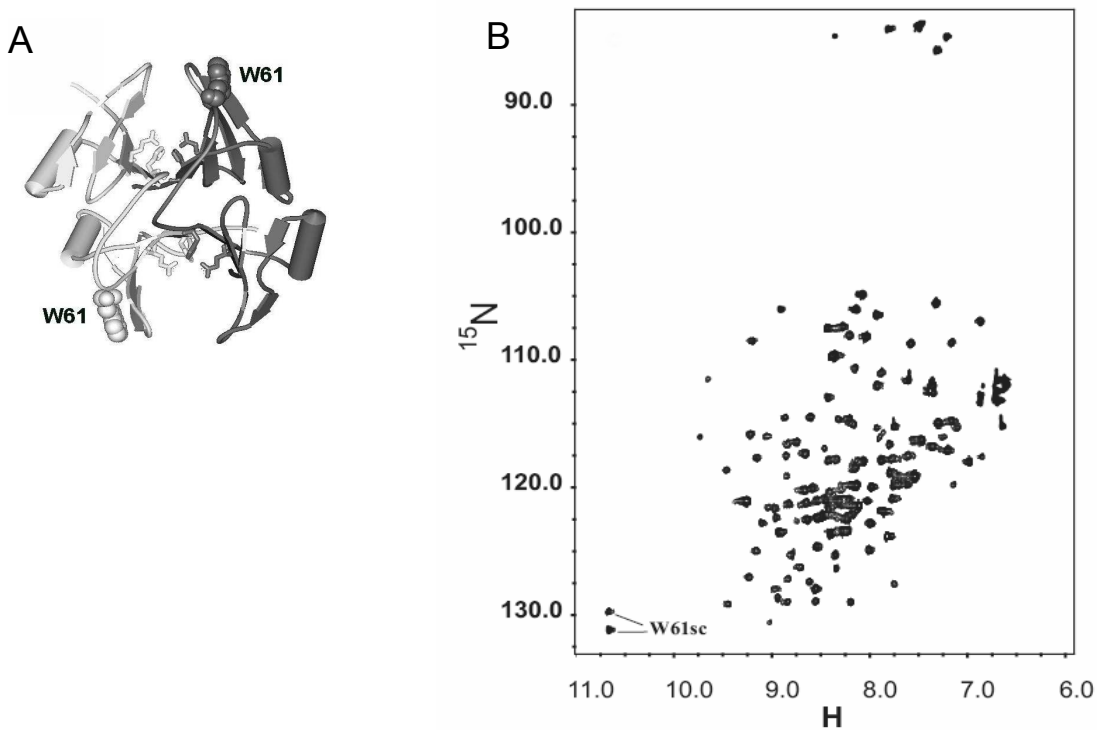
Figure 6.5: A) Structure of *E. coli* GlxI showing the location of Trp61 B) ^{1}H-^{15}N HSQC spectrum of wild type GlxI apoenzyme with labelled resonance peaks for Trp61.

Although assignment of all peaks in the *E. coli* GlxI ^{1}H-^{15}N HSQC spectrum has not yet been performed, the systematic NiCl$_2$ titration of wild type GlxI permits the observation of subtle protein backbone reorganization. These conformational differences were not previously revealed in crystallographic or circular dichroism analysis. Following titration of one equivalent of Ni^{2+} ions into the GlxI sample, the spectrum reveals splitting for several peaks, indicative of asymmetries in the dimer environment that accompany metal binding. The chemical shifts for the Trp61 residues remain constant during Ni^{2+} titration of the enzyme (Figures 6.6 and 6.8). Additionally, spatially distinct shifts in spectral peaks are also observed, which are indicative of uniform backbone reorganizations at

specific locations in both monomers of the native enzyme (Figure 6.7). A key implication of these spectral features of the titrated enzyme is that wild type *E. coli* GlxI does not possess a uniform dimer environment and that the holoprotein assumes a conformation distinct relative to the apoenzyme when it acquires activating Ni^{2+} ions.

The changes in peak distribution/splitting are essentially complete after titration with one equivalent of Ni^{2+} into apoGlxI (Figures 6.6, 6.7 and 6.8). Superimposition of the spectra following one-equivalent and two-equivalent additions of Ni^{2+} to *E. coli* GlxI indicate that little change in protein conformation occurs when titrated past one-half of the total active sites. The data implies that the active enzyme saturates for metal binding at one equivalent Ni^{2+} per dimer. This data is consistent with ITC and ICP-AES studies as well as activity versus metal content plots indicating that *E. coli* GlxI exhibits half-of-the-sites metal binding under the conditions examined.
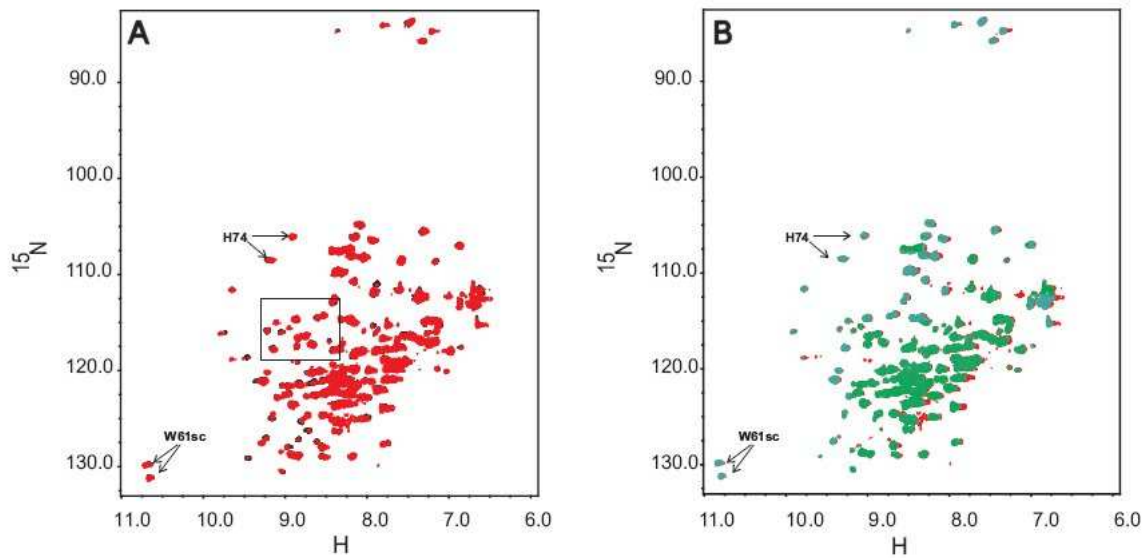
Figure 6.6: A) Overlay of apoGlxI spectrum (black) with 1:1 Ni2+:GlxI in solution (red) B) Overlay of spectra for 1:1 Ni2+:GlxI (green) and 2:1 Ni2+:GlxI (red). Resonances labelled H74 and W61sc are associated with His74 backbone resonances and Trp61 side chain resonances respectively. The box in A) denotes the area of the spectra where peak splitting occurs during metal titration. An expanded view of this region is shown in Figure 6.7.
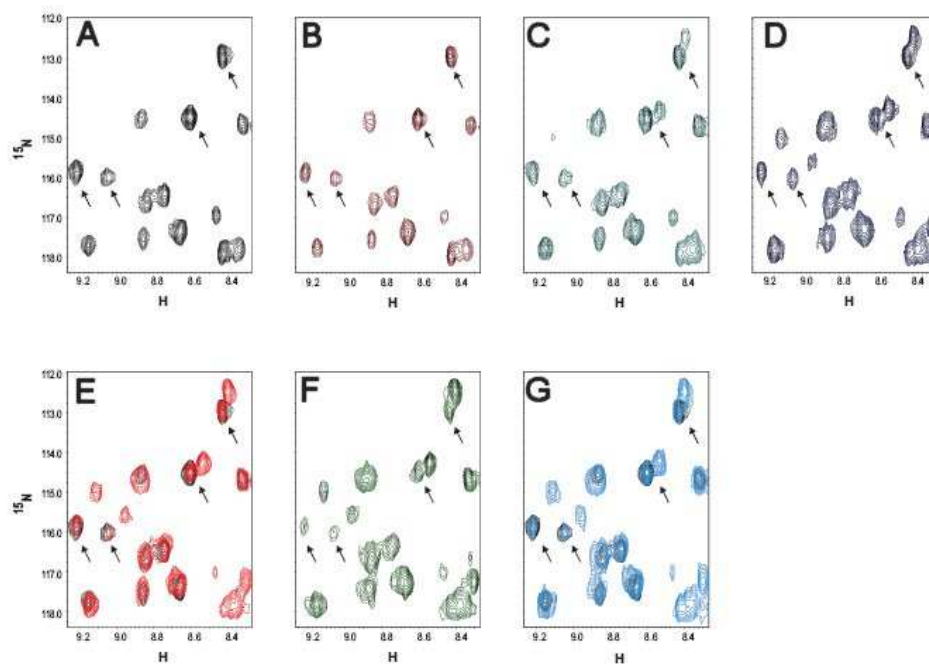
Figure 6.7: Selected resonances (indicated by arrows in wild type GlxI that split in response to Ni²⁺ binding. Each panel represents resonances an overlay of the apoenzyme spectrum (black) with non-black titration spectra at increasing metal:dimer ratios: A) 0:1 B) 0.25:1 C) 0.5:1 D) 0.75:1 E) 1:1 F) 1.5:1 G) 2:1.
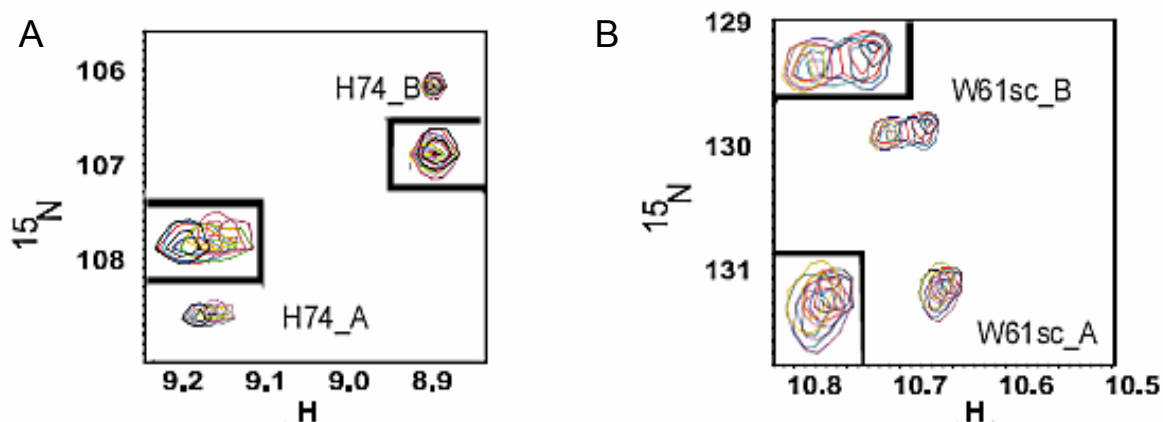
Figure 6.8: Chemical shift changes accompanying metal binding in wild type GlxI for A)His74 and B) Trp61 side-chain N-H resonances. Colours of resonances denote positions metal:dimer ratios of 0:1 (black), 0.4:1 (green), 0.6:1 (purple), 0.8:1 (yellow), 1:1 (red), 1.5:1 (brown) and 2:1 (blue). Display of these resonances is enlarged (inset) for clearer illustration.

^{1}H-^{15}N HSQC NMR spectra were also obtained for the H74Q variant of *E. coli* GlxI, which has been previously characterized for metal activation. This metal versus activity titration data is described thoroughly in the Master's dissertation of Nicole Sukdeo. This active site variant was chosen for ^{1}H-^{15}N HSQC NMR analyses to identify the peaks associated with the His74 metal ligand. Additionally, the yields of recombinantly expressed H74Q GlxI are superior to those for the H5Q and double active site histidine variant H5Q/H74Q GlxI (both have been previously described), so it was a suitable candidate for ^{15}N-labelling where yields of protein tend to be more conservative. The 1D proton NMR spectrum for H74Q GlxI was indicative of a well-folded dimeric protein comparable to the 1D spectrum for the wild type enzyme. The overall distribution of ^{1}H-^{15}N HSQC peaks for the H74Q dimer is quite similar to those observed for the wild type enzyme. Particularly the backbone resonances in the chemical shift range ^{15}N 103-111 ppm, ^{1}H 7.1-8 ppm are spatially arranged in an identical manner comparing the wild type and H74Q spectra. This conservation of protein structure is

162

expected, as His74 is primarily a metal binding residue and likely not a great contributor to the structural configuration of the overall dimer.

There are some notable differences between the ^{1}H-^{15}N HSQC spectra of the wild type *E. coli* GlxI and this active site variant. The most prominent difference is the absence of two resonances in the H74Q GlxI spectrum that are located at ^{15}N 106 ppm, ^{1}H 8.96 ppm and ^{15}N 108.5 ppm, ^{1}H 9.25 ppm in the wild type *E. coli* GlxI spectrum (Figure 6.8). During NiCl$_2$ titration of the wild type enzyme it is also observed that the peak with the chemical shifts ^{15}N 108.5 ppm, ^{1}H 9.25 ppm translocates in the spectrum in the presence of Ni^{2+} whereas the peak at ^{15}N 106 ppm, ^{1}H 8.96 ppm does not (Figure 6.9). These peaks in the wild type spectrum are likely representative of the His74 backbone amide resonances and their difference and their absence in the H74Q spectrum is plausible given the glutamine substitution. Furthermore the presence of two peaks that can be assigned to each of the active site His74 residues in the homodimer indicates inherent asymmetry of the active sites in the wild type apo- and holo-enzyme (Figure 6.9). In accordance with half-of-the-sites metallation of *E. coli* GlxI the chemical shift change for only one of the two peaks implies metal ion binding at only one active site in the native apoenzyme. Other notable features of the H74Q variant spectrum are several resonances that are translocated relative to the analogous resonance in the wild type GlxI spectrum (Figure 6.9). It is possible that these chemical shift differences indicate a subtle reconfiguration of hydrogen-bonding that is strongly influenced by the presence of His74 in the polypeptide. Consequently the lower activity (and weaker metal binding) observed for H74Q GlxI may be the result of ligand substitution inducing unfavorable changes in the second sphere coordination environment.
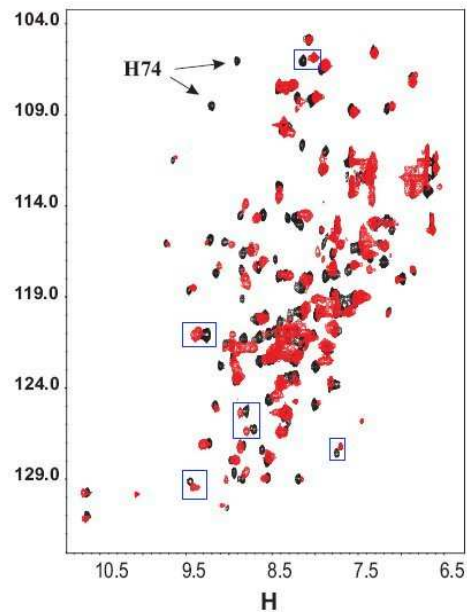
Figure 6.9: Overlay of wild type apoGlxI spectrum (black) with the apoH74Q-GlxI spectrum (red). The resonances associated with His74 residues in the wild type spectrum are indicated with arrows (H74). Resonances that are shifted in both monomers of the H74Q variant relative to wild type GlxI are indicated with blue boxes.

The *E. coli* GlxI H74Q variant has been characterized previously by metal versus activity titration. The relative activation of the enzyme with different divalent metal ions ($Ni^{2+} > Co^{2+} > Mn^{2+} > Cd^{2+}$) is similar to the wild type GlxI although the activity is almost abolished (specific activity of H74Q is approximately 1% of the V_{max} reported for wild type *E. coli* GlxI) as a consequence of the ligand substitution. The metal titrations indicate that the metal affinity of the variant GlxI is attenuated. Wild type *E. coli* GlxI exhibits maximal activation when titrated with reconstituting metal ions (Ni^{2+}, Co^{2+}, Mn^{2+}, Cd^{2+}) when titrated from the apo-form to one equivalent of metal per homodimer in solution. The H74Q GlxI variant reaches maximal activation when titrated from the apoform closer to two equivalents of metal ion per dimer. Although calorimetric or equilibrium

164

dialysis data have not been used to characterize metal affinity of this variant, these titrations

demonstrate the essential role of His74 for binding catalytic metal ions in *E. coli* GlxI.

NiCl$_2$ titration of the ^{15}N-labelled H74Q GlxI enzyme also demonstrates the compromised

metal-binding capacity of this variant. ^{1}H-^{15}N HSQC spectra of the apo-form H74Q compared to the

spectra of the enzyme with one equivalent of Ni^{2+} reveals no significant shift in the backbone ^{15}N and

^{1}H chemical shift values (data not shown). This contrasts significantly with Ni^{2+} titration of wild type

GlxI where peak splitting and/or re-orientation is observable with the introduction of only 0.25

equivalents of Ni^{2+} to the preparation of apoenzyme. One important attribute of the ^{1}H-^{15}N HSQC

NMR spectra obtained for the H74Q variant is that the two peaks associated with the indole ring

nitrogen resonances from Trp61 are still visible as observed in the wild type spectrum. This implies

that a degree of dimer asymmetry is present in the variant, which is plausible, as the histidine to

glutamine substitution is not positioned to significantly alter the native structure of the enzyme.

However the absence of spectral changes accompanying metal titration indicates an inability of the

variant to assume the active metal-binding conformation, in spite of the subtle nature of the apo- to

holoenzyme conversion.

6.6.2 Titration of Ni^{2+}-Reconstituted *E. coli* GlxI with *S*-{2-[3-(hexyloxy)benzoyl]vinyl}glutathione

In an effort to characterize subtle structural changes of the wild type *E. coli* GlxI enzyme that would

accompany substrate/substrate analogue binding, the Ni^{2+}-reconstituted enzyme (re-metallated during

NiCl$_2$ titration experiment) was incrementally titrated with a comparably strong inhibitor. *S*-{2-[3-

(hexyloxy)benzoyl]vinyl}glutathione (Figure 6.10) and its interaction with *E. coli* GlxI has previously

been characterized in an electrospray time-of-flight mass spectrometric examination of GlxI-inhibitor

complexes (184). This compound was one of several S-substituted glutathione analogues screened

against *E. coli* GlxI previously. This inhibitor has a micromolar inhibition constant for *E. coli* GlxI, with a published IC$_{50}$ value of approximately 57 µM (184).
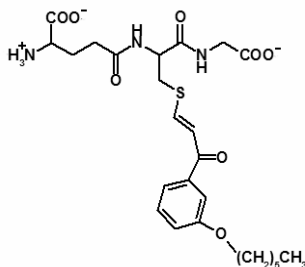
Figure 6.10: Structure of *S*-{2-[3-(hexyloxy)benzoyl]vinyl}glutathione

Mass spectrometric and enzyme kinetic studies indicate that the dimeric enzyme can bind *S*-{2-[3-(hexyloxy)benzoyl]vinyl}glutathione in the apo- and Ni^{2+}-reconstituted forms (184). *E. coli* GlxI is also capable of binding two molecules of *S*-{2-[3-(hexyloxy)benzoyl]vinyl}glutathione based on an ESMS-monitored titration of apo-GlxI (184). For monometallated *E. coli* GlxI, this finding implies that both apo- and holo- active sites of enzyme can bind inhibitors (and possibly substrates). Alternatively, this inhibitor stoichiometry might imply that the mode of *E. coli* GlxI inhibition involves indiscriminate interaction with both active sites.

The substrate analog *S*-{2-[3-(hexyloxy)benzoyl]vinyl}glutathione was solubilized in 100% dimethyl sulfoxide (DMSO) and titrated into the holoenzyme preparation as a millimolar concentration working stock so as to minimize any detrimental effects of this organic solvent on the protein structure. The overall distribution of peaks in the ^{1}H-^{15}N HSQC NMR spectra during titration remains the same indicating that the protein structure is stable in low concentrations of DMSO. When Ni^{2+}-GlxI is exposed to *S*-{2-[3-(hexyloxy)benzoyl]vinyl}glutathione at 1:1 inhibitor to dimer in solution, the peak at ^{15}N 106 ppm, ^{1}H 8.96 ppm does not change in chemical shift whereas the peak at ^{15}N 108.5 ppm, ^{1}H 9.25 ppm remains stationary (Figure 6.11 B). These two peaks once again are

associated with the backbone amide resonances of the His74 active site residues in the homodimer (Figure 6.11). What is interesting to note about these changes accompanying binding of this glutathione analog is that the monometallated enzyme would appear to bind the inhibitor initially at the active site that is not metallated, whereas titrating the apoenzyme with Ni^{2+} results in re-organization of the enzyme for metal binding at the other end of the dimer. These inferences are based on the H74 resonances identified through ^1H-^{15}N HSQC analysis of H74Q GlxI and the observation of a differential response of the two H74 to metal binding versus inhibitor binding.
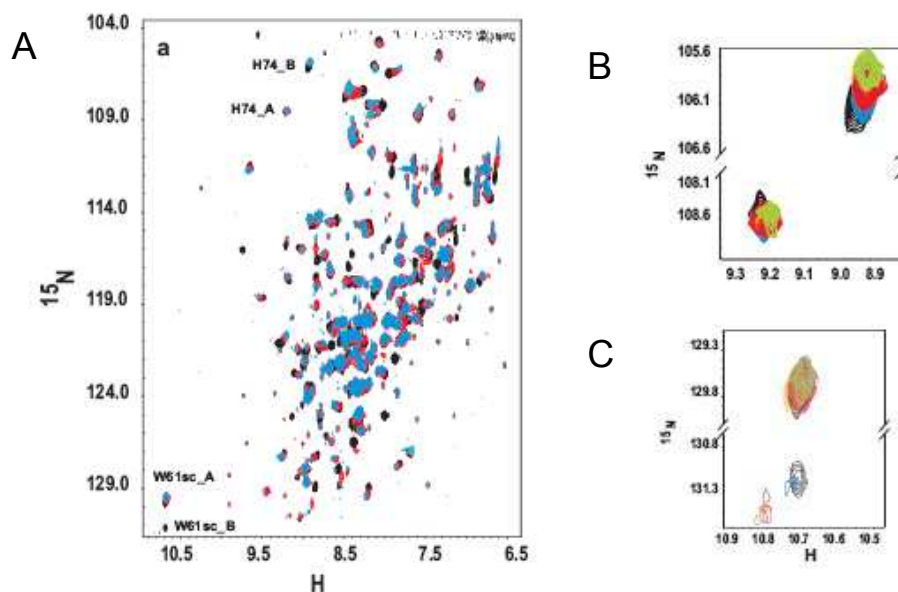
Figure 6.11 A) Overlay of NMR spectrum for wild type Ni^{2+}-reconstituted GlxI pre-inhibitor (black), after titration to 1:1 inhibitor to dimer (red) and following titration to 2:1 inhibitor to dimer (blue). The resonances associated with residues His74 and Trp61 are labelled in the spectrum B) Chemical shift perturbations of His74 accompanying inhibitor binding in the following inhibitor:dimer ratios: 0:1 (black), 0.5:1 (blue), 1:1 (red) and 2:1(green). C) Chemical shift perturbations of Trp61 accompanying inhibitor binding in the following inhibitor:dimer ratios: 0:1 (black), 0.5:1 (blue), 1:1 (red) and 2:1(green).

These results should be interpreted cautiously as the *S*-{2-[3-(hexyloxy)benzoyl]vinyl}glutathione is an inhibitor of GlxI and therefore not a true representation of the substrate. The observed chemical shift changes may actually reflect the inhibitor-induced assumption of an inactive *E. coli* GlxI conformation instead of the substrate-binding conformation. However these observations again indicate that there is very little structural reorganization of the enzyme that accompanies binding of substrate analogues.

One aspect of catalysis that cannot be resolved by the ^{1}H-^{15}N HSQC NMR analysis described in this chapter is the dynamics of the water molecules observed as metal ligands in crystal structures of the resting holoenzyme. XAS studies of *E. coli* GlxI in complexes with *S*-D-lactoylglutathione and *S*-octylglutathione indicate that the incoming substrate/analogue molecule displaces neither active site histidine residue (65). However hydroxamate inhibitor binding to *E. coli* GlxI results in the displacement of both water ligands (65). XAS shows that inhibitor binding to *E. coli* GlxI results in displacement of an active site Glu residue that could function as a catalytic base (65). Eventual assignment of all peaks in the *E. coli* GlxI ^{1}H-^{15}N HSQC NMR spectrum should prove useful in determining whether any metal coordination changes involving glutamate accompanies the binding of incoming substrate/inhibitor.

6.7 Discussion

E. coli GlxI is by no means the only metalloprotein in the biochemical literature for which half-of-the-sites metal binding is relevant to the active holoform. Porphobilinogen synthase serves as a paradigm for this phenomenon.

Porphobilinogen synthases (PBGS) are a family of enzymes that catalyze the asymmetric condensation of two 5-aminolevulinic acid molecules (185). This reaction constitutes the first common step in tetrapyrrole biosynthesis (185).

168

Like GlxI, PBGS enzymes can be divided into two metal activation classes, specifically

those requiring Zn^{2+} for activation and those activated by Mg^{2+} ions (185). The native PBGS

enzymes from human and *Drosophila melanogaster* are homo-octameric tetramers of dimers (186,

187). The monomer possesses an $\alpha_8\beta_8$ barrel tertiary structure and the catalytic site is situated at the

C-terminal regions of the β-strands that converge at the top of the barrel cavity (185, 188). The

dimers are assembled so that the N-terminal arm of each monomer wraps along the periphery of the

adjacent subunit (Figure 6.12). This configuration is very similar to the positioning of the N-terminal

arm contact with the opposite monomer in the human GlxI homodimer (185, 188). The β-barrels in

the dimer are positioned so that the barrel cavities are oriented at right angles to each other (188).

Yeast and mammalian PBGS enzymes have two binding sites for the zinc ions (Figure 6.12). The site

designated ZnA is not the catalytic site, but a region for binding of a non-essential Zn^{2+} ion (185).

The active site Zn^{2+} binds to a location designated ZnB (Figure 6.12)(185).

PBGS enzymes from different organisms exhibit different stoichiometries of catalytic Zn^{2+}-

binding. For example human PBGS has only four active sites per octamer that are Zn^{2+}-occupied

whereas the yeast enzyme has full occupancy of all eight catalytic sites per octamer (186). The *D.*

melanogaster PBGS (DmPBGS) has been investigated in depth concerning Zn^{2+}-binding and is the

only PBGS for which half-of-the-sites metal binding has been described in detail (189).

Maximal activity of DmPBGS is observed at a pH of 8 when the purified enzyme is assayed

without addition of exogenous metal ions (189). This active octamer possesses 0.5 - 0.7 Zn atoms per

subunit (monomer) (189). The addition of $ZnCl_2$ at 10 mM concentration significantly decreases

activity and the metal occupancy in this case is 1.5 Zn atoms per subunit (189). This implies that

inhibitory Zn atoms bind to DmPBGS with the stoichiometry of one atom per monomer (189). The

dissociation constant for Zn^{2+} at the inhibitory site is ~ 5 mM which is comparable to the K_d for ZnA

metal ions in mammalian PBGS (189). Therefore the inhibitory binding site in DmPBGS might be analogous to ZnA sites in PBGS from other sources (189). The removal of catalytic Zn^{2+} from DmPBGS requires more of the chelator *o*-phenanthroline in the presence of the substrate 5-aminolevulinic acid (ALA) than when ALA is absent, indicating that the substrate may engage in coordination of the active site metal (189).

Potential sites for Zn^{2+} binding on DmPBGS have been identified using a homology model for the enzyme based on the structure of yeast PBGS (Figure 6.12) (188, 189). The active site Zn^{2+} ion is coordinated by three Cys residues, which are 120, 122, and 130 (189). The residues that correspond to the ZnA site of yeast and mammalian PBGS are Cys219 and His10 (Figure 6.12) (189). These two residues are situated on different monomers of the dimeric subunit. Cys219 is located on the N-terminal arm that forms the lid over the active site of its parent monomer (189). Ligation to a second Zn atom would depend on whether the lid was open or closed, with the closed configuration facilitating metal ligation alongside His10 (189).
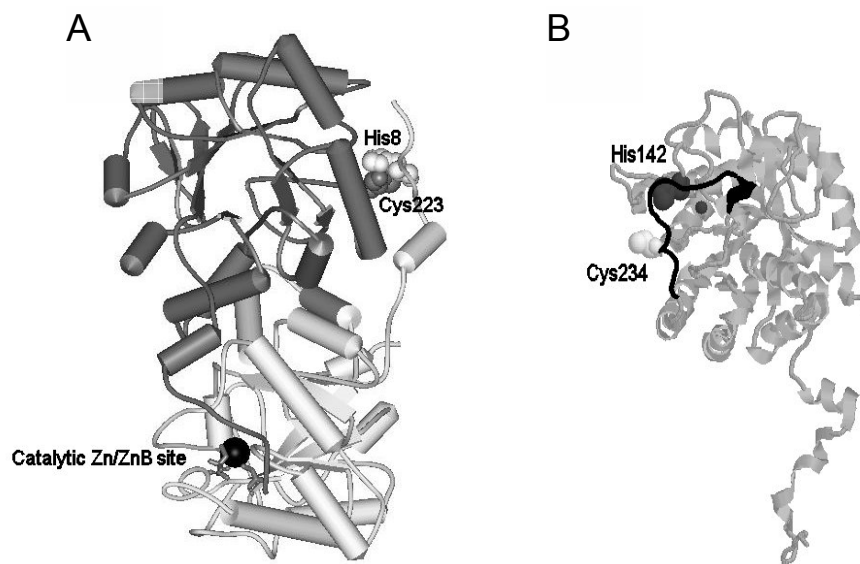
Figure 6.12: A) Structure of human PBGS dimer (PDB ID: 1E51) showing ZnB site and residues for non-essential Zn atom binding (ZnA site) B) Structure of yeast PBGS monomer (PDB ID: 1H7P) showing the mobile lid region (black) and the ligands associated with non-essential Zn atom binding (ZnA site)

If the second site contains Zn, then the enzyme inhibition will occur because the active site is closed off to incoming substrate (189). Mutation of His10 to Phe generates a DmPBGS variant that is not inhibited by exposure to Zn^{2+} ions, indicating that the non-catalytic metal site reduces enzyme activity (189). The variant binds the inhibitory Zn^{2+} ion with the stoichiometry of 0.5 atoms per monomer. Because Cys219 is part of the ZnA site (non-essential but non-inhibitory) there cannot be simultaneous Zn occupancy of this site as well as the inhibitory metal site (189). The data indicates that there are three sites for Zn binding on DmPBGS; the catalytic site, the ZnA site and an inhibitory site. Kundrat *et al.* have postulated that each of the Zn binding sites on DmPBGS exhibit half-of-the-sites occupancy and that during the catalytic cycle only four of the eight monomers have catalytic

Zn^{2+}-bound. Different crystal structures of yeast PBGS reveal that the N-terminal arm which forms the active site lid can be found in dissimilar positions that influence whether the ZnA or inhibitory metal sites are available for binding (189).

One model that Kundrat *et al.* proposed is that Cys 219 coordinates the Zn atom in the inhibitory site as well as the ZnA site, but the site containing the metal is dependent upon the lid position (open versus closed). A closed lid would facilitate Zn^{2+} binding at the inhibitory site with His10 and Cys219 as ligands. The open lid conformation allows metal occupancy at ZnA where the ligands would be Cys219 and His129. The experimental data implies that the DmPBGS octamer can have Zn simultaneously bound to ZnA and the inhibitory site, so half of the lids must be open while the other half are closed (189).

A "reciprocating motion model" for conformational change during DmPBGS's catalytic cycle can account for the alternating occupancy of ZnA and inhibitory sites in each monomer (189). This model provides an explanation for half-of-the-sites metal binding and half-of-the-sites reactivity that has been observed in PBGS enzymes. Crystallography on PBGS has shown product molecules bound to only half of the active sites (189). Other studies have shown that product release from PBGS requires the binding of substrate in an adjacent monomer, so that the lid closure over incoming product is a reciprocal motion in the protein that facilitates lid opening in the porphobilinogen-containing active site (189). This mechanistic evidence for a reciprocal catalytic cycle in the enzyme may correlate to a model of reciprocating subunit metallation in PBGS enzymes.

The GlxI dimer does not undergo significant conformational changes when the substrate analogue binds to the enzyme. The lack of evidence for large domain motions provides little support for the possibility that GlxI has a reciprocal motion component in its catalytic cycle. The half-of-the-sites metal occupancy is not uniform amongst GlxI enzymes, since human and yeast GlxI have two

172

Zn atoms per dimer, whereas the *E. coli* GlxI has only one (51, 147, 190). Active site mutagenesis studies on *P. falciparum* GlxI indicate that this di-metallated enzyme has two functioning catalytic sites that may exhibit cooperativity for substrate binding and turnover (8).

Whether *E. coli* GlxI has half-of-the-sites reactivity in parallel with its metal content still needs to be determined. One possible approach is to perform ITC analysis on Ni^{2+}-substituted *E. coli* GlxI with a micromolar potency inhibitor such as *S*-{2-[3-(hexyloxy)benzoyl]vinyl}glutathione. The isotherm can be used to enumerate the number of inhibitor molecules bound, which in turn can indicate the number of substrate-receptive active sites. A serious limitation to this approach is that this inhibitor may bind to both active sites as a means of inhibiting catalysis. Also the data would have to be interpreted with caution, as inhibitors are not truly representative of the normal substrate. Another experimental approach to investigate half-of-the-sites reactivity in *E. coli* GlxI would be to create an active fused dimer by site-directed mutagenesis. The active sites in a monomeric *E. coli* GlxI can be probed for metal occupancy and activity by selectively mutagenizing one active site or the other. This approach would be similar to that used by Deponte *et al.* in their investigation of *P. falciparum* GlxI (8). The availability of a fused-dimer variant would also allow the kinetics of each active site to be determined by amino-acid replacement to inactive one site versus another.

The work presented in this chapter describes convincing biophysical evidence in favor of half-of-the-sites binding of metal (Ni^{2+}) in *E. coli* GlxI. This data indicates that full occupancy of both active sites does not occur readily in solution as observed in the *E. coli* holo-GlxI crystal structures (Ni^{2+}, Cd^{2+}, Co^{2+} and Zn^{2+} substituted) (52). The *E. coli* GlxI backbone resonances from ^1H-^{15}N HSQC NMR do not indicate major domain motions that accompany metal binding, but rather subtle reorientations of small, discrete regions of the protein. This is in keeping with the crystal structure data, indicating that the overall structural configuration of the of the apo- and holoforms of *E. coli* GlxI are conserved regardless of the metal content (52).

173

Another key experiment awaiting completion is the incremental titration of *E. coli* GlxI with Zn^{2+} ions. Since the Zn^{2+}-substituted *E. coli* GlxI is an inactive holoform, there must be a structural reason for why this metal does not confer catalytic activity in the enzyme. A Zn^{2+}-titration monitored by ^{1}H ^{15}N HSQC NMR on labelled *E. coli* apo-GlxI, a comparison of Zn2+-induced resonance shifts Ni^{2+}-induced changes can be made. Any differences in the peak shifts comparing the Ni^{2+} and Zn^{2+} titrations will permit identification of any different re-organizations in the GlxI polypeptide that are specific to binding of a certain type of metal ion. This experiment would therefore be designed to assess whether the second sphere metal environment in *E. coli* GlxI differs depending on whether Ni^{2+} or Zn^{2+}- is bound. The second sphere ligands are the amino acids that have hydrogen bonding interaction with the primary metal ligands in the protein. These residues may be influential in positioning the active site ligands, and optimizing the site for one activating metal ion versus another. The data obtained from this additional titration would be a seminal contribution to the literature on GlxI because it would constitute the first potential explanation for control of metal selectivity in *E. coli* GlxI.

Subsequent investigation of this phenomenon should also involve identification of residues at sites where the polypeptide backbone undergoes reconfiguration in relation to the metal ion. The residues subject to re-orientation during apoenzyme to holoenzyme conversion would be indicative of the "second sphere" metal ligands in the enzyme. It is likely that the extended coordination network identified by NMR methods will consist of residues that are influential structural determinants of metal specificity in *E. coli* GlxI.

Summary

The data presented in this dissertation encompasses structure-function, protein-protein interaction and comparative biochemical studies of Glx system enzymes in the Honek laboratory. Characterization of the *E. coli* GlxII has provided information about overall metal selectivity in the GlxI system as a whole. *E. coli* GlxII is conserved for metal activation and contains the conserved metal-binding residues present in previously characterized orthologous GlxII enzymes. This finding clarifies that the Ni^{2+}/Co^{2+} activation of *E. coli* GlxI is not mirrored in the metal selectivity of GlxII, so that the metal activation of the hydrolase is well conserved across phylogenetic divisions.

The biochemical investigation of *P. aeruginosa* GlxI enzymes is an extension of previous comparative studies with enzyme from different bacterial sources. This investigation was significant for confirming that all three GlxI homologs encoded in the PAO1 genome were for active MG-GSH isomerizing enzymes but with differing metal activation properties. The reason for the presence of three GlxI enzymes in *P. aeruginosa* remains as yet unknown.

The *in vivo* metal center assembly of *E. coli* GlxI was investigated for its potential dependence on the Ni^{2+}-metallochaperone SlyD. The previously described characterization indicates no detectable correlation between the amount of GlxI activity in *E. coli* and the presence/absence of the *slyD* gene in the organism. This indicates that there is likely no Ni^{2+} release from SlyD to GlxI in during cytosolic formation of active holoenzyme. Therefore further research is necessary to determine whether *E. coli* GlxI requires metallochaperones *in vivo*.

The HSQC-NMR analysis of *E. coli* GlxI from the apo- to holoenzyme (Ni^{2+}-substituted) form is a continuation of previous biophysical studies on the nature of metal binding in this model protein. The observation of maximal structural perturbation with only one equivalent Ni^{2+} per dimer converges with other data implying half-of-the-sites metal binding in this GlxI (51, 60).

The investigations described in this dissertation add to the general understanding of the metal selectivity within the Glx system. If the metal selectivities differ between the GlxI and GlxII enzymes within a single organism, there should be different mechanisms for regulating their production on the basis of metal availability. This adds to the complexity of regulating the activity of the Glx system *in vivo*. Future investigations of the Glx system activity *in situ* should reveal how rates of MG production and metal availability contribute to regulating expression of both detoxification enzymes (i.e. GlxI and GlxII). Further developments in understanding Ni^{2+}-homeostasis in *E. coli* will allow additional studies of metal delivery to GlxI *in vitro* and *in vivo*.

The mechanistic and structural studies of *E. coli* GlxI described in this work are meaningful contributions to the field of metalloenzyme biochemistry. These studies provide a foundation to further investigate the nature of metal selectivity in GlxI as the mechanistic attributes of the Zn^{2+}- and non-Zn^{2+}-activated enzymes are similar. The half-of-the-sites metal binding exhibited by *E. coli* GlxI constitutes an excellent system for studying the relationship what asymmetries are present in an apparent homodimer and how they contribute to differences between catalytic sites. The biochemical properties of *E. coli* GlxI provides an important example of how enzyme activities can be conserved while fundamental attributes such as metal selectivity can diverge.

References

1. Kalapos, M. P. (1999) Methylglyoxal in Living Organisms: Chemistry, Biochemistry, Toxicology and Biological Implications. *Toxicol. Lett. 110*, 145-175.

2. Marasinghe, G. P., Sander, I. M., Bennett, B., Periyannan, G., Yang, K. W., Makaroff, C. A., and Crowder, M. W. (2005) Structural Studies on a Mitochondrial Glyoxalase II. *J. Biol. Chem. 280*, 40668-40675.

3. Sukdeo, N., Clugston, S. L., Daub, E., and Honek, J. F. (2004) Distinct Classes of Glyoxalase I: Metal Specificity of the *Yersinia pestis*, *Pseudomonas aeruginosa* and *Neisseria meningitidis* Enzymes. *Biochem. J. 384*, 111-117.

4. Campos-Bermudez, V. A., Leite, N. R., Krog, R., Costa-Filho, A. J., Soncini, F. C., Oliva, G., and Vila, A. J. (2007) Biochemical and Structural Characterization of *Salmonella typhimurium* Glyoxalase II: New Insights into Metal Ion Selectivity. *Biochemistry. 46*, 11069-11079.

5. Fersht, A. (1999) Kinetic Isotope Effects, in *Structure and mechanism in protein science: a guide to enzyme catalysis and protein folding* (M. R. Julet, and G. L. Hadler, Eds.) pp 96-97-99, W.H. Freeman and Company, New York.

6. Zhang, J. W., Butland, G., Greenblatt, J. F., Emili, A., and Zamble, D. B. (2005) A Role for SlyD in the *Escherichia coli* Hydrogenase Biosynthetic Pathway. *J. Biol. Chem. 280*, 4360-4366.

7. Leach, M. R., Zhang, J. W., and Zamble, D. B. (2007) The Role of Complex Formation between the *Escherichia coli* Hydrogenase Accessory Factors HypB and SlyD. *J. Biol. Chem. 282*, 16177-16186.

8. Deponte, M., Sturm, N., Mittler, S., Harner, M., Mack, H., and Becker, K. (2007) Allosteric Coupling of Two Different Functional Active Sites in Monomeric *Plasmodium falciparum* Glyoxalase I. *J. Biol. Chem. 282*, 28419-28430.

9. Bergdoll, M., Eltis, L. D., Cameron, A. D., Dumas, P., and Bolin, J. T. (1998) All in the Family: Structural and Evolutionary Relationships among Three Modular Proteins with Diverse Functions and Variable Assembly. *Protein Sci. 7*, 1661-1670.

10. Inoue, Y., and Kimura, A. (1995) Methylglyoxal and Regulation of its Metabolism in Microorganisms. *Adv. Microb. Physiol. 37*, 177-227.

11. Racker, E. (1951) The Mechanism of Action of Glyoxalase. *J. Biol. Chem. 190,* 685-696.

12. Speer, O., Morkunaite-Haimi, S., Liobikas, J., Franck, M., Hensbo, L., Linder, M. D., Kinnunen, P. K., Wallimann, T., and Eriksson, O. (2003) Rapid Suppression of Mitochondrial Permeability Transition by Methylglyoxal. Role of Reversible Arginine Modification. *J. Biol. Chem. 278*, 34757-34763.

13. Li, Y., Cohenford, M. A., Dutta, U., and Dain, J. A. (2008) The Structural Modification of DNA Nucleosides by Nonenzymatic Glycation: An *in Vitro* Study Based on the Reactions of Glyoxal and Methylglyoxal with 2'-Deoxyguanosine. *Anal. Bioanal Chem. 390*, 679-688.

14. Vander Jagt, D. L., and Hunsaker, L. A. (2003) Methylglyoxal Metabolism and Diabetic Complications: Roles of Aldose Reductase, Glyoxalase-I, Betaine Aldehyde Dehydrogenase and 2-Oxoaldehyde Dehydrogenase. *Chem. Biol. Interact. 143-144*, 341-351.

15. Zeng, J., and Davies, M. J. (2005) Evidence for the Formation of Adducts and S-(Carboxymethyl)Cysteine on Reaction of Alpha-Dicarbonyl Compounds with Thiol Groups on Amino Acids, Peptides, and Proteins. *Chem. Res. Toxicol. 18*, 1232-1241.

16. Lo, T. W., Westwood, M. E., McLellan, A. C., Selwood, T., and Thornalley, P. J. (1994) Binding and Modification of Proteins by Methylglyoxal Under Physiological Conditions. A Kinetic and Mechanistic Study with N Alpha-Acetylarginine, N Alpha-Acetylcysteine, and N Alpha-Acetyllysine, and Bovine Serum Albumin. *J. Biol. Chem. 269*, 32299-32305.

17. Thornalley, P. J. (2007) Dietary AGEs and ALEs and Risk to Human Health by their Interaction with the Receptor for Advanced Glycation Endproducts (RAGE)--an Introduction. *Mol. Nutr. Food Res. 51*, 1107-1110.

18. Ahmed, N., and Thornalley, P. J. (2002) Chromatographic Assay of Glycation Adducts in Human Serum Albumin Glycated *in Vitro* by Derivatization with 6-Aminoquinolyl-N-Hydroxysuccinimidyl-Carbamate and Intrinsic Fluorescence. *Biochem. J. 364*, 15-24.

19. Staehelin, M. (1959) Inactivation of Virus Nucleic Acid with Glyoxal Derivatives. *Biochim. Biophys. Acta. 31*, 448-454.

20. Krymkiewicz, N., Dieguez, E., Rekarte, U. D., and Zwaig, N. (1971) Properties and Mode of Action of a Bactericidal Compound (=methylglyoxal) Produced by a Mutant of *Escherichia coli*. *J. Bacteriol. 108*, 1338-1347.

21. Frischmann, M., Bidmon, C., Angerer, J., and Pischetsrieder, M. (2005) Identification of DNA Adducts of Methylglyoxal. *Chem. Res. Toxicol. 18*, 1586-1592.

22. Ponces Freire, A., Ferreira, A., Gomes, R., and Cordeiro, C. (2003) Anti-Glycation Defences in Yeast. *Biochem. Soc. Trans. 31*, 1409-1412.

23. Brownlee, J. M., Carlson, E., Milne, A. C., Pape, E., and Harrison, D. H. (2006) Structural and Thermodynamic Studies of Simple Aldose Reductase-Inhibitor Complexes. *Bioorg. Chem. 34*, 424-444.

24. Kawamura, M., Eisenhofer, G., Kopin, I. J., Kador, P. F., Lee, Y. S., Tsai, J. Y., Fujisawa, S., Lizak, M. J., Sinz, A., and Sato, S. (1999) Aldose Reductase, a Key Enzyme in the Oxidative Deamination of Norepinephrine in Rats. *Biochem. Pharmacol. 58*, 517-524.

25. Wermuth, B., Burgisser, H., Bohren, K., and von Wartburg, J. P. (1982) Purification and Characterization of Human-Brain Aldose Reductase. *Eur. J. Biochem. 127*, 279-284.

26. Warren, J. C., Murdock, G. L., Ma, Y., Goodman, S. R., and Zimmer, W. E. (1993) Molecular Cloning of Testicular 20 Alpha-Hydroxysteroid Dehydrogenase: Identity with Aldose Reductase. *Biochemistry. 32*, 1401-1406.

27. Yabe-Nishimura, C., Nishinaka, T., Iwata, K., and Seo, H. G. (2003) Up-Regulation of Aldose Reductase by the Substrate, Methylglyoxal. *Chem. Biol. Interact. 143-144*, 317-323.

28. Richard, J. P. (1991) Kinetic Parameters for the Elimination Reaction Catalyzed by Triosephosphate Isomerase and an Estimation of the Reaction's Physiological Significance. *Biochemistry. 30*, 4581-4585.

29. Cooper, R. A., and Anderson, A. (1970) The Formation and Catabolism of Methylglyoxal during Glycolysis in *Escherichia Coli. FEBS Lett. 11*, 273-276.

30. Hopper, D. J., and Cooper, R. A. (1972) The Purification and Properties of *Escherichia coli* Methylglyoxal Synthase. *Biochem. J. 128*, 321-329.

31. Murata, K., Fukuda, Y., Watanabe, K., Saikusa, T., Shimosaka, M., and Kimura, A. (1985) Characterization of Methylglyoxal Synthase in *Saccharomyces cerevisiae. Biochem. Biophys. Res. Commun. 131*, 190-198.

32. Cooper, R. A. (1974) Methylglyoxal Formation during Glucose Catabolism by *Pseudomonas saccharophila*. Identification of Methylglyoxal Synthase. *Eur. J. Biochem. 44*, 81-86.

33. Huang, K., Rudolph, F. B., and Bennett, G. N. (1999) Characterization of Methylglyoxal Synthase from *Clostridium acetobutylicum* ATCC 824 and its use in the Formation of 1, 2-Propanediol. *Appl. Environ. Microbiol. 65*, 3244-3247.

34. Cooper, R. A. (1984) Metabolism of Methylglyoxal in Microorganisms. *Annu. Rev. Microbiol. 38*, 49-68.

35. Ferguson, G. P., Totemeyer, S., MacLean, M. J., and Booth, I. R. (1998) Methylglyoxal Production in Bacteria: Suicide Or Survival? *Arch. Microbiol. 170*, 209-218.

36. Murata, K., Saikusa, T., Fukuda, Y., Watanabe, K., Inoue, Y., Shimosaka, M., and Kimura, A. (1986) Metabolism of 2-Oxoaldehydes in Yeasts. Possible Role of Glycolytic Bypath as a Detoxification System in L-Threonine Catabolism by *Saccharomyces Cerevisiae. Eur. J. Biochem. 157*, 297-301.

37. Ray, M., and Ray, S. (1987) Aminoacetone Oxidase from Goat Liver. Formation of Methylglyoxal from Aminoacetone. *J. Biol. Chem. 262*, 5974-5977.

38. Urata, G., and Granick, S. (1963) Biosynthesis of Alpha-Aminoketones and the Metabolism of Aminoacetone. *J. Biol. Chem. 238*, 811-820.

39. Elliott, W. H. (1959) Amino-Acetone; its Isolation and Role in Metabolism. *Nature. 183*, 1051-1052.

40. Casazza, J. P., Felver, M. E., and Veech, R. L. (1984) The Metabolism of Acetone in Rat. *J. Biol. Chem. 259*, 231-236.

41. Mukaihara, T., Tamura, N., Murata, Y., and Iwabuchi, M. (2004) Genetic Screening of Hrp Type III-Related Pathogenicity Genes Controlled by the HrpB Transcriptional Activator in *Ralstonia solanacearum. Mol. Microbiol. 54*, 863-875.

42. Tamura, N., Murata, Y., and Mukaihara, T. (2005) Isolation of *Ralstonia solanacearum hrpB* Constitutive Mutants and Secretion Analysis of hrpB-Regulated Gene Products that Share Homology with Known Type III Effectors and Enzymes. *Microbiology. 151*, 2873-2884.

43. Shi, L., Adkins, J. N., Coleman, J. R., Schepmoes, A. A., Dohnkova, A., Mottaz, H. M., Norbeck, A. D., Purvine, S. O., Manes, N. P., Smallwood, H. S., Wang, H., Forbes, J., Gros, P., Uzzau, S., Rodland, K. D., Heffron, F., Smith, R. D., and Squier, T. C. (2006) Proteomic Analysis of *Salmonella enterica* Serovar Typhimurium Isolated from RAW 264.7 Macrophages: Identification of a Novel Protein that Contributes to the Replication of Serovar Typhimurium Inside Macrophages. *J. Biol. Chem. 281*, 29131-29140.

44. Passalacqua, K. D., Bergman, N. H., Lee, J. Y., Sherman, D. H., and Hanna, P. C. (2007) The Global Transcriptional Responses of *Bacillus anthracis* Sterne (34F2) and a Delta sodA1 Mutant to Paraquat Reveal Metal Ion Homeostasis Imbalances during Endogenous Superoxide Stress. *J. Bacteriol. 189*, 3996-4013.

45. Korithoski, B., Levesque, C. M., and Cvitkovitch, D. G. (2007) Involvement of the Detoxifying Enzyme Lactoylglutathione Lyase in *Streptococcus mutans* Aciduricity. *J. Bacteriol. 189*, 7586-7592.

46. Davis, K. A., and Williams, G. R. (1966) Cation Activation of Glyoxalase I. *Biochim. Biophys. Acta. 113*, 393-395.

47. Uotila, L., and Koivusalo, M. (1975) Purification and Properties of Glyoxalase I from Sheep Liver. *Eur. J. Biochem. 52*, 493-503.

48. Han, L. P., Schimandle, C. M., Davison, L. M., and Vander Jagt, D. L. (1977) Comparative Kinetics of Mg^{2+}-, Mn^{2+}-, Co^{2+}-, and Ni^{2+}-Activated Glyoxalase I. Evaluation of the Role of the Metal Ion. *Biochemistry. 16*, 5478-5484.

49. Mannervik, B., Lindstrom, L., and Bartfai, T. (1972) Partial Purification and Characterization of Glyoxalase I from Porcine Erythrocytes. *Eur. J. Biochem. 29*, 276-281.

50. Aronsson, A. C., Marmstal, E., and Mannervik, B. (1978) Glyoxalase I, a Zinc Metalloenzyme of Mammals and Yeast. *Biochem. Biophys. Res. Commun. 81*, 1235-1240.

51. Clugston, S. L., Barnard, J. F., Kinach, R., Miedema, D., Ruman, R., Daub, E., and Honek, J. F. (1998) Overproduction and Characterization of a Dimeric Non-Zinc Glyoxalase I from *Escherichia coli*: Evidence for Optimal Activation by Nickel Ions. *Biochemistry. 37*, 8754-8763.

52. He, M. M., Clugston, S. L., Honek, J. F., and Matthews, B. W. (2000) Determination of the Structure of *Escherichia coli* Glyoxalase I Suggests a Structural Basis for Differential Metal Activation. *Biochemistry. 39*, 8719-8727.

53. Cameron, A. D., Olin, B., Ridderstrom, M., Mannervik, B., and Jones, T. A. (1997) Crystal Structure of Human Glyoxalase I--Evidence for Gene Duplication and 3D Domain Swapping. *EMBO J. 16*, 3386-3395.

54. Armstrong, R. N. (2000) Mechanistic Diversity in a Metalloenzyme Superfamily. *Biochemistry. 39*, 13625-13632.

55. McCarthy, A. A., Baker, H. M., Shewry, S. C., Patchett, M. L., and Baker, E. N. (2001) Crystal Structure of Methylmalonyl-Coenzyme A Epimerase from *P. shermanii*: A Novel Enzymatic Function on an Ancient Metal Binding Scaffold. *Structure. 9*, 637-646.

56. Clugston, S. L., Daub, E., and Honek, J. F. (1998) Identification of Glyoxalase I Sequences in *Brassica oleracea* and *Sporobolus stapfianus*: Evidence for Gene Duplication Events. *J. Mol. Evol. 47*, 230-234.

57. Frickel, E. M., Jemth, P., Widersten, M., and Mannervik, B. (2001) Yeast Glyoxalase I is a Monomeric Enzyme with Two Active Sites. *J. Biol. Chem. 276*, 1845-1849.

58. Iozef, R., Rahlfs, S., Chang, T., Schirmer, H., and Becker, K. (2003) Glyoxalase I of the Malarial Parasite *Plasmodium falciparum*: Evidence for Subunit Fusion. *FEBS Lett. 554*, 284-288.

59. Saint-Jean, A. P., Phillips, K. R., Creighton, D. J., and Stone, M. J. (1998) Active Monomeric and Dimeric Forms of *Pseudomonas putida* Glyoxalase I: Evidence for 3D Domain Swapping. *Biochemistry. 37*, 10345-10353.

60. Clugston, S. L., Yajima, R., and Honek, J. F. (2004) Investigation of Metal Binding and Activation of *Escherichia coli* Glyoxalase I: Kinetic, Thermodynamic and Mutagenesis Studies. *Biochem. J. 377*, 309-316.

61. Sellin, S., Eriksson, L. E., Aronsson, A. C., and Mannervik, B. (1983) Octahedral Metal Coordination in the Active Site of Glyoxalase I as Evidenced by the Properties of Co(II)-Glyoxalase I. *J. Biol. Chem. 258*, 2091-2093.

62. Sellin, S., Eriksson, L. E., and Mannervik, B. (1987) Electron Paramagnetic Resonance Study of the Active Site of Copper-Substituted Human Glyoxalase I. *Biochemistry. 26*, 6779-6784.

63. Ridderstrom, M., Cameron, A. D., Jones, T. A., and Mannervik, B. (1998) Involvement of an Active-Site Zn^{2+} Ligand in the Catalytic Mechanism of Human Glyoxalase I. *J. Biol. Chem. 273*, 21623-21628.

64. Cameron, A. D., Ridderstrom, M., Olin, B., Kavarana, M. J., Creighton, D. J., and Mannervik, B. (1999) Reaction Mechanism of Glyoxalase I Explored by an X-Ray Crystallographic Analysis of the Human Enzyme in Complex with a Transition State Analogue. *Biochemistry. 38*, 13480-13490.

65. Davidson, G., Clugston, S. L., Honek, J. F., and Maroney, M. J. (2001) An XAS Investigation of Product and Inhibitor Complexes of Ni-Containing GlxI from *Escherichia coli*: Mechanistic Implications. *Biochemistry. 40*, 4569-4582.

66. Clugston, S. L., and Honek, J. F. (2000) Identification of Sequences Encoding the Detoxification Metalloisomerase Glyoxalase I in Microbial Genomes from several Pathogenic Organisms. *J. Mol. Evol. 50*, 491-495.

67. Vickers, T. J., Greig, N., and Fairlamb, A. H. (2004) A Trypanothione-Dependent Glyoxalase I with a Prokaryotic Ancestry in *Leishmania major*. *Proc. Natl. Acad. Sci. U. S. A. 101*, 13186-13191.

68. Padmanabhan, P. K., Mukherjee, A., Singh, S., Chattopadhyaya, S., Gowri, V. S., Myler, P. J., Srinivasan, N., and Madhubala, R. (2005) Glyoxalase I from *Leishmania donovani*: A Potential Target for Anti-Parasite Drug. *Biochem. Biophys. Res. Commun. 337*, 1237-1248.

69. Greig, N., Wyllie, S., Vickers, T. J., and Fairlamb, A. H. (2006) Trypanothione-Dependent Glyoxalase I in *Trypanosoma cruzi*. *Biochem. J. 400*, 217-223.

70. Krauth-Siegel, R. L., Meiering, S. K., and Schmidt, H. (2003) The Parasite-Specific Trypanothione Metabolism of *Trypanosoma* and *Leishmania* . *Biol. Chem. 384*, 539-549.

71. Ariza, A., Vickers, T. J., Greig, N., Armour, K. A., Dixon, M. J., Eggleston, I. M., Fairlamb, A. H., and Bond, C. S. (2006) Specificity of the Trypanothione-Dependent *Leishmania major* Glyoxalase I: Structure and Biochemical Comparison with the Human Enzyme. *Mol. Microbiol. 59*, 1239-1248.

72. Uotila, L. (1973) Purification and Characterization of S-2-Hydroxyacylglutathione Hydrolase (Glyoxalase II) from Human Liver. *Biochemistry. 12*, 3944-3951.

73. Schwyzer, R., and Hurlimann, C. (1954) Coenzyme A. Model Reactions of the Enzymic Activation of Acyl Derivatives of Coenzyme A. *Helv. Chim. Acta. 37*, 155-166.

74. Ridderstrom, M., Saccucci, F., Hellman, U., Bergman, T., Principato, G., and Mannervik, B. (1996) Molecular Cloning, Heterologous Expression, and Characterization of Human Glyoxalase II. *J. Biol. Chem. 271*, 319-323.

75. Ridderstrom, M., and Mannervik, B. (1997) Molecular Cloning and Characterization of the Thiolesterase Glyoxalase II from *Arabidopsis thaliana*. *Biochem. J. 322 (Pt 2)*, 449-454.

76. Crowder, M. W., Maiti, M. K., Banovic, L., and Makaroff, C. A. (1997) Glyoxalase II from *A. Thaliana* Requires Zn(II) for Catalytic Activity. *FEBS Lett. 418*, 351-354.

77. Melino, S., Capo, C., Dragani, B., Aceto, A., and Petruzzelli, R. (1998) A Zinc-Binding Motif Conserved in Glyoxalase II, Beta-Lactamase and Arylsulfatases. *Trends Biochem. Sci. 23*, 381-382.

78. Cameron, A. D., Ridderstrom, M., Olin, B., and Mannervik, B. (1999) Crystal Structure of Human Glyoxalase II and its Complex with a Glutathione Thiolester Substrate Analogue. *Structure. 7*, 1067-1078.

79. Zang, T. M., Hollman, D. A., Crawford, P. A., Crowder, M. W., and Makaroff, C. A. (2001) *Arabidopsis* Glyoxalase II Contains a zinc/iron Binuclear Metal Center that is Essential for Substrate Binding and Catalysis. *J. Biol. Chem. 276*, 4788-4795.

80. Schilling, O., Wenzel, N., Naylor, M., Vogel, A., Crowder, M., Makaroff, C., and Meyer-Klaucke, W. (2003) Flexible Metal Binding of the Metallo-Beta-Lactamase Domain: Glyoxalase II Incorporates Iron, Manganese, and Zinc *in Vivo*. *Biochemistry. 42*, 11777-11786.

81. Wenzel, N. F., Carenbauer, A. L., Pfiester, M. P., Schilling, O., Meyer-Klaucke, W., Makaroff, C. A., and Crowder, M. W. (2004) The Binding of Iron and Zinc to Glyoxalase II Occurs Exclusively as Di-Metal Centers and is Unique within the Metallo-Beta-Lactamase Family. *J. Biol. Inorg. Chem. 9*, 429-438.

82. Bebrone, C. (2007) Metallo-Beta-Lactamases (Classification, Activity, Genetic Organization, Structure, Zinc Coordination) and their Superfamily. *Biochem. Pharmacol. 74*, 1686-1701.

83. Ball, J. C., and Vander Jagt, D. L. (1981) S-2-Hydroxyacylglutathione Hydrolase (Glyoxalase II): Active-Site Mapping of a Nonserine Thiolesterase. *Biochemistry. 20*, 899-905.

84. Ragsdale, S. W. (1998) Nickel Biochemistry. *Curr. Opin. Chem. Biol. 2*, 208-215.

85. Lipscomb, W. N., and Strater, N. (1996) Recent Advances in Zinc Enzymology. *Chem. Rev. 96*, 2375-2434.

86. Vander Jagt, D. L., and Han, L. P. (1973) Deuterium Isotope Effects and Chemically Modified Coenzymes as Mechanism Probes of Yeast Glyoxalase-I. *Biochemistry. 12*, 5161-5167.

87. Chari, R. V., and Kozarich, J. W. (1981) Deuterium Isotope Effects on the Product Partitioning of Fluoromethylglyoxal by Glyoxalase I. Proof of a Proton Transfer Mechanism. *J. Biol. Chem. 256*, 9785-9788.

88. Rae, C., O'Donoghue, S. I., Bubb, W. A., and Kuchel, P. W. (1994) Stereospecificity of Substrate Usage by Glyoxalase 1: Nuclear Magnetic Resonance Studies of Kinetics and Hemithioacetal Substrate Conformation. *Biochemistry. 33*, 3548-3559.

89. Forzi, L., and Sawers, R. G. (2007) Maturation of [NiFe]-Hydrogenases in *Escherichia coli*. *Biometals. 20*, 565-578.

90. Leach, M. R., and Zamble, D. B. (2007) Metallocenter Assembly of the Hydrogenase Enzymes. *Curr. Opin. Chem. Biol. 11*, 159-165.

91. Hottenrott, S., Schumann, T., Pluckthun, A., Fischer, G., and Rahfeld, J. U. (1997) The *Escherichia coli* SlyD is a Metal Ion-Regulated Peptidyl-Prolyl cis/trans-Isomerase. *J. Biol. Chem. 272*, 15697-15701.

92. Stover, C. K., Pham, X. Q., Erwin, A. L., Mizoguchi, S. D., Warrener, P., Hickey, M. J., Brinkman, F. S., Hufnagle, W. O., Kowalik, D. J., Lagrou, M., Garber, R. L., Goltry, L., Tolentino, E., Westbrock-Wadman, S., Yuan, Y., Brody, L. L., Coulter, S. N., Folger, K. R., Kas, A., Larbig, K., Lim, R., Smith, K., Spencer, D., Wong, G. K., Wu, Z., Paulsen, I. T., Reizer, J., Saier, M. H., Hancock, R. E., Lory, S., and Olson, M. V. (2000) Complete Genome Sequence of *Pseudomonas aeruginosa* PAO1, an Opportunistic Pathogen. *Nature. 406*, 959-964.

93. Koonin, E. V., Makarova, K. S., and Aravind, L. (2001) Horizontal Gene Transfer in Prokaryotes: Quantification and Classification. *Annu. Rev. Microbiol. 55*, 709-742.

94. Groisman, E. A., and Ochman, H. (1993) Cognate Gene Clusters Govern Invasion of Host Epithelial Cells by *Salmonella typhimurium* and *Shigella flexneri. EMBO J. 12*, 3779-3787.

95. Salama, N. R., and Falkow, S. (1999) Genomic Clues for Defining Bacterial Pathogenicity. *Microbes Infect. 1*, 615-619.

96. Frost, L. S., Leplae, R., Summers, A. O., and Toussaint, A. (2005) Mobile Genetic Elements: The Agents of Open Source Evolution. *Nat. Rev. Microbiol. 3*, 722-732.

97. Dobrindt, U., Hochhut, B., Hentschel, U., and Hacker, J. (2004) Genomic Islands in Pathogenic and Environmental Microorganisms. *Nat. Rev. Microbiol. 2*, 414-424.

98. Hurles, M. (2004) Gene Duplication: The Genomic Trade in Spare Parts. *PLoS Biol. 2*, E206.

99. Marri, P. R., Bannantine, J. P., and Golding, G. B. (2006) Comparative Genomics of Metabolic Pathways in *Mycobacterium* Species: Gene Duplication, Gene Decay and Lateral Gene Transfer. *FEMS Microbiol. Rev. 30*, 906-925.

100. Brichta, D. M., Azad, K. N., Ralli, P., and O'Donovan, G. A. (2004) *Pseudomonas aeruginosa* Dihydroorotases: A Tale of Three *pyrC*s. *Arch. Microbiol. 182*, 7-17.

101. Winsor, G. L., Lo, R., Sui, S. J., Ung, K. S., Huang, S., Cheng, D., Ching, W. K., Hancock, R. E., and Brinkman, F. S. (2005) *Pseudomonas aeruginosa* Genome Database and PseudoCAP: Facilitating Community-Based, Continually Updated, Genome Annotation. *Nucleic Acids Res. 33*, D338-43.

102. Rothmel, R. K., Chakrabarty, A. M., Berry, A., and Darzins, A. (1991) Genetic Systems in *Pseudomonas*, in *Bacterial Genetic Systems* (J. H. Miller, Ed.) pp 485-514, Academic Press, New York.

103. Paulsen, I. T., Press, C. M., Ravel, J., Kobayashi, D. Y., Myers, G. S., Mavrodi, D. V., DeBoy, R. T., Seshadri, R., Ren, Q., Madupu, R., Dodson, R. J., Durkin, A. S., Brinkac, L. M., Daugherty, S. C., Sullivan, S. A., Rosovitz, M. J., Gwinn, M. L., Zhou, L., Schneider, D. J., Cartinhour, S. W., Nelson, W. C., Weidman, J., Watkins, K., Tran, K., Khouri, H., Pierson, E. A., Pierson, L. S.,3rd, Thomashow, L. S., and Loper, J. E. (2005) Complete Genome Sequence of the Plant Commensal *Pseudomonas fluorescens* Pf-5. *Nat. Biotechnol. 23*, 873-878.

104. Palleroni, N. J., and Moore, E. R. B. (2004) Taxonomy of Pseudomonads: Experimental Approaches, in *Pseudomonas: Genomics, Life Style and Molecular Architecture* (J. Ramos, Ed.) pp 3-44, Kluwer Academic/Plenum Publishers, New York.

185

105. Nelson, K. E., Weinel, C., Paulsen, I. T., Dodson, R. J., Hilbert, H., Martins dos Santos, V. A., Fouts, D. E., Gill, S. R., Pop, M., Holmes, M., Brinkac, L., Beanan, M., DeBoy, R. T., Daugherty, S., Kolonay, J., Madupu, R., Nelson, W., White, O., Peterson, J., Khouri, H., Hance, I., Chris Lee, P., Holtzapple, E., Scanlan, D., Tran, K., Moazzez, A., Utterback, T., Rizzo, M., Lee, K., Kosack, D., Moestl, D., Wedler, H., Lauber, J., Stjepandic, D., Hoheisel, J., Straetz, M., Heim, S., Kiewitz, C., Eisen, J. A., Timmis, K. N., Dusterhoft, A., Tummler, B., and Fraser, C. M. (2002) Complete Genome Sequence and Comparative Analysis of the Metabolically Versatile *Pseudomonas putida* KT2440. *Environ. Microbiol. 4*, 799-808.

106. Buell, C. R., Joardar, V., Lindeberg, M., Selengut, J., Paulsen, I. T., Gwinn, M. L., Dodson, R. J., Deboy, R. T., Durkin, A. S., Kolonay, J. F., Madupu, R., Daugherty, S., Brinkac, L., Beanan, M. J., Haft, D. H., Nelson, W. C., Davidsen, T., Zafar, N., Zhou, L., Liu, J., Yuan, Q., Khouri, H., Fedorova, N., Tran, B., Russell, D., Berry, K., Utterback, T., Van Aken, S. E., Feldblyum, T. V., D'Ascenzo, M., Deng, W. L., Ramos, A. R., Alfano, J. R., Cartinhour, S., Chatterjee, A. K., Delaney, T. P., Lazarowitz, S. G., Martin, G. B., Schneider, D. J., Tang, X., Bender, C. L., White, O., Fraser, C. M., and Collmer, A. (2003) The Complete Genome Sequence of the *Arabidopsis* and Tomato Pathogen *Pseudomonas syringae* pv. Tomato DC3000. *Proc. Natl. Acad. Sci. U. S. A. 100*, 10181-10186.

107. Jensen, L. J., Skovgaard, M., Sicheritz-Pontén, T., Hansen, N. T., Johansson, H., Jorgenson, M. K., Kiil, K., Hallin, P. F., and Ussery, D. (2004) Comparative Genomics of Four *Pseudomonas* Species, in *Pseudomonas: Genomics, Life Style and Molecular Architecture* (J. Ramos, Ed.) Kluwer Academic/Plenum Publishers, New York.

108. Sukdeo, N., and Honek, J. F. (2007) *Pseudomonas aeruginosa* Contains Multiple Glyoxalase I-Encoding Genes from both Metal Activation Classes. *Biochim. Biophys. Acta. 1774*, 756-763.

109. Bergmeyer, H. U. (1983) Glyoxalase I, in *Methods of Enzymatic Analysis* (H. U. Bergmeyer, Ed.) 3rd ed., pp 217-218, Verlag Chemie, Deerfield Beach.

110. Cliffe, E. E., and Waley, S. G. (1961) The Mechanism of the Glyoxalase I Reaction, and the Effect of Ophthalmic Acid as an Inhibitor. *Biochem. J. 79*, 475-482.

111. Vince, R., Daluge, S., and Wadd, W. B. (1971) Studies on the Inhibition of Glyoxalase I by S-Substituted Glutathiones. *J. Med. Chem. 14*, 402-404.

112. Vander Jagt, D. L., Han, L. P., and Lehman, C. H. (1972) Kinetic Evaluation of Substrate Specificity in the Glyoxalase-I-Catalyzed Disproportionation of -Ketoaldehydes. *Biochemistry. 11*, 3735-3740.

113. Bergmeyer, H. U. (1984) Methylglyoxal, in *Methods of Enzymatic Analysis* 3rd ed., pp 593, Verlag Chemie, Deerfield Beach.

114. Ellman, G. L. (1959) Tissue Sulfhydryl Groups. *Arch. Biochem. Biophys. 82*, 70-77.

115. Collier, H. B. (1973) Letter: A Note on the Molar Absorptivity of Reduced Ellman's Reagent, 3-Carboxylato-4-Nitrothiophenolate. *Anal. Biochem. 56*, 310-311.

116. Gasteiger, E., Hoogland, C., Gattiker, A., Duvaud, S., Wilkins, M. R., Appel, R. D., and Bairoch, A. (2005) Protein Identification and Analysis Tools on the ExPASy Server, in *The Proteomics Protocols Handbook* (J. M. Walker, Ed.) Humana Press, Totowa, NJ.

117. Bobrowska-Grzesik, E., and Grossman, A. M. (1996) Derivative Spectrophotometry in the Determination of Metal Ions with 4-(Pyridyl-2-Azo)Resorcinol (PAR). *Anal. Bioanal Chem. 354*, 498-502.

118. Ramsaywak, P. C., Labbe, G., Siemann, S., Dmitrienko, G. I., and Guillemette, J. G. (2004) Molecular Cloning, Expression, Purification, and Characterization of Fructose 1,6-Bisphosphate Aldolase from *Mycobacterium tuberculosis*--a Novel Class II A Tetramer. *Protein Expr. Purif. 37*, 220-228.

119. Davis, K. A., and Williams, G. R. (1969) Glyoxalase I, a Lyase Or an Oxidoreductive Isomerase? *Can. J. Biochem. 47*, 553-556.

120. Sellin, S., and Mannervik, B. (1984) Metal Dissociation Constants for Glyoxalase I Reconstituted with Zn^{2+}, Co^{2+}, Mn^{2+}, and Mg^{2+}. *J. Biol. Chem. 259*, 11426-11429.

121. Richter, U., and Krauss, M. (2001) Active Site Structure and Mechanism of Human Glyoxalase I-an *Ab Initio* Theoretical Study. *J. Am. Chem. Soc. 123*, 6973-6982.

122. Creighton, D. J., and Hamilton, D. S. (2001) Brief History of Glyoxalase I and what we have Learned about Metal Ion-Dependent, Enzyme-Catalyzed Isomerizations. *Arch. Biochem. Biophys. 387*, 1-10.

123. Davidson, G., Clugston, S. L., Honek, J. F., and Maroney, M. J. (2000) XAS Investigation of the Nickel Active Site Structure in *Escherichia coli* Glyoxalase I. *Inorg. Chem. 39*, 2962-2963.

124. McClelland, M., Sanderson, K. E., Spieth, J., Clifton, S. W., Latreille, P., Courtney, L., Porwollik, S., Ali, J., Dante, M., Du, F., Hou, S., Layman, D., Leonard, S., Nguyen, C., Scott, K., Holmes, A., Grewal, N., Mulvaney, E., Ryan, E., Sun, H., Florea, L., Miller, W., Stoneking, T., Nhan, M., Waterston, R., and Wilson, R. K. (2001) Complete Genome Sequence of *Salmonella enterica* Serovar Typhimurium LT2. *Nature. 413*, 852-856.

125. Keseler, I. M., Collado-Vides, J., Gama-Castro, S., Ingraham, J., Paley, S., Paulsen, I. T., Peralta-Gil, M., and Karp, P. D. (2005) EcoCyc: A Comprehensive Database Resource for *Escherichia coli*. *Nucleic Acids Res. 33*, D334-7.

126. O'Young, J., Sukdeo, N., and Honek, J. F. (2007) *Escherichia coli* glyoxalase II is a Binuclear Zinc-Dependent Metalloenzyme. *Arch. Biochem. Biophys. 459*, 20-26.

127. Sambrook, J., and Russell, D. W. (2001) *Molecular Cloning: A Laboratory Manual.* Cold Spring Harbour Laboratory Press, Cold Spring Harbour, NY.

128. Akoachere, M., Iozef, R., Rahlfs, S., Deponte, M., Mannervik, B., Creighton, D. J., Schirmer, H., and Becker, K. (2005) Characterization of the Glyoxalases of the Malarial Parasite *Plasmodium falciparum* and Comparison with their Human Counterparts. *Biol. Chem. 386*, 41-52.

129. Talesa, V., Rosi, G., Bistoni, F., Marconi, P., Norton, S. J., and Principato, G. B. (1990) Presence of a Plant-Like Glyoxalase II in *Candida albicans*. *Biochem. Int. 21*, 397-403.

130. Bito, A., Haider, M., Briza, P., Strasser, P., and Breitenbach, M. (1999) Heterologous Expression, Purification, and Kinetic Comparison of the Cytoplasmic and Mitochondrial Glyoxalase II Enzymes, Glo2p and Glo4p, from *Saccharomyces cerevisiae*. *Protein Expr. Purif. 17*, 456-464.

131. Dragani, B., Cocco, R., Ridderstrom, M., Stenberg, G., Mannervik, B., and Aceto, A. (1999) Unfolding and Refolding of Human Glyoxalase II and its Single-Tryptophan Mutants. *J. Mol. Biol. 291*, 481-490.

132. Walasek, P., and Honek, J. F. (2005) Nonnatural Amino Acid Incorporation into the Methionine 214 Position of the Metzincin *Pseudomonas aeruginosa* Alkaline Protease. *BMC Biochem. 6*, 21.

133. Franzen, V. (1956) *Chem. Ber. 89*, 1020.

134. Franzen, V. (1957) *Chem. Ber. 90*, 623.

135. Rose, I. A. (1957) Mechanism of the Action of Glyoxalase I. *Biochim. Biophys. Acta. 25*, 214-215.

136. Seemann, J. E., and Schulz, G. E. (1997) Structure and Mechanism of L-Fucose Isomerase from *Escherichia coli. J. Mol. Biol. 273*, 256-268.

137. Joerger, A. C., Gosse, C., Fessner, W. D., and Schulz, G. E. (2000) Catalytic Action of Fuculose 1-Phosphate Aldolase (Class II) as Derived from Structure-Directed Mutagenesis. *Biochemistry. 39*, 6033-6041.

138. Topper, Y. J. (1957) On the Mechanism of Action of Phosphoglucose Isomerase and Phosphomannose Isomerase. *J. Biol. Chem. 225*, 419-425.

139. Williams, L., Nguyen, T., Li, Y., Porter, T. N., and Raushel, F. M. (2006) Uronate Isomerase: A Nonhydrolytic Member of the Amidohydrolase Superfamily with an Ambivalent Requirement for a Divalent Metal Ion. *Biochemistry. 45*, 7453-7462.

140. Himo, F., and Siegbahn, P. E. (2001) Catalytic Mechanism of Glyoxalase I: A Theoretical Study. *J. Am. Chem. Soc. 123*, 10280-10289.

141. Hall, S. S., Doweyko, A. M., and Jordan, F. (1976) Glyoxalase I Enzyme Studies. 2. Nuclear Magnetic Resonance Evidence for an Enediol-Proton Transfer Mechanism. *J. Am. Chem. Soc. 98*, 7460-7461.

142. Northrop, D. B. (1975) Steady-State Analysis of Kinetic Isotope Effects in Enzymic Reactions. *Biochemistry. 14*, 2644-2651.

143. Walsh, C. (1979) Kinetic Isotope Effects, in *Enzymatic Reaction Mechanisms* (A. C. Bartlett, and L. W. McCombs, Eds.) pp 108, W. H. Freeman and Company, San Fransisco.

144. Scheiner, S. (2000) Calculation of Isotope Effects from First Principles. *Biochim. Biophys. Acta. 1458*, 28-42.

145. Feierberg, I., Luzhkov, V., and Aqvist, J. (2000) Computer Simulation of Primary Kinetic Isotope Effects in the Proposed Rate-Limiting Step of the Glyoxalase I Catalyzed Reaction. *J. Biol. Chem. 275*, 22657-22662.

146. Sommer, A., Fischer, P., Krause, K., Boettcher, K., Brophy, P. M., Walter, R. D., and Liebau, E. (2001) A Stress-Responsive Glyoxalase I from the Parasitic Nematode *Onchocerca volvulus*. *Biochem. J. 353*, 445-452.

147. Ridderstrom, M., and Mannervik, B. (1996) Optimized Heterologous Expression of the Human Zinc Enzyme Glyoxalase I. *Biochem. J. 314 (Pt 2)*, 463-467.

148. Lincoln, S. F. (2005) Mechanistic Studies of Metal Aqua Ions: A Semi-Historical Perspective. *Helvetica Chimica Acta. 88*, 523.

149. Barnum, D. W. (1983) Hydrolysis of Cations. Formation Constants and Standard Free Energies of Formation of Hydroxy Complexes. *Inorg. Chem. 22*, 2297.

150. Faine, S. (1959) Iron as a Growth Requirement for Pathogenic *Leptospira*. *J. Gen. Microbiol. 20*, 246-251.

151. Lowe, R. H., and Evans, H. J. (1962) Cobalt Requirement for the Growth of Rhizobia. *J. Bacteriol. 83*, 210-211.

152. Finstein, M. S., and Delwiche, C. C. (1965) Molybdenum as a Micronutrient for Nitrobacter. *J. Bacteriol. 89*, 123-128.

153. Bartha, R., and Ordal, E. J. (1965) Nickel-Dependent Chemolithotrophic Growth of Two *Hydrogenomonas* Strains. *J. Bacteriol. 89*, 1015-1019.

154. Dixon, N. E., Gazzola, T. C., blakeley, R. L., and Zermer, B. (1975) Letter: Jack Bean Urease (EC 3.5.1.5). A Metalloenzyme. A Simple Biological Role for Nickel? *J. Am. Chem. Soc. 97*, 4131-4133.

155. Mulrooney, S. B., and Hausinger, R. P. (2003) Nickel Uptake and Utilization by Microorganisms. *FEMS Microbiol. Rev. 27*, 239-261.

156. Soriano, A., and Hausinger, R. P. (1999) GTP-Dependent Activation of Urease Apoprotein in Complex with the UreD, UreF, and UreG Accessory Proteins. *Proc. Natl. Acad. Sci. U. S. A. 96*, 11140-11144.

157. Colpas, G. J., Brayman, T. G., Ming, L. J., and Hausinger, R. P. (1999) Identification of Metal-Binding Residues in the *Klebsiella aerogenes* Urease Nickel Metallochaperone, UreE. *Biochemistry. 38*, 4078-4088.

158. Soriano, A., Colpas, G. J., and Hausinger, R. P. (2000) UreE Stimulation of GTP-Dependent Urease Activation in the UreD-UreF-UreG-Urease Apoprotein Complex. *Biochemistry. 39*, 12435-12440.

159. Lutz, S., Jacobi, A., Schlensog, V., Bohm, R., Sawers, G., and Bock, A. (1991) Molecular Characterization of an Operon (Hyp) Necessary for the Activity of the Three Hydrogenase Isoenzymes in *Escherichia coli*. *Mol. Microbiol. 5*, 123-135.

160. Navarro, C., Wu, L. F., and Mandrand-Berthelot, M. A. (1993) The *Nik* operon of *Escherichia coli* Encodes a Periplasmic Binding-Protein-Dependent Transport System for Nickel. *Mol. Microbiol. 9*, 1181-1191.

161. Vignais, P. M., Billoud, B., and Meyer, J. (2001) Classification and Phylogeny of Hydrogenases. *FEMS Microbiol. Rev. 25*, 455-501.

162. Adams, M. W. (1990) The Structure and Mechanism of Iron-Hydrogenases. *Biochim. Biophys. Acta. 1020*, 115-145.

163. Atanassova, A., and Zamble, D. B. (2005) *Escherichia coli* HypA is a Zinc Metalloprotein with a Weak Affinity for Nickel. *J. Bacteriol. 187*, 4689-4697.

164. Leach, M. R., Sandal, S., Sun, H., and Zamble, D. B. (2005) Metal Binding Activity of the *Escherichia coli* Hydrogenase Maturation Factor HypB. *Biochemistry. 44*, 12229-12238.

165. Suzuki, R., Nagata, K., Yumoto, F., Kawakami, M., Nemoto, N., Furutani, M., Adachi, K., Maruyama, T., and Tanokura, M. (2003) Three-Dimensional Solution Structure of an Archaeal FKBP with a Dual Function of Peptidyl Prolyl Cis-Trans Isomerase and Chaperone-Like Activities. *J. Mol. Biol. 328*, 1149-1160.

166. Berggard, T., Linse, S., and James, P. (2007) Methods for the Detection and Analysis of Protein-Protein Interactions. *Proteomics. 7*, 2833-2842.

167. Estojak, J., Brent, R., and Golemis, E. A. (1995) Correlation of Two-Hybrid Affinity Data with *in Vitro* Measurements. *Mol. Cell. Biol. 15*, 5820-5829.

168. Deane, C. M., Salwinski, L., Xenarios, I., and Eisenberg, D. (2002) Protein Interactions: Two Methods for Assessment of the Reliability of High Throughput Observations. *Mol. Cell. Proteomics. 1*, 349-356.

169. Outten, C. E., and O'Halloran, T. V. (2001) Femtomolar Sensitivity of Metalloregulatory Proteins Controlling Zinc Homeostasis. *Science. 292*, 2488-2492.

170. De Pina, K., Desjardin, V., Mandrand-Berthelot, M. A., Giordano, G., and Wu, L. F. (1999) Isolation and Characterization of the *nikR* gene Encoding a Nickel-Responsive Regulator in *Escherichia coli*. *J. Bacteriol. 181*, 670-674.

171. Wu, L. F., Mandrand-Berthelot, M. A., Waugh, R., Edmonds, C. J., Holt, S. E., and Boxer, D. H. (1989) Nickel Deficiency Gives Rise to the Defective Hydrogenase Phenotype of *hydC* and *Fnr* mutants in *Escherichia coli*. *Mol. Microbiol. 3*, 1709-1718.

172. Nelson, D. L., and Kennedy, E. P. (1971) Magnesium Transport in *Escherichia Coli*. Inhibition by Cobaltous Ion. *J. Biol. Chem. 246*, 3042-3049.

173. Niegowski, D., and Eshaghi, S. (2007) The CorA Family: Structure and Function Revisited. *Cell Mol. Life Sci. 64*, 2564-2574.

174. Grass, G., Franke, S., Taudte, N., Nies, D. H., Kucharski, L. M., Maguire, M. E., and Rensing, C. (2005) The Metal Permease ZupT from *Escherichia coli* is a Transporter with a Broad Substrate Spectrum. *J. Bacteriol. 187*, 1604-1611.

175. Rodrigue, A., Effantin, G., and Mandrand-Berthelot, M. A. (2005) Identification of *rcnA* (*yohM*), a Nickel and Cobalt Resistance Gene in *Escherichia coli*. *J. Bacteriol. 187*, 2912-2916.

176. Iwig, J. S., Rowe, J. L., and Chivers, P. T. (2006) Nickel Homeostasis in *Escherichia coli* - the *rcnR-rcnA* Efflux Pathway and its Linkage to NikR Function. *Mol. Microbiol. 62*, 252-262.

177. Koch, D., Nies, D. H., and Grass, G. (2007) The RcnRA (YohLM) System of *Escherichia coli*: A Connection between Nickel, Cobalt and Iron Homeostasis. *Biometals. 20*, 759-771.

178. Ranquet, C., Ollagnier-de-Choudens, S., Loiseau, L., Barras, F., and Fontecave, M. (2007) Cobalt Stress in *Escherichia coli*. the Effect on the Iron-Sulfur Proteins. *J. Biol. Chem. 282*, 30442-30451.

179. Johansen, K. S., Svendsen, I. I., and Rasmussen, S. K. (2000) Purification and Cloning of the Two Domain Glyoxalase I from Wheat Bran. *Plant Sci. 155*, 11-20.

180. Becker, K., Rahlfs, S., Nickel, C., and Schirmer, R. H. (2003) Glutathione--Functions and Metabolism in the Malarial Parasite *Plasmodium Falciparum*. *Biol. Chem. 384*, 551-566.

181. Bradford, M. M. (1976) A Rapid and Sensitive Method for the Quantitation of Microgram Quantities of Protein Utilizing the Principle of Protein-Dye Binding. *Anal. Biochem. 72*, 248-254.

182. Bodenhausen, G., and Ruben, D. J. (1980) Natural Abundance Nitrogen-15 NMR by Enhanced Heteronuclear Spectroscopy. *Chemical Physics Letters. 69*, 185-189.

183. States, D. J., Haberkorn, R. A., and Ruben, D. J. (1982) A Two-Dimensional Nuclear Overhauser Experiment with Pure Absorption Phase in Four Quadrants. *Journal of Magnetic Resonance. 48*, 286-292.

184. Stokvis, E., Clugston, S. L., Honek, J. F., and Heck, A. J. (2000) Characterization of Glyoxalase I (*E. coli*)-Inhibitor Interactions by Electrospray Time-of-Flight Mass Spectrometry and Enzyme Kinetic Analysis. *J. Protein Chem. 19*, 389-397.

185. Jaffe, E. K. (2000) The Porphobilinogen Synthase Family of Metalloenzymes. *Acta Crystallogr. D Biol. Crystallogr. 56*, 115-128.

186. Jaffe, E. K., Martins, J., Li, J., Kervinen, J., and Dunbrack, R. L.,Jr. (2001) The Molecular Mechanism of Lead Inhibition of Human Porphobilinogen Synthase. *J. Biol. Chem. 276*, 1531-1537.

187. Jaffe, E. K. (2003) Investigations on the Metal Switch Region of Human Porphobilinogen Synthase. *J. Biol. Inorg. Chem. 8*, 176-184.

188. Erskine, P. T., Senior, N., Awan, S., Lambert, R., Lewis, G., Tickle, I. J., Sarwar, M., Spencer, P., Thomas, P., Warren, M. J., Shoolingin-Jordan, P. M., Wood, S. P., and Cooper, J. B. (1997) X-Ray Structure of 5-Aminolaevulinate Dehydratase, a Hybrid Aldolase. *Nat. Struct. Biol. 4*, 1025-1031.

189. Kundrat, L., Martins, J., Stith, L., Dunbrack, R. L.,Jr, and Jaffe, E. K. (2003) A Structural Basis for Half-of-the-Sites Metal Binding Revealed in *Drosophila melanogaster* Porphobilinogen Synthase. *J. Biol. Chem. 278*, 31325-31330.

190. Marmstal, E., and Mannervik, B. (1978) Subunit Structure of Glyoxalase I from Yeast. *FEBS Lett. 85*, 275-278.